A CORRELATION POLARIMETER FOR DEEP SPACE TRACKING

Wolff-Rüdiger Zimmermann

NAVAL POSTGRADUATE SCHOOL
Monterey, California

THESIS

A CORRELATION POLARIMETER
FOR DEEP SPACE TRACKING

by

Wolff-Rüdiger Zimmermann

Thesis Advisor: J.E. Ohlson

September 1973

Approved for public release; distribution unlimited.

A Correlation Polarimeter for Deep Space Tracking

by

Wolff-Rüdiger Zimmermann
Kapitänleutnant (Lieutenant Commander), Federal German Navy
M.S., Naval Postgraduate School, 1973

Submitted in partial fulfillment of the
requirements for the degree of

ELECTRICAL ENGINEER

from the

NAVAL POSTGRADUATE SCHOOL
September 1973

ABSTRACT

The tracking polarimeter implemented on the 64-meter National Aeronautics and Space Administration/Jet Propulsion Laboratory (NASA/JPL) parabolic antenna at Goldstone, California uses a pair of waveguide quarter-wave plates to allow synthesis of a rotating cross-polarized linear feed system, and a phase-locked-loop (PLL) to coherently determine an error signal from the signal component in the error channel. This error signal drives the feed system until the error axis is orthogonal to the signal axis.

Because the PLL has the normal "loss of lock" problem at low signal-to-noise ratios a correlation polarimeter has been developed. The PLL is replaced by a multiplier as a correlator. The correlation between the signal components in the reference and error channels accomplishes a detection of the error signal because both have same phase, since they are just different projections of the same signal vector.

The analysis, the investigation of the theory by means of a working model, the development of the actual correlation polarimeter and the test series performed are described.

TABLE OF CONTENTS

LIST OF TABLES

Table

LIST OF FIGURES

Figure

Figure

Figure

ACKNOWLEDGEMENT

The author is indebted to G.S. Levy, B. Seidel, B. Parham, R. Mitchell, and all others, of the Jet Propulsion Laboratory, for their support and cooperation.

I. INTRODUCTION

In many applications, it is desired to measure the plane of polarization of a linearly polarized signal, e.g. Faraday rotation in the terrestrial ionosphere or in the corona of the sun.

Present schemes for measuring the polarization plane of a narrowband linearly polarized signal are optimum for high signal-to-noise ratio (SNR) but are not optimum and usually do not work at all when the SNR is small. A system for which the SNR must be moderately high to be optimum is shown in Fig. 1. This is called a coherent polarimeter and it is very similar to amplitude comparison monopulse angle tracking [1]. The key feature of this system is the use of a rotatable feed system which may be electronically synthesized or purely mechanical. It may

- mechanically rotate a cross-polarized feed [2,3]
- synthesize a cross-polarized feed by phase comparison in the receiver at IF [2,3]
- use a rotatable quarter-wave plate waveguide section behind a stationary horn [4]

The latter scheme is the most sensitive and accurate of the three. The operation of the coherent polarimeter is easy to follow. The reference and error channel signals are the projections of the received electric field vector upon the reference and error axes. When the reference

axis is perfectly aligned with the linearly polarized signal, the reference channel has all the signal power and the phase locked loop (PLL) is locked to the signal. The error channel has no signal component so the motor is driven only by the system noise. When the reference channel is slightly misaligned with the signal axis, the error channel has a signal component and by means of the coherent detector an error signal proportional to magnitude and sign of the angle error is developed which drives the feed system back so that the error axis is orthogonal to the signal axis.

The performance of this system deteriorates rapidly as the SNR in the PLL approaches unity. The difficulty is due primarily to the inability of the PLL to remain locked at low SNR, which can result from a weak signal, a high noise environment or doppler spreading of the signal. The correlation polarimeter which is subject of this thesis eliminates the "loss of lock" problem inherent for low SNR.

Note that Fig. 2 is of the form of the classical monopulse angle tracking radar [1]. In the present application, however, a continuous noise-like signal rather than relatively clean radar pulses are of concern.

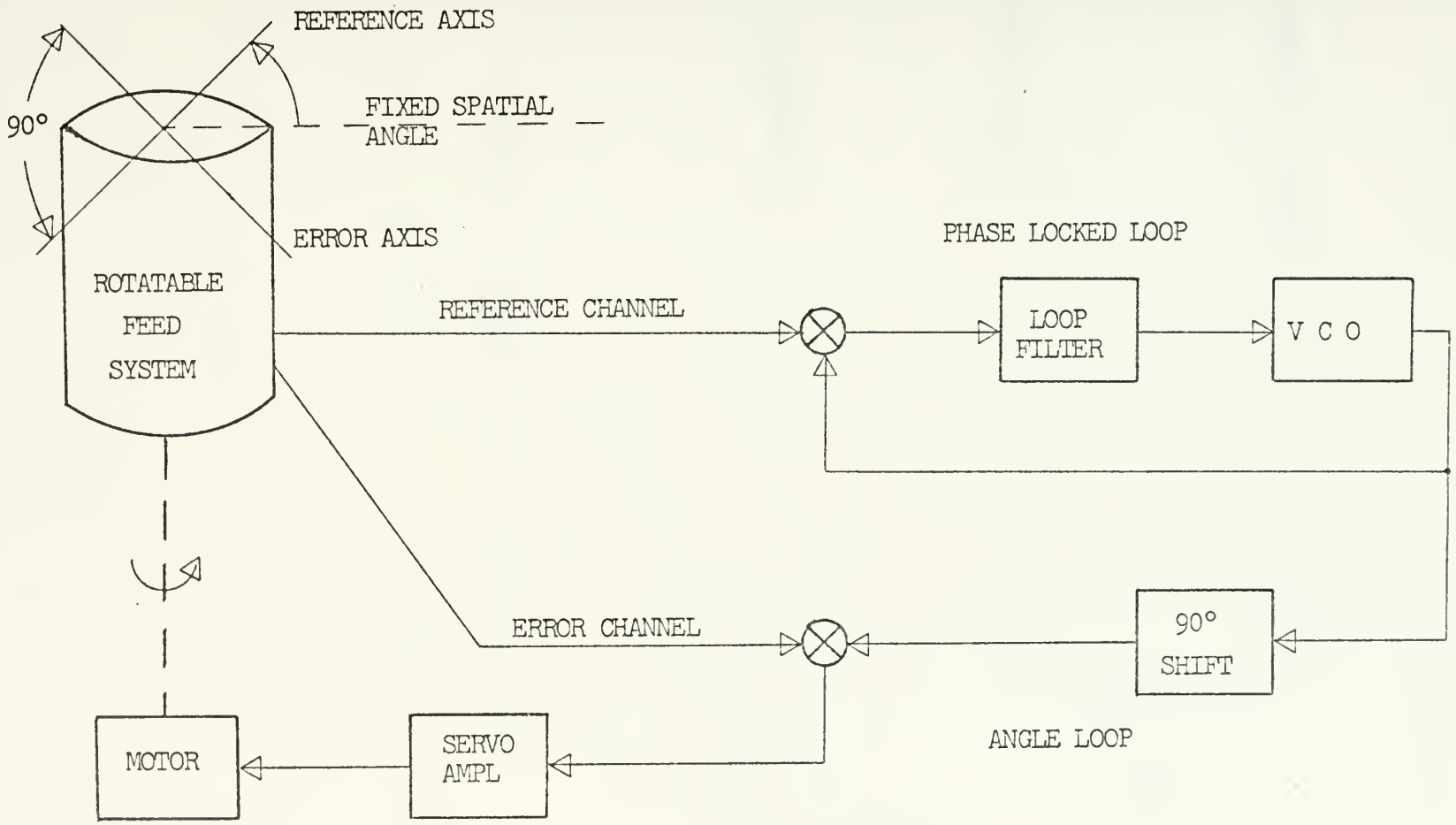

Figure 1. COHERENT POLARIMETER

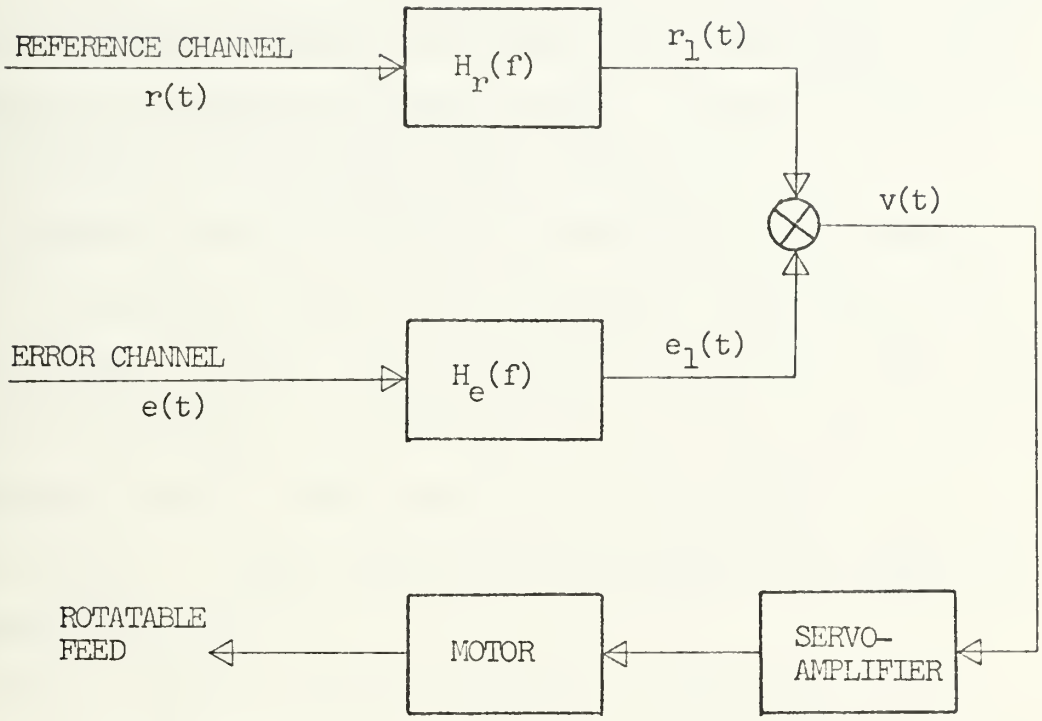

Figure 2. CORRELATION POLARIMETER MODEL

II. BASIC OPERATION OF THE CORRELATION POLARIMETER

It has been shown by Ohlson [4] that the basic correlation polarimeter scheme is optimal when the signal can be modeled as a Gaussian random process. Much of this and the next chapter is based upon this article.

A model of the correlation polarimeter is presented in Fig. 2, where $H_r(f)$ and $H_e(f)$ represent all filtering in the system. In Fig. 3 the system is shown with some additional items such as automatic gain control (AGC), automatic frequency control (AFC), and a second multiplier with wide band inputs. A more practical correlation polarimeter is presented in Fig. 4.

It is assumed that the reference and error channel signals are developed by use of a rotatable feed system such as shown in Fig. 1. The actual method of implementing the feed system is of no consequence here.

The heuristic idea behind the correlation polarimeter is that if the PLL cannot do a good job at low SNR, because it loses lock often, the function it performs should be done by a suitable substitute. The PLL attempts to make a good estimate of the signal phase so that it can coherently detect the signal component in the error channel. If the PLL cannot hold lock, then a correlation of the signal component in the reference channel r(t) with the signal component in the error channel e(t) will also accomplish

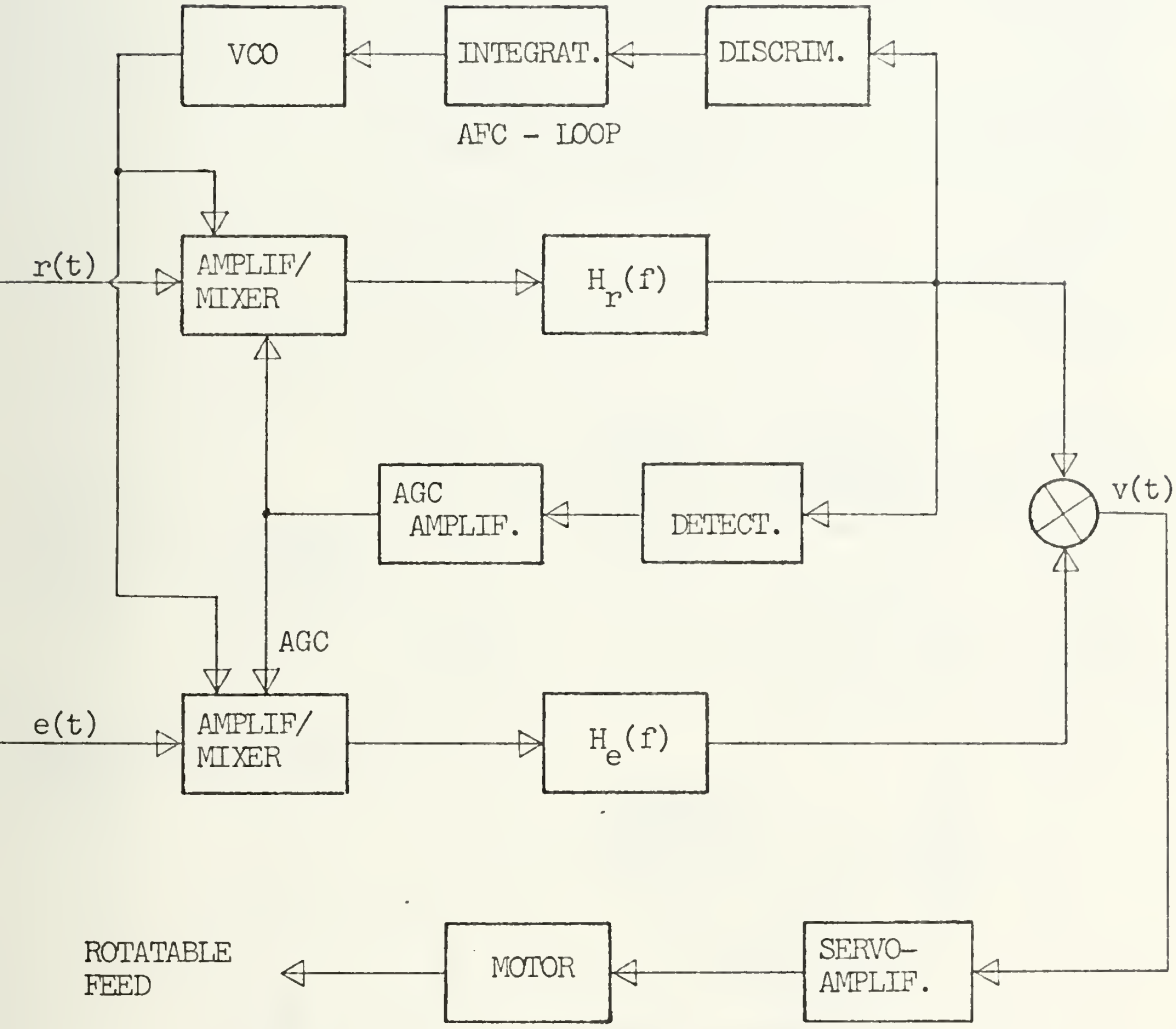

Figure 3. CORRELATION POLARIMETER MODEL
(with AGC- and AFC-loop)

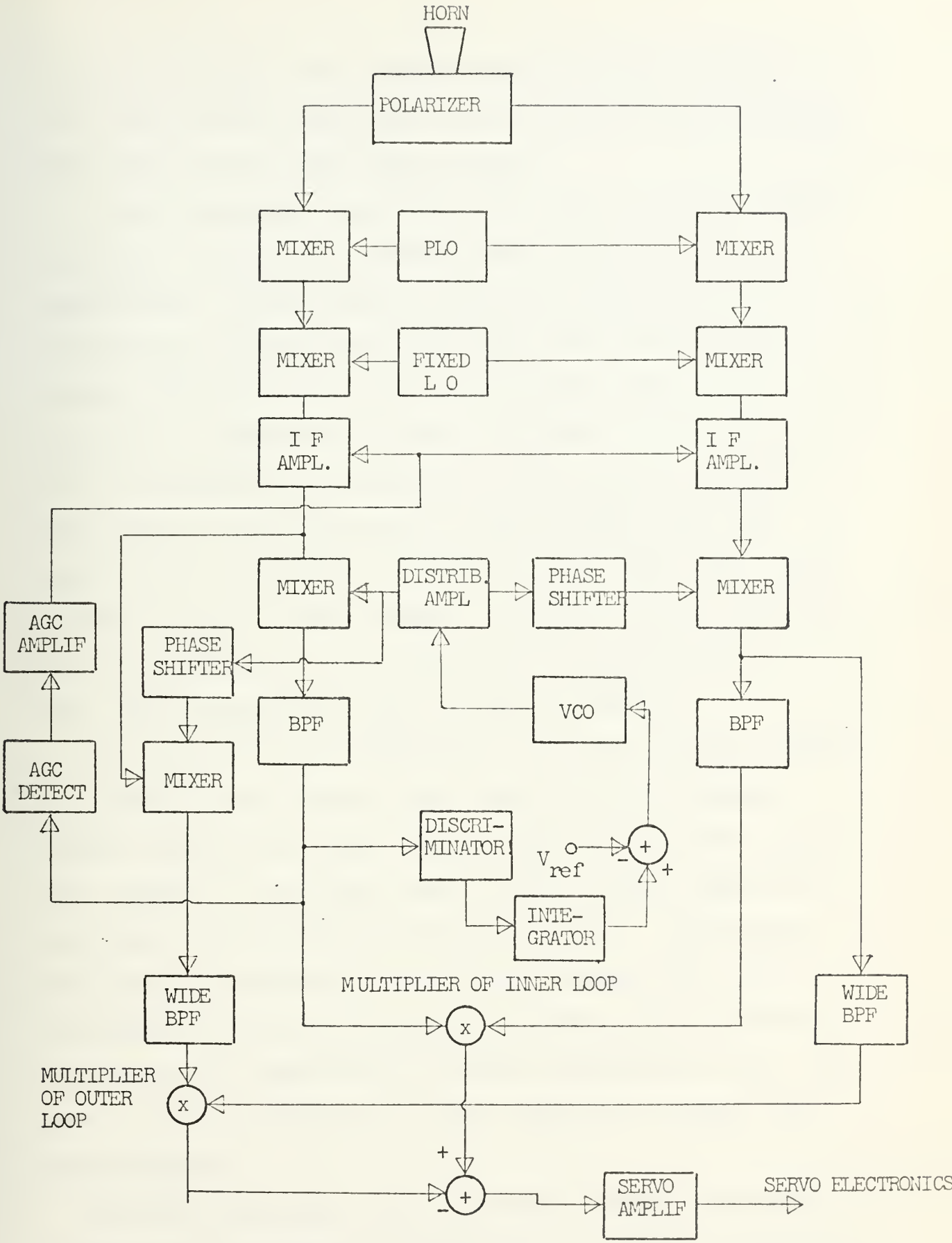

Figure 4. PRACTICAL CORRELATION POLARIMETER

a detection of the error channel signal because r(t) and e(t) must have the same phase, since they are just different projections of the same signal vector.

In the practical system the inner loop is used to detect the signal in the error channel which is disturbed by the system noise. (This loop is used in the analysis of the polarimeter.) In the outer loop with the wide band-pass filters (BPF) the SNR is low so the signal power can be neglected in comparison to the noise power. In the loop only the linearly polarized noise power will be detected which then is subtracted with a proper factor from the output of the inner loop, so that only the real signal will produce the servo input voltage. If more linearly polarized noise is received by the polarimeter the power levels in both loops increase and will continue to cancel.

The function of the AGC (Fig. 5) in the reference channel is to maintain the signal power output in the reference channel constant and thus also the input to the servo system. Thus changes in the power level of the received signal will not affect the function of the servo system. The detector will give the envelope of the filter output. This then is differenced with the AGC reference voltage. The difference is averaged and amplified in the AGC amplifier and then fed back to the IF-amplifiers in both channels to adjust their gains properly.

The AFC loop should stabilize mixer output frequencies to the center frequency of the BPF's. It detects frequency

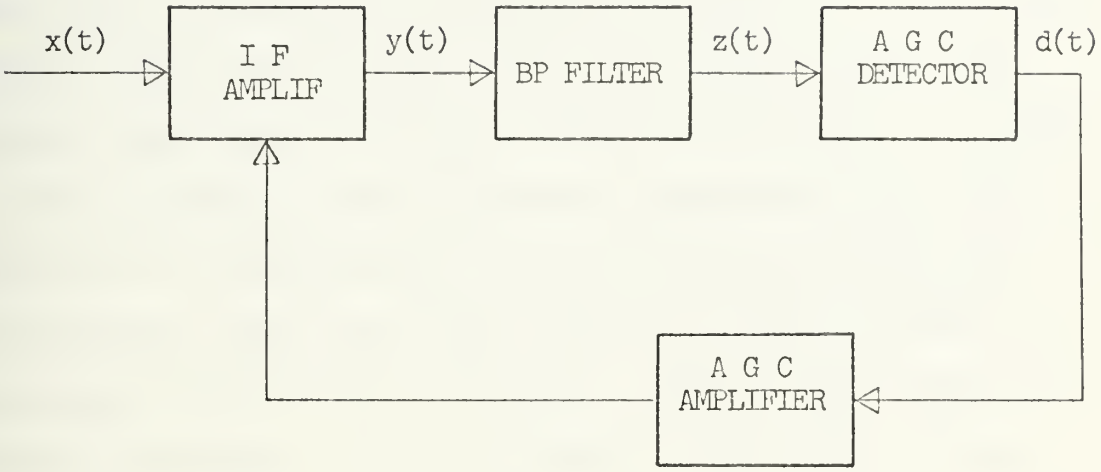

Figure 5. AGC LOOP

changes due to drift in the system by the discriminator. Its output DC voltage is a function of the frequency offset. The voltage polarity depends on the direction of the frequency offset. This DC voltage is then integrated and compared with the reference voltage. If there is a difference between these two voltages the output frequency of the voltage controlled oscillator (VCO) is changed in this way so that the mixer output frequency approaches the center frequency of the band-pass filters. At this point the discriminator will have zero output voltage, so that the integrator output stays constant. Thus the VCO frequency remains unchanged. A block diagram of the AFC is shown in Fig. 6.

The programmable local oscillator (PLO) of the first mixer stage is needed because there is no automatic tuning of the system as in the coherent polarimeter with the PLL. With the PLO the frequency change due to the variable doppler shift caused by the spacecraft and earth motions is eliminated. The PLO uses doppler predictions calculated from spacecraft orbit and motion of the earth.

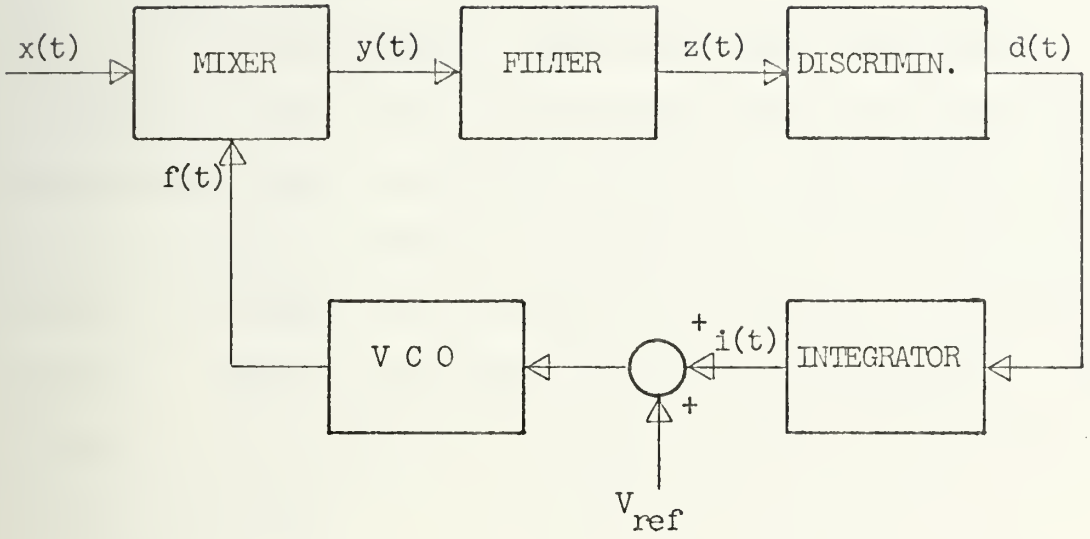

Figure 6. AFC LOOP

III. SYSTEM ANALYSIS

A. CORRELATOR OUTPUT

In the following the signal and noise components of the correlator output v(t) are derived using the correlation polarimeter model as shown in Fig. 2. The received signal as seen with the antenna's aperture s(t) is linearly polarized at an angle θ with respect to a reference xy-coordinate system. One now can define the reference and error channel signals as the projection of the received signal upon the coordinate axes.

Thus

$$r(t) = s(t)\cos\theta + n_r(t) \tag{1}$$

$$e(t) = s(t)\sin\theta + n_e(t) \tag{2}$$

S(t) is assumed to have the auto-correlation function

$$R_s(\tau) = E[s(t+\tau)\, s(t)] \tag{3}$$

where $E[\cdot]$ denotes statistical expectation, and the corresponding power spectrum is

$$S_s(f) = \int_{-\infty}^{\infty} R_s(\tau) \exp(-j2\pi f\tau)\, d\tau \,. \tag{4}$$

All other autocorrelations and power spectral densities are defined similarly.

The noises $n_r(t)$ and $n_e(t)$ are assumed to be independent, white zero-mean Gaussian random processes with double-sided power spectral densities:

$$S_{n_r}(f) = N_r = kT_r/2 \tag{5}$$

$$S_{n_e}(f) = N_e = kT_e/2 \tag{6}$$

where k is Boltzmann's constant and T_r and T_e are the system noise temperatures in the reference and error channels. From (5), (6) and (4) their autocorrelation functions are:

$$R_{n_r}(\tau) = N_r\,\delta(\tau) \tag{7}$$

$$R_{n_e}(\tau) = N_e\,\delta(\tau) \tag{8}$$

All voltages are assumed to be on 1-ohm impedances so the units in (5), (6), and (4) are watts/Hz, and also the average signal power is given by

$$P_s = E[s^2(t)] = R_s(0) \tag{9}$$

Now the statistics of v(t) in Fig. 2 will be examined. Knowledge of the mean and spectrum of v(t), given θ, are

sufficient to characterize the rms system error, σ_θ. From Fig. 2 it can be seen that

$$r_1(t) = \int_{-\infty}^{\infty} h_r(t-\tau)r(\tau)\, d\tau \tag{10}$$

where $h_r(t)$ is the impulse response corresponding to $H_r(f)$, i.e., $H_r(f)$ is the Fourier transform of $h_r(t)$. Making a similar definition for $h_e(t)$ to get

$$e_1(t) = \int_{-\infty}^{\infty} h_e(t-\tau)e(\tau)\, d\tau \tag{11}$$

Now since

$$v(t) = r_1(t)\, e_1(t) \tag{12}$$

and using (1), (2), (10), and (11) the correlator output becomes

$$v(t) = \int_{-\infty}^{\infty}\int_{-\infty}^{\infty} h_r(t-\tau_1)h_e(t-\tau_2)[s(\tau_1)\cos\theta + n_r(\tau_1)][s(\tau_2) \sin\theta + n_e(\tau_2)]\, d\tau_1\, d\tau_2 \tag{13}$$

By taking the expectation of v(t), conditioned upon θ, the system S-curve $S(\theta)$ is obtained:

$$S(\theta) = E[v(t)|\theta] = \cos\theta \sin\theta \int_{-\infty}^{\infty}\int_{-\infty}^{\infty} h_r(t-\tau_1)h_e(t-\tau_2) R_S(\tau_1-\tau_2)\, d\tau_1\, d\tau_2 \tag{14}$$

Parseval's theorem and the Fourier transform allows (14) to be rewritten as

$$S(\theta) = \cos\theta \sin\theta \int_{-\infty}^{\infty} H(f)\cdot S_s(f)\, df \qquad (15)$$

where for brevity

$$H(f) = H_r(f)\, H_e^*(f) \qquad (15a)$$

It should be noted that the S-curve in (15) was found without needing the assumption that $s(t)$, $n_r(t)$ and $n_e(t)$ were Gaussian random processes. To evaluate system performance this assumption, however, will be needed and is invoked at this point. Now the autocorrelation function is calculated for $v(t)$, conditional upon θ, using (3) to obtain

$$R_v(\tau) = E[v(t+\tau)v(\tau)|\theta] = E[r_1(t+\tau)e_1(t+\tau)r_1(t)e_1(t)|\theta]. \qquad (16)$$

Until stated to the contrary, all autocorrelations and spectra are conditioned upon θ being held constant. Since $n_r(t)$ and $n_e(t)$ are zero-mean Gaussian random processes, $r_1(t)$ and $e_1(t)$ are also zero-mean and Gaussian because $H_r(f)$ and $H_e(f)$ are linear operators. Thus one may use the identity for the expectation of the product of four Gaussian random variables [6]

$$E[X_1X_2X_3X_4] = E[X_1X_2]E[X_3X_4] + E[X_1X_3]E[X_2X_4] + E[X_1X_4]E[X_2X_3] \tag{17}$$

Thus

$$R_v(\tau) = R_{r_1}(\tau)R_{e_1}(\tau) + R^2_{r_1e_1}(0) + R_{r_1e_1}(\tau)\, R_{r_1e_1}(-\tau) \tag{18}$$

The autocorrelations are defined as (3) while

$$R_{r_1e_1}(\tau) = E[r_1(t+\tau)\, e_1(t)|\theta] \tag{19}$$

The Fourier transform of (18) is

$$\begin{aligned} S_v(f) = {} & S_{r_1}(f) \otimes S_{e_1}(f) + R^2_{r_1e_1}(0)\, \delta(f) \\ & + S_{r_1e_1}(f) \otimes S^*_{r_1e_1}(f) \end{aligned} \tag{20}$$

where $\otimes$ denotes the convolution and (*) denotes complex conjugation.

The second term in (20) is due to the average value of v(t) found in (19). In particular, $R^2_{r_1e_1}(0) = E^2[v(t)|\theta] = E^2[r_1(\tau)e_1(\tau)|\theta] = S^2(\theta)$. Therefore, it is chosen to represent v(t) as

$$v(t) = S(\theta) + n(t) \tag{21}$$

where the spectrum of n(t) is the first and third term of (20)

$$S_n(f) = S_{r_1}(f) \otimes S_{e_1}(f) + S_{r_1 e_1}(f) \otimes S^*_{r_1 e_1}(f). \quad (22)$$

From Fig. 2, (1) and (2) it can be shown that

$$S_{r_1}(f) = |H_r(f)|^2 [\cos^2\theta \, S_s(f) + N_r] \quad (23)$$

Similarly,

$$S_{e_1}(f) = |H_e(f)|^2 [\sin^2\theta \, S_s(f) + N_e] \quad (24)$$

To find $S_{r_1 e_1}$ one observes from Fig. 2 that

$$r_1(t) = \int_{-\infty}^{\infty} h_r(t-\tau) \, r(\tau) \, d\tau \quad (10)$$

$$e_1(t) = \int_{-\infty}^{\infty} h_e(t-\tau) \, e(\tau) \, d\tau \quad (11)$$

where $h_r(t)$ and $h_e(t)$ are the filter impulse responses which are the inverse Fourier transforms of $H_r(f)$ and $H_e(f)$.

From (10), (11), and (19), the crosscorrelation is found as

$$R_{r_1 e_1}(\tau) = \int_{-\infty}^{\infty} \int_{-\infty}^{\infty} h_r(t+\tau-\tau_1) h_e(t-\tau_2) E\{[s(\tau_1)\cos\theta + n_r(\tau_1)]$$

$$[s(\tau_2)\sin\theta + n_e(\tau_2)] | \theta\} \, d\tau_1 \, d\tau_2 \quad (25)$$

Since $n_r(t)$ and $n_e(t)$ are independent

$$R_{r_1e_1}(\tau) = \cos\theta \sin\theta \int_{-\infty}^{\infty}\int_{-\infty}^{\infty} h_r(t+\tau-\tau_1)h_e(t-\tau_2) R_s(\tau_1-\tau_2)\, d\tau_1\, d\tau_2 \tag{26}$$

The Fourier transform is

$$S_{r_1e_1}(f) = \cos\theta \sin\theta\, H_e^*(f)\, H_r(f)\, S_s(f) \tag{27}$$

One now may argue that since the servo loop bandwidth will be much smaller than the bandwidth of n(t), over the small servo loop bandwidth the noise spectrum is constant, and over the servo bandwidth therefore it is

$$S_n(f) = S_n(0) \tag{28}$$

Thus, n(t) is approximated very well as a white Gaussian process with power spectral density

$$S_n(f) = S_n(0) = \int_{-\infty}^{\infty} [S_{r_1}(f)S_{e_1}(f) + |S_{r_1e_1}(f)|^2]\, df \tag{29}$$

which becomes

$$S_n(f) = N_eN_r \int_{-\infty}^{\infty} |H(f)|^2 df + (N_e\cos^2\theta + N_r\sin^2\theta) \int_{-\infty}^{\infty} |H(f)|^2 S_s(f)df + 2\cos^2\theta \sin^2\theta \int_{-\infty}^{\infty} |H(f)|^2 S_s^2(f)df \tag{30}$$

by using (23), (24), and (27).

It should be noted that in the analysis and in the derivation of the performance of the correlation polarimeter only the product of $H_r(f)$ and the complex conjugate of $H_e(f)$, defined as $H(f) = H_r(f)\, H_e^*(f)$, is of significance. Thus, without losing generality in the mathematics one can easily omit the band-pass filters in one of the branches, not only in the inner loop but also in the outer loop. The latter has not been used in the analysis.

Because both the AGC and the AFC loops need as their inputs the reference signal (this should be received only if the polarimeter feed system is aligned perfectly) only the BPF in the error channel branch could be omitted. That means simply that $H_r(f) = H(f)$ and $H_e(f) = 1$. If the reference and the error channel signals are filtered by $H_r(f)$ and $H_e(f)$ respectively or if only the reference signal frequency is filtered by $H(f)$ the result will be the same in both cases.

In practice it is impossible to eliminate the error channel filters due to the phase response of filters. Only if filters with absolutely constant phase over the entire bandwidth were available could the error channel BPF be eliminated. The effects of filter phase response are further discussed in Section III.B.2.

B. SYSTEM PERFORMANCE

1. General Expression for the RMS-Angle Error due to Noise

The input signal of the servo system is given as

$$v(t) = S(\theta) + n(t) \qquad (21)$$

where

$$S(\theta) = E[r_1(t)e_1(t)|\theta] \tag{19}$$

$$= \cos\theta \sin\theta \int_{-\infty}^{\infty} H(f) \cdot S_s(f)\, df \tag{15}$$

and for small θ, $\cos\theta \simeq 1$, $\sin\theta \approx \theta$ so that

$$S(\theta) = \theta \int_{-\infty}^{\infty} H(f) \cdot S_s(f)\, df \tag{31}$$

The integral is constant for a certain H(f) and a given signal power density $S_s(f)$; thus

$$S(\theta) = K\,\theta \tag{32}$$

where, in general, K is a function of filter frequency response and signal power density

$$K = \int_{-\infty}^{\infty} H(f) \cdot S_s(f)\, df \tag{33}$$

The servo input now becomes

$$v(t) = K\,\theta + n(t) \tag{34}$$

where θ is the difference between the signal polarization angle θ_s and the polarizer angle θ_p

$$\theta = \theta_s - \theta_p \tag{35}$$

The system can be modeled as shown in Figure 7.

In order to find the rms angle error due to the system's noise θ_s is arbitrarily set equal to zero. In Figure 6 now the entry point of n(t) may be moved back to the first summing node where its power spectral density is attenuated by the factor K^2. The modified block diagram is shown in Figure 8.

The transfer function of this system is

$$F(s) = \frac{K\,G(s)}{1 + K\,G(s)}$$

$$= \frac{1}{1 + \frac{1}{K\,G(s)}} \tag{36}$$

The single sided noise bandwidth of this system (servo loop) can be defined as

$$W_S = \frac{\int_0^\infty |F(f)|^2\, df}{|F(0)|^2} \tag{37}$$

For a servo system that tracks with zero position error it is required that

$$|F(0)| = 1$$

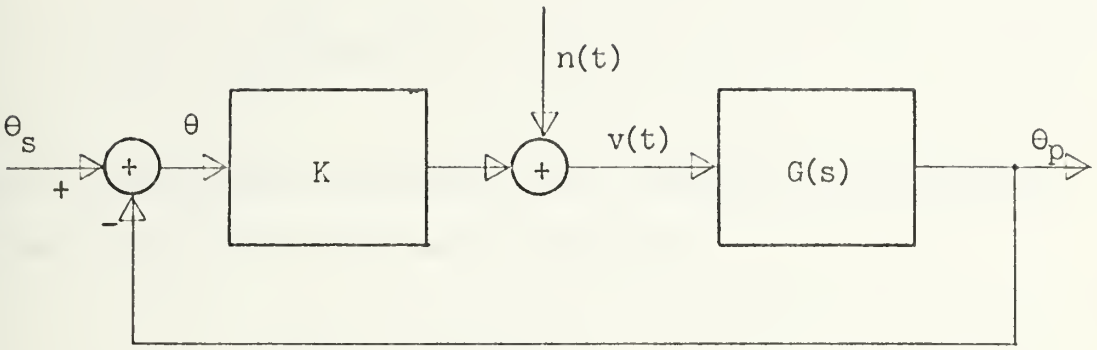

Figure 7. POLARIZATION TRACKING LOOP

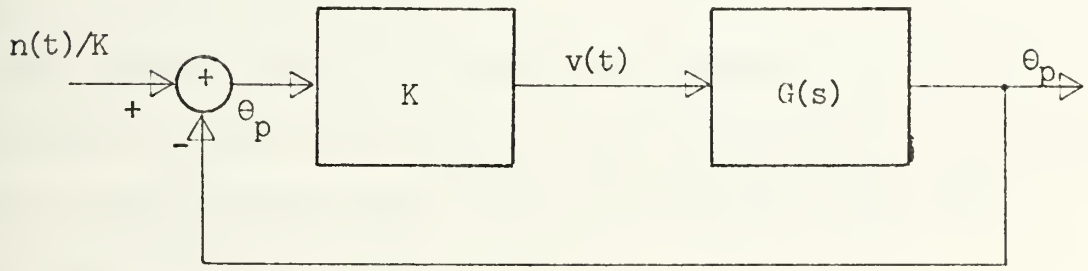

Figure 8. POLARIZATION TRACKING LOOP

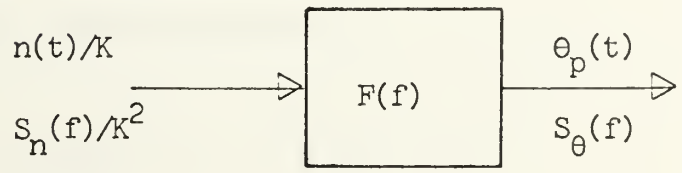

Figure 9. POLARIZATION TRACKING LOOP
(with transfer function F)

Thus the noise bandwidth becomes

$$W_S = \int_0^\infty |F(f)|^2 \, df \tag{38}$$

Figure 9 shows the rearranged block diagram of the system. The rms angle error due to the noise is

$$\sigma_\theta^2 = E[\theta^2(t)] - E^2[\theta(t)] \tag{39}$$

$$= R_\theta(0) - R_\theta(\infty)$$

but $R_\theta(\infty) = E^2[\theta(t)] = 0$ because the input to the linear system, $n(t)$, has zero mean.

The spectral density of the output process is merely the product of the input density times the system's response. From the block diagram (Fig. 8) it can be seen that the output spectral density is

$$S_\theta(f) = |F(f)|^2 \frac{S_n(f)}{K^2} \tag{40}$$

The mean-square voltage of the output process $\theta(t)$ - the rms angle error - can be found as

$$\sigma_\theta^2 = R_\theta(0) = \int_{-\infty}^\infty S_\theta(f) \, df \tag{41}$$

$$= \frac{1}{2\pi} \int_{-\infty}^\infty S_\theta(\omega) \, d\omega$$

$$= \frac{1}{2\pi K^2} \int_{-\infty}^\infty |F(\omega)|^2 \, S_n(\omega) \, d\omega \tag{42}$$

In the system analysis of the correlation polarimeter the noise power spectral density is calculated (30), furthermore it was shown that n(t) can be approximated as a white Gaussian process.

Assuming small angle θ the double-sided density in (30) becomes

$$S_n(f) = N_e N_r \int_{-\infty}^{\infty} |H(f)|^2 \, df + N_e \int_{-\infty}^{\infty} |H(f)|^2 \, S_s(f) \, df \tag{43}$$

The single-sided noise bandwidth of the system's BPF as defined in (15a)

$$W_n = \frac{\int_0^{\infty} |H(f)|^2 \, df}{|H(f_o)|^2} \tag{44}$$

The maximum filter response occurs at frequency f_o and is assumed to be unity; thus the expression for the noise bandwidth reduces to

$$W_n = \int_0^{\infty} |H(f)|^2 \, df \tag{45}$$

and the equation (43) becomes

$$S_n(f) = 2N_e N_r W_n + N_e I \tag{46}$$

where for brevity

$$I = \int_{-\infty}^{\infty} |H(f)|^2 S_s(f)\, df \qquad (47)$$

Using (40), (41), and (46) the rsm angle error in general can be expressed as

$$\sigma_\theta^2 = \frac{2 W_S S_n(f)}{K^2} \qquad (48)$$

$$\sigma_\theta^2 = \frac{2 N_e W_S}{K^2} (2 N_r W_n + I) \qquad (49)$$

2. Phase Response of the Filter

In this section the effect of the filter phase response on the correlator output, the noise spectral density, and the rms angle error are derived.

a. Correlator Output

The correlator output v(t) is derived in III.B.1 as

$$v(t) = S(\theta) + n(t) = E[v(t)] + n(t) \qquad (21)$$

where

$$E[v(t)] = S(\theta) = \cos\theta \sin\theta \int_{-\infty}^{\infty} H(f) S_s(f)\, df \qquad (15)$$

$$\approx \theta \int_{-\infty}^{\infty} H(f) S_s(f)\, df \qquad (31)$$

With E[v(t)] and $S_s(f)$ to be real h(t), the filter impulse response, has to be a real function too.

The Fourier transform of a real function has a real part that is even and an imaginary part that is odd [6]. The Fourier transform of the real time function h(t) is given as

$$H(f) = \int_{-\infty}^{\infty} h(t)\, e^{-j\,2\pi ft}\, dt \qquad (50)$$

This transform may be written as

$$H(f) = \int_{-\infty}^{\infty} h(t) \cos 2\pi ft\, dt - j \int_{-\infty}^{\infty} h(t) \sin 2\pi ft\, dt \qquad (51)$$

The real part of this function is even since

$$Re[H(f)] = \int_{-\infty}^{\infty} h(t) \cos 2\pi ft\, dt = Re[H(-f)] \qquad (52)$$

and the imaginary part is odd since

$$Im[H(f)] = \int_{-\infty}^{\infty} h(t) \sin 2\pi ft\, dt = - Im[H(-f)] \qquad (53)$$

Using these facts (31) can be written as

$$E[v(t)] = \theta \int_{-\infty}^{\infty} \{Re[H(f)] + j\, Im[H(f)]\}\, S_s(f)\, df \qquad (54)$$

$$E[v(t)] = \theta \{2 \int_0^\infty \mathrm{Re}[H(f)]\, S_s(f)\, df + j \int_0^\infty \mathrm{Im}[H(-f)]\, S_s(f)\, df - j \int_0^\infty \mathrm{Im}[H(-f)]\, S_s(f) df$$

$$= 2\theta \int_0^\infty \mathrm{Re}[H(f)]\, S_s(f)\, df \qquad (55)$$

$$= K\theta \qquad (32)$$

This is the expected real function; only the real part of the filter's frequency response is effective in the multiplier output, v(t).

The complex filter response is

$$H(f) = \mathrm{Re}[H(f)] + j\, \mathrm{Im}[H(f)] \qquad (56)$$

$$= [(\mathrm{Re}[H(f)])^2 + (\mathrm{Im}[H(f)])^2]^{\frac{1}{2}}\, e^{j\phi(f)} \qquad (57)$$

$$= |H(f)|\, e^{j\phi(f)} \qquad (58)$$

where

$$\phi(f) = \tan^{-1} \frac{\mathrm{Im}[H(f)]}{\mathrm{Re}[H(f)]} \qquad (59)$$

The frequency response rewritten gives

$$H(f) = |H(f)| \cos \phi(f) + j\, |H(f)| \sin \phi(f) \qquad (60)$$

so the phase response of the filter effects the multiplier output, v(t), with the cosine of the phase angle.

$$v(t) = \theta \int_{-\infty}^{\infty} |H(f)| \cos \phi(f)\, S_s(f)\, df + n(t) \qquad (61)$$

$$= K\,\theta + n(t) \qquad (34)$$

Thus K is generally defined now as

$$K = 2 \int_{0}^{\infty} \mathrm{Re}[H(f)] S_s(f)\, df = \int_{-\infty}^{\infty} |H(f)| \cos \phi(f) S_s(f)\, df \qquad (62)$$

b. Noise Power Spectral Density and RMS Angle Error

The noise power spectral density of n(t) is given by Equation (43)

$$S_n(f) = N_e N_r \int_{-\infty}^{\infty} |H(f)|^2\, df + N_r \int_{-\infty}^{\infty} |H(f)|^2 S_s(f)\, df \qquad (43)$$

which only depends upon the magnitude of the band-pass filter response; it is independent of the phase response.

From (40) in connection with (55) and (60) it can be seen that the phase response of the filter enters in the power spectral density of the servo output, $S_\theta(f)$, which is

$$S_\theta(f) = \frac{S_n(f)\, |F(f)|^2}{K^2} \qquad (40)$$

where K is defined in (62).

The rms angle error is phase dependent because K is. It can be expressed using (38) as

$$\sigma_\theta^2 = \frac{2 W_S S_n(f)}{K^2} \tag{48}$$

Substituting for $S_n(f)$ the rms angle error becomes

$$\sigma_\theta^2 = \frac{2 W_S N_e}{K^2} \int_{-\infty}^{\infty} |H(f)|^2 (N_r + S_s(f)) \, df \tag{63}$$

The real part of the filter response affects the expected value of the multiplier output, E[v(t)], and thus the rms angle error.

3. Optimum Filter in the Correlation Polarimeter

In the following section the optimum filter of the correlation polarimeter is derived. This filter should be optimal in noise rejection, but on the other hand maximum signal power should pass the band-pass filter. Thus a realization of the optimum filter would mean a maximization of the performance of the system.

a. Frequency and Phase Response of the Optimum Filter

The filter response should provide maximum servo input voltage

$$v(t) = S(\theta) + n(t) \tag{21}$$

That means H(f) should maximize

$$S(\theta) = \theta \int_{-\infty}^{\infty} H(f)\, S_s(f)\, df \tag{31}$$

$$= K\, \theta \tag{32}$$

where K is defined for real time function h(t) as

$$K = \int_{-\infty}^{\infty} |H(f)| \cos \phi(f)\, S_s(f)\, df \tag{62}$$

This maximization is done subject to

$$S_n(f) = N_e \int_{-\infty}^{\infty} |H(f)|^2 (N_r + S_s(f))\, df = A'$$

which means the constraint is to keep the spectral noise power spectral density constant, because the noise is assumed to be Gaussian and white over the bandwidth of the filter.

This constraint can be modified to

$$A = \int_{-\infty}^{\infty} |H(f)|^2 (N_r + S_s(f))\, df \tag{64}$$

where A is arbitrary.

The method of calculus of variation used is presented in [6]. Let

$$K = \int_{-\infty}^{\infty} Z(f,H)\, df \quad \text{and}$$

$$A = \int_{-\infty}^{\infty} Z_1(f,H)\, df$$

form

$$Z_o = Z + Z_1$$

and apply the Euler-Lagrange condition. Thus

$$Z_o = Re[H(f)]S_s(f) + \lambda\{(Re[H(f)])^2 + (Im[H(f)])^2\}[N_r+S_s(f)] \tag{65}$$

where λ is the Lagrange multiplier.

One has to set the partial derivatives of Z_o with respect to the real part and the imaginary part of the filter response H(f) equal to zero

$$\frac{\partial Z_o}{\partial Re[H(f)]} = 0 = S_s(f) + 2\lambda Re[H(f)]\ (N_r+S_s(f)) \tag{66}$$

$$\frac{\partial Z_o}{\partial Im[H(f)]} = 0 = 2\lambda Im[H(f)]\ (N_r+S_s(f)) \tag{67}$$

Solving these two simultaneous equations the filter response becomes

$$Re\ H(f) = \frac{-\ S_s(f)}{2\lambda(N_r + S_s(f))} \tag{68}$$

$$Im\ H(f) = 0 \tag{69}$$

Substituting these expressions into (43) λ is found to be

$$\lambda = \left\{ \frac{1}{4A} \int_{-\infty}^{\infty} \frac{S_s^2(f)\, df}{N_r + S_s(f)} \right\}^{\frac{1}{2}} \tag{70}$$

Using this result in (68) the filter response becomes

$$H(f) = \frac{- S_s(f)}{2\,(N_r + S_s(f)) \left\{ \frac{1}{4A} \int_{-\infty}^{\infty} \frac{S_s^2(f)}{N_r + S_s(f)}\, df \right\}^{\frac{1}{2}}} \tag{71}$$

But the radical is a constant, so

$$H(f) = C \frac{1}{1 + \frac{N_r}{S_s(f)}} \tag{72}$$

and since A is arbitrary

$$H(f) = \frac{1}{1 + N_r/S_s(f)} \tag{73}$$

In this frequency response of the band-pass filter of the correlation polarimeter the frequency dependence is given by the power spectral density of the received signal. Because the signal is real and its power spectral density function is a real function of the frequency, the filter frequency is a real function too. Thus the optimum filter has zero-phase response.

b. Correlator Output (Multiplier Output)

With the optimum filter in the system the multiplier output (servo input) becomes

$$v(t) = \theta \int_{-\infty}^{\infty} \frac{S_s(f)\, df}{1 + N_r/S_s(f)} + n(t) \qquad (74)$$

To maximize this voltage, v(t), the filter must have the frequency response as derived in (73). This response of the filter changes with the power spectral density of the signal; the shape of the signal spectrum is important. Depending on the SNR a filter bandwidth has to be selected.

But in practice these required changes of the filter frequency response for optimum v(t) are not realizable. Therefore the optimum filter can only be approximated by selecting from a bank of different band-pass filters, the filter with the bandwidth large enough to get almost all signal power through but as small as possible to limit the noise power. By means of a spectrum analyzer the signal spectrum in front of the filters can be examined in real-time and according to the observed signal bandwidth the proper filter can be selected.

In addition this spectrum analyzer tells how well the PLO and the AFC loop are working; the signal should always be centered around the center-frequency of the filters. The analyzer must have a high frequency resolution to indicate the slightest change in signal bandwidth.

Besides the Faraday rotation, a spectral broadening of the signal has been observed in solar occultations [7]. During the spacecraft's approach of the sun the increase in polarization angle and broadening of the spectrum of the signal occur together.

Because of the desire for high resolution with the spectrum analyzer it will have a very slow sweep time and a storage oscilloscope or a strip chart recorder must be used for display.

c. Noise Spectral Density

For the optimum filter the noise power spectral density becomes

$$S_n(0) = \int_{-\infty}^{\infty} \frac{N_e\,(S_s(f) + N_r)}{(1 + \frac{N_r}{S_s(f)})^2}\,df \qquad (75)$$

Which simplified gives

$$S_n(0) = N_e \int_{-\infty}^{\infty} \frac{S_s(f)}{1 + \frac{N_r}{S_s(f)}}\,df \qquad (76)$$

In Equations (75) and (76) N_e and N_r are the reference channel and error channel noise power spectral densities as defined in (5) and (6).

d. Rms Angle Error

The rms angle error of the system is also a function of the frequency response of the optimum filter. From (33), (47), (49), (5), (6), and (73)

$$\sigma_\theta^2 = \frac{W_S\ k\ T_e}{K^2} \int_{-\infty}^{\infty} \frac{N_r + S_s(f)}{(1 + N_r/S_s(f))^2}\ df \qquad (77)$$

which can be simplified to

$$\sigma_\theta^2 = \frac{k\ T_e\ W_S}{\int_{-\infty}^{\infty} \frac{S_s^2(f)\ df}{S_s(f) + N_r}} \qquad (78)$$

4. Special Cases

The rms angle error is determined now for the special case where the filter frequency response is assumed to be real and unity. The total signal power is available at the filter output under the assumption that the filter with unity gain over the signal bandwidth is wide enough to let pass all the received signal power, denoted as P_s.

For $H(f) = 1$ it is

$$I = \int_{-\infty}^{\infty} |H(f)|^2 S_s(f)df = \int_{-\infty}^{\infty} H(f)S_s(f)df = P_s = K \qquad (79)$$

From (49), (63), (5) and (6) the rms angle error for this special case is calculated

$$\sigma_\theta^2 = \frac{k\ T_e\ W_S}{P_s^2} (k\ T_r\ W_n + P_s)$$

$$= \frac{k\ T_e\ W_S}{P_s} \left(1 + \frac{k\ T_r\ W_n}{P_s}\right) \qquad (80)$$

For an overshooting zero tracking servo system in response to a unit step input, the time τ (defined as response time) to the first crossing of unit output is related to the low-pass single-sided noise bandwidth W_S by

$$\tau W_S = Q \tag{81}$$

where Q is a function of the system's damping ratio ξ[3]. The rms angle error becomes

$$\sigma_\theta^2 = \frac{k T_e Q}{P_s \tau} F_D \tag{82}$$

where F_D is the degradation factor of the reference channel and is defined as

$$F_D = 1 + \frac{k T_r W_n}{P_s} \tag{83}$$

As a special case of the servo system let it have the response of a first order low-pass filter, so from (36)

$$F(f) = \frac{1}{1 + \frac{1}{P_s \, a/j2\pi f}} \tag{84}$$

Integrating this in the limit from 0 to ∞ the low-pass single-sided bandwidth is found as

$$W_S = \frac{a P_s}{4} \tag{85}$$

Defining the system response time τ as

$$\tau = 1/a\ P_s \tag{86}$$

then the rms noise angle error due to the system noise for this very special case is simply

$$\sigma_\theta^2 = \frac{k\ T_e}{4\ P_s\ \tau}\ F_D \tag{87}$$

By increasing the system response time the rms angle error can be decreased.

C. PERFORMANCE OF COHERENT POLARIMETER

For comparison, the rms angle error of the coherent polarimeter calculated by Ohlson [4]

$$\sigma_\theta^2 = \frac{k\ T_e\ W_S}{P_s} \left\{ \frac{I_o\left(\frac{2\ P_s}{k\ T_r\ W_n}\right)}{I_1\left(\frac{2\ P_s}{k\ T_r\ W_n}\right)} \right\}^2 \tag{88}$$

$$= \frac{k\ T_e}{4\ P_s\ \tau}\ F_D \tag{87}$$

In (87) and (88) we also assumed a first order loop with a single-sided system noise bandwidth of

$$W_S = \int_0^\infty \frac{1}{1 + \omega^2\tau^2}\ \frac{d\omega}{2\pi} = \frac{1}{4\tau} \tag{89}$$

In the final equations for both polarimeters, (87) and (88)

k = Boltzmann's constant

T_e = error channel operating temperature

T_r = reference channel operating temperature

τ = time constant of servo system

W_n = IF bandwidth for correlation polarimeter

= loop bandwidth of coherent polarimeter at RF (i.e. twice lowpass noise bandwidth)

P_s = signal power

I_o & I_1 = Bessel functions of imaginary arguments

F_D = reference channel degradation factor

In Fig. 10 both degradation factors are plotted versus the SNR of the reference channel.

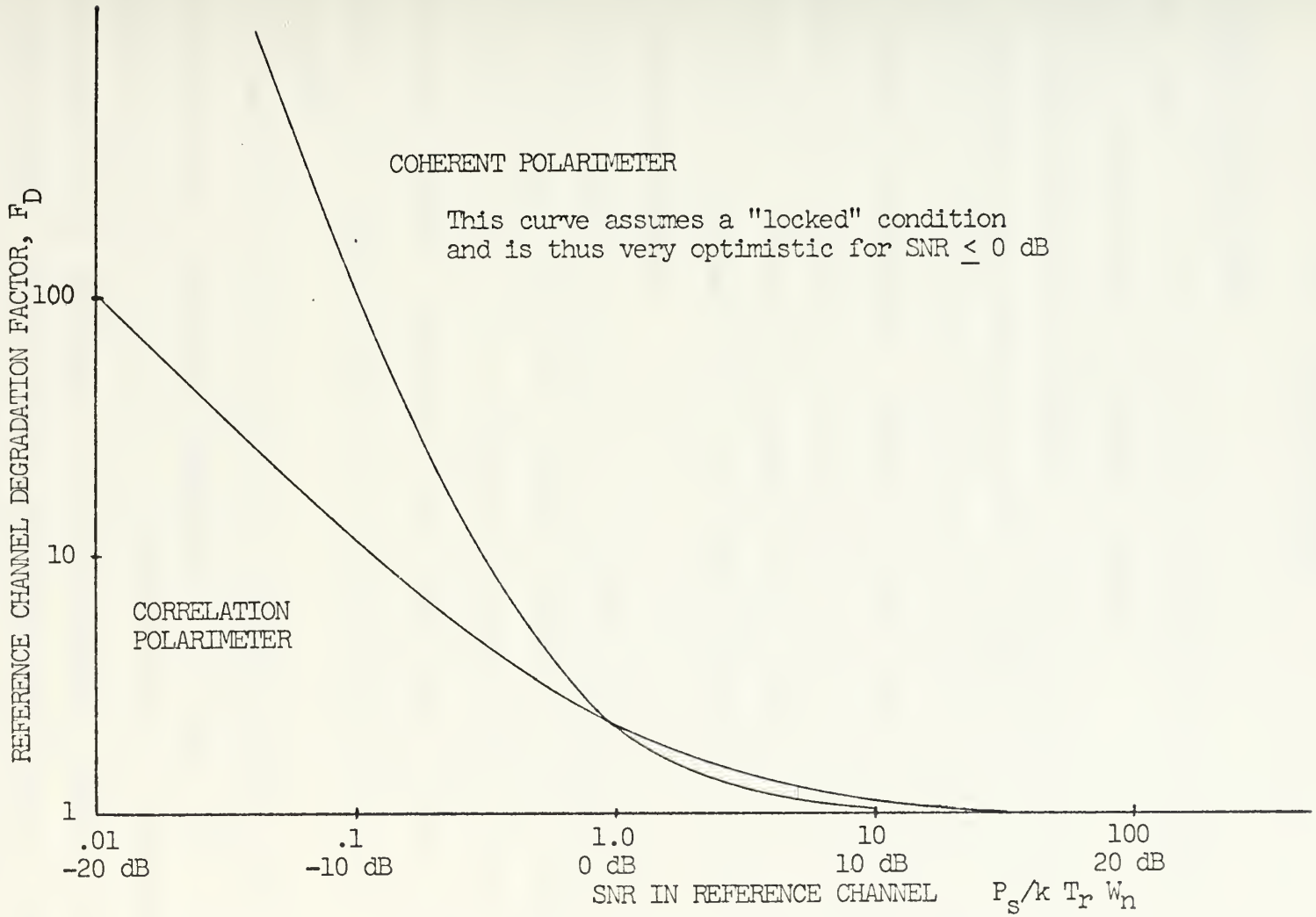

Figure 10. REFERENCE CHANNEL DEGRADATION FACTOR VERSUS SNR IN REFERENCE CHANNEL

IV. WORKING MODEL

A. SYSTEM DESCRIPTION

The theory of the correlation polarimeter has successfully been proved with the working model.

The simplified block diagram of this is shown in Fig. 11; the actual test-set-up is shown in Fig. 12-17. The working model represents an equivalent of the inner loop of the practical polarimeter. This loop has been used in the analysis of the correlation polarimeter and its performance [Section III]. The derived equations and results are therefore valid for the model too. The PLO, AGC loop, and the AFC loop were omitted.

A known signal (sine-wave) of 470 MHz was transmitted from a $\lambda/2$-dipole. With two crossed dipoles of $\lambda/2$, turned by a DC-servo-system, the transmitted signal was received and the polarization angle of it was measured by means of a digital shaft angle encoder and a potentiometer on the motor shaft.

The received reference and error channel signals were mixed down to the operation frequency of 110 KHz. This frequency was picked since most components for the working model were already available in this frequency range. With the phase shifter in the local oscillator input line to the mixer in the error channel phase differences between both channels have been balanced out, so that both multiplier inputs had equal phase. A trombone-line served as phase shifter.

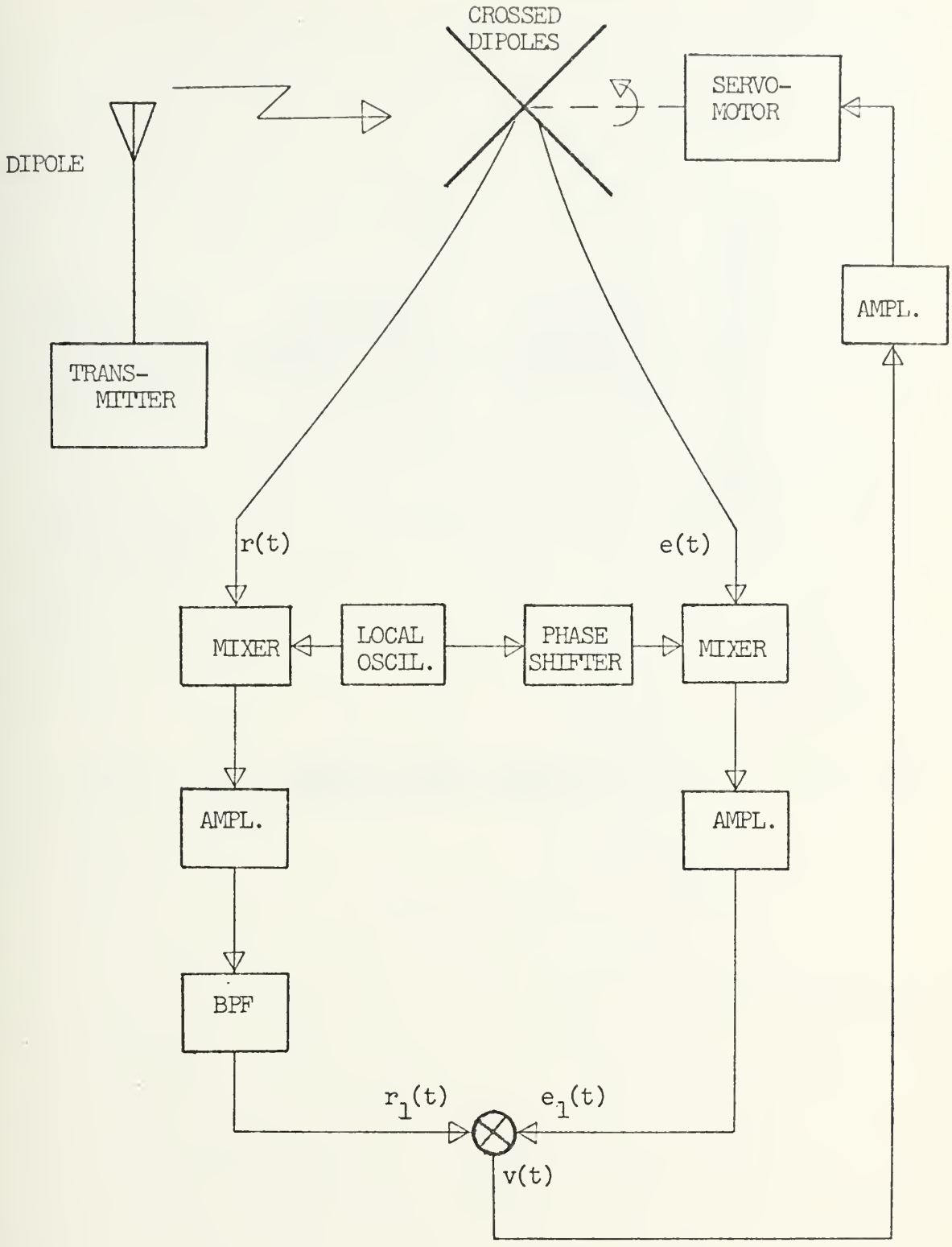

Figure 11. SIMPLIFIED WORKING MODEL

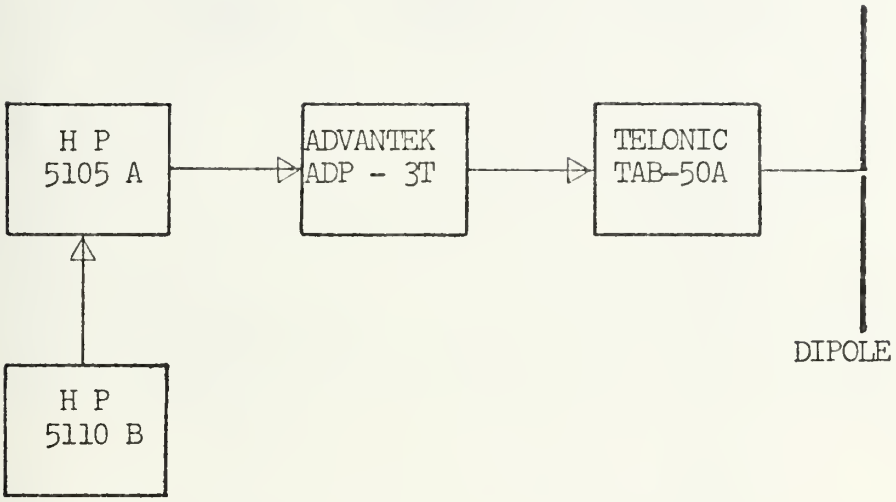

Figure 12. WORKING MODEL, TEST-SET-UP OF TRANSMITTING PORTION

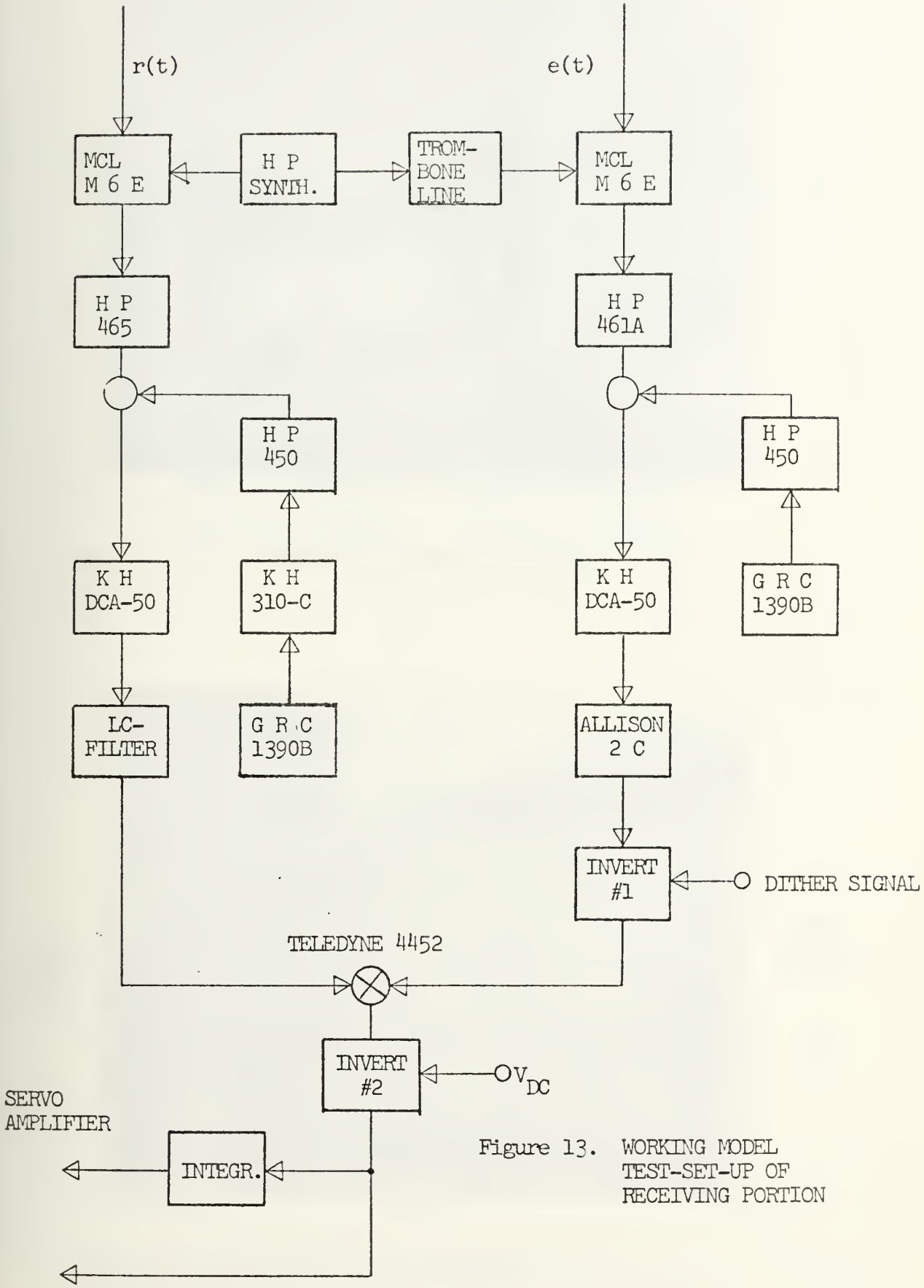

Figure 13. WORKING MODEL TEST-SET-UP OF RECEIVING PORTION

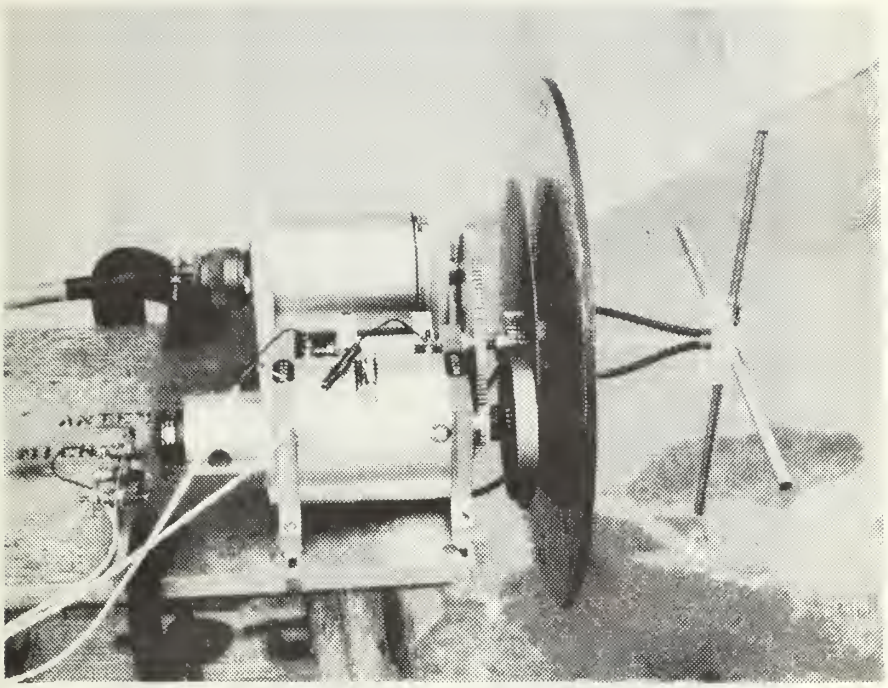

Figure 14. RECEIVING CROSSED DIPOLES

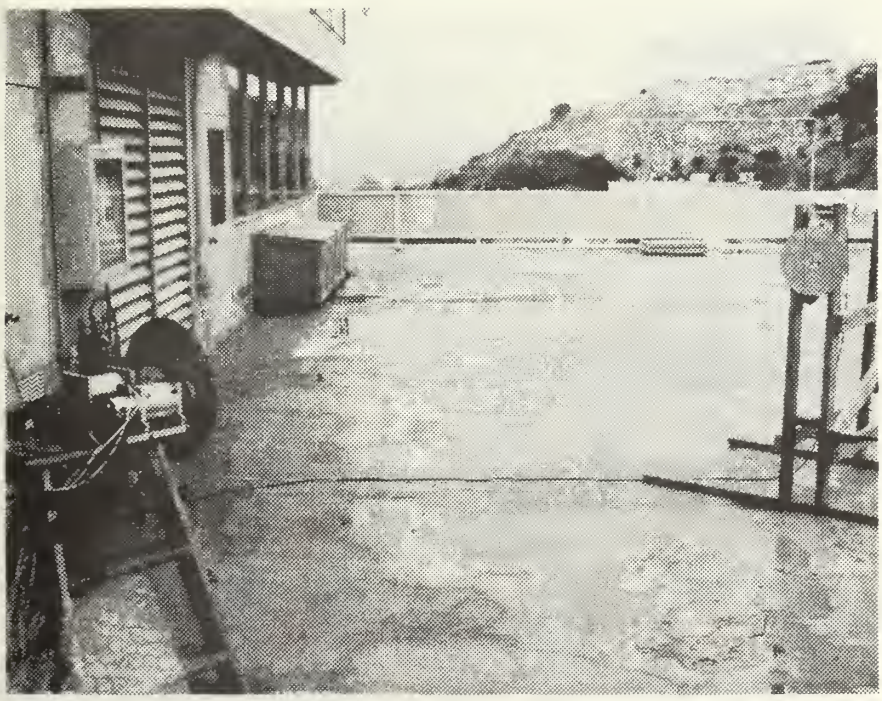

Figure 15. TEST-SET-UP, ANTENNAS

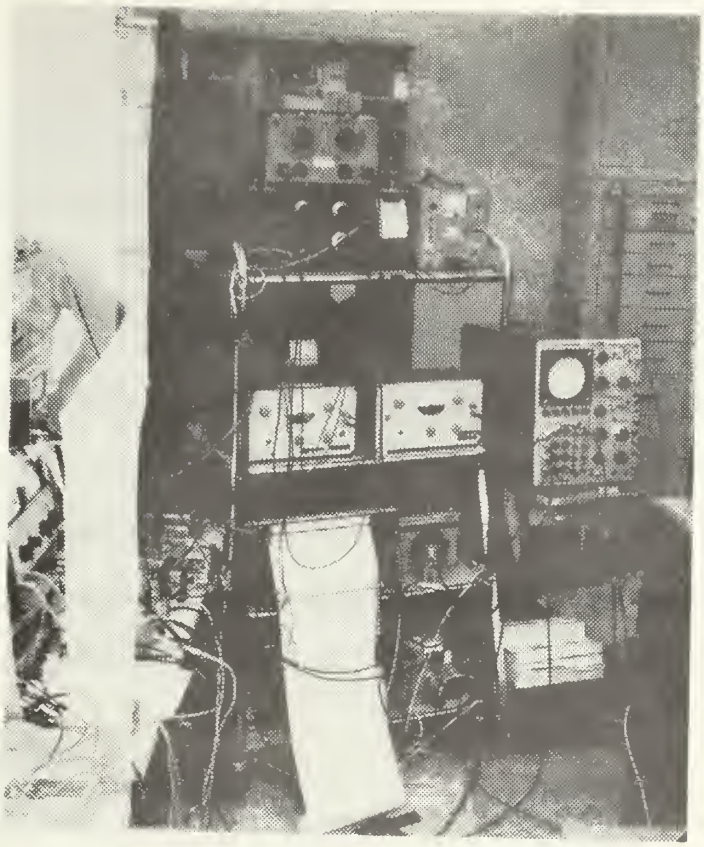

Figure 16.
TEST-SET-UP #1

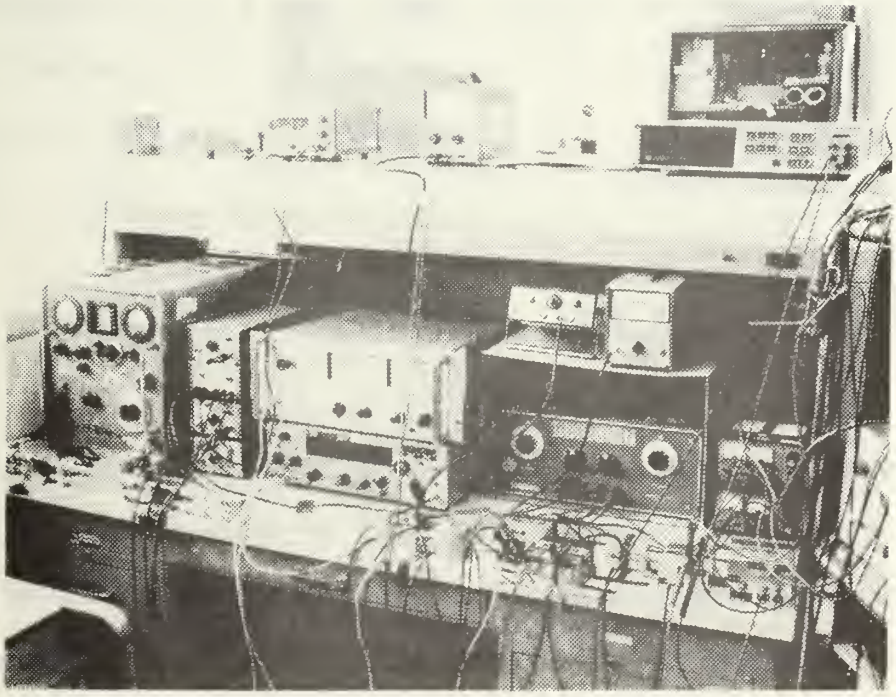

Figure 17. TEST-SET-UP #2

In interconnecting the system components the proper impedance matching was taken into account.

The effects of noise in both channels on the polarization angle error were investigated by having a noise generator connected in each channel. To determine the noise spectral density in the system the rms noise voltages behind the BPF's were measured, with no signal present. Because the frequency response curves of these filters were known, the noise spectral densities could be calculated.

B. TEST SERIES

1. Testing the Components of the Model

a. Dipoles

The dipoles were built from aluminum tubing with a diameter of 0.8 cm. Their length required to resonate at the frequency of 470 MHz and to provide a radiation resistance of 50Ω was determined by the following approximation [8].

$$\text{Physical length (cm)} = \frac{5905 \times 2.54 \times K}{f\ (\text{MHz})} \qquad (90)$$

where K is the factor by which a free-space half wavelength must be multiplied to find the resonant length as a function of the ratio of free-space half wavelength to conductor diameter, known as the "length/diameter ratio." K was taken from Fig. 18 for the particular length/diameter ratio.

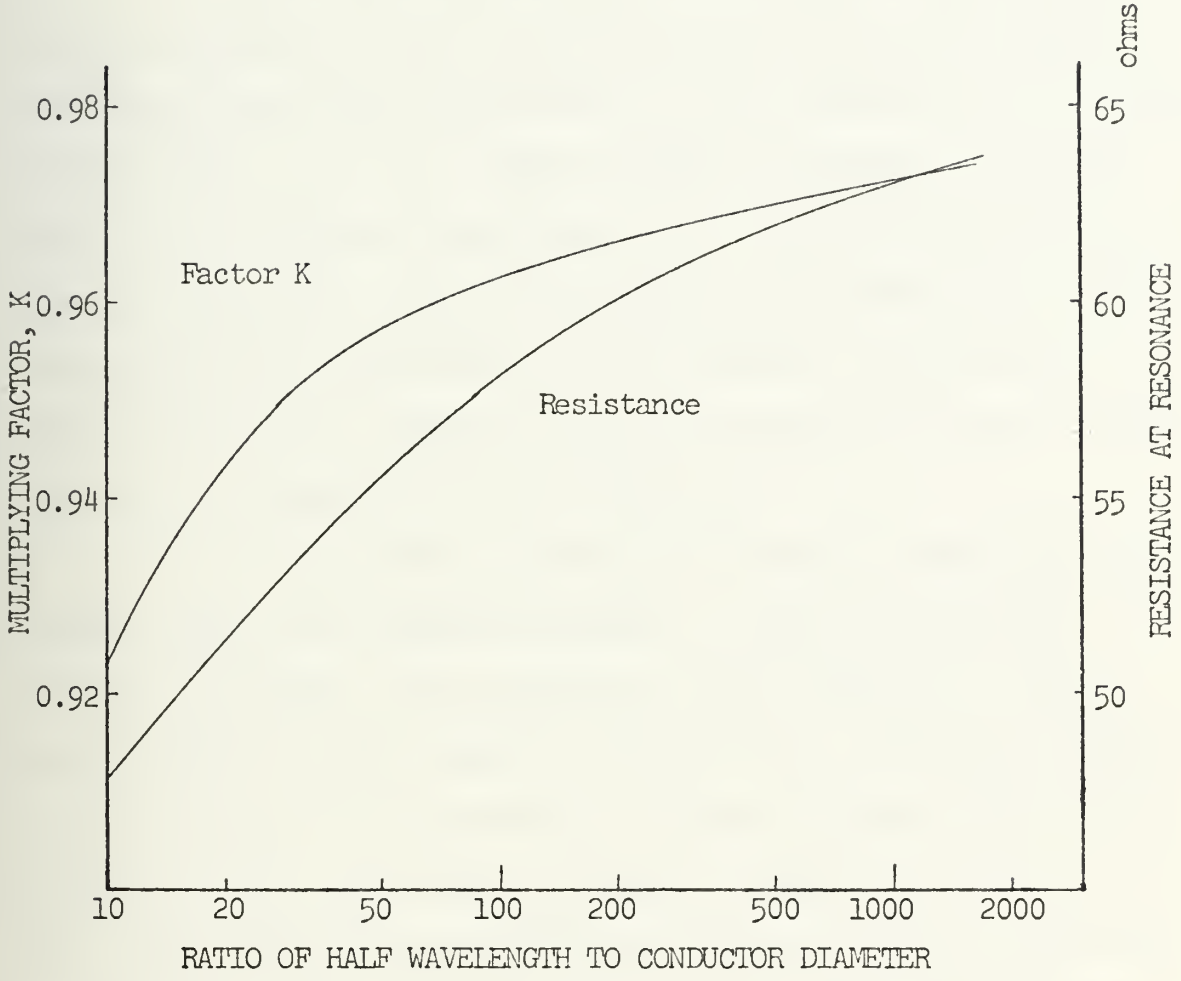

Figure 18. FACTOR K AND RADIATION RESISTANCE OF A HALF-WAVE ANTENNA VERSUS LENGTH/DIAMETER RATIO, [8].

The physical lengths of the dipoles used in the working model were 14.6 cm.

Behind the single transmitter dipole and the crossed dipoles of the receiving portion circular plastic shields covered with aluminum foil were mounted in a distance of $\lambda/4$ (Fig. 14, 15). They provided the same reflecting area for all dipole positions, i.e. scattering from the system components behind the dipoles was prevented. On the other hand the performance of the dipoles was increased because the wave reflected by the aluminum foil was in phase with the transmitted or received one.

A 470 MHz sine-wave of constant amplitude transmitted from the transmitting part of the working model (signal generator, RF amplifier, and a single $\lambda/2$ dipole) was received by the crossed dipole pair. Frequency changes to both sides of the nominal 470 MHz frequency resulted, as expected, in a decrease of received signal amplitude and at the same time the maximum values received by the reference and by the error channel dipole (when these dipoles were aligned with the transmitting dipole) were no longer equal.

For various angles of the crossed dipoles with respect to the transmitting dipole the received amplitudes in both were measured by means of a vector voltmeter. (Transmitted signal had frequency of 470 MHz and constant amplitude.)

The amplitudes changed with the cosine of the angle, and both channels had the required angle difference

of 90°. The signal amplitudes are plotted versus angle in Fig. 19.

b. Multiplier

The multiplier was tested using set-up as shown in Fig. 20. Of interest was the linearity of the multiplier operation for different signal levels, especially with one input approaching zero value. On the other hand it was important to see that the multiplier output was the expected function of the amplitudes of both inputs and the phase difference between them.

The multiplier output DC-voltage as function of the amplitudes of the input signals is plotted in Fig. 21 and 22. For strong input signals the multiplier functioned perfectly linear. With decreasing signal strength the multiplication was slightly incorrect, the output voltage curve shows a change in slope. Fig. 23 shows the DC-output voltage of the multiplier versus the phase difference between the input signals. It varies with the cosine of the phase difference. Here the multiplier output is offset by about 80 mvolts because inverter #2 was not used in this test for zeroing.

c. Amplifiers

The two amplifiers used in either channel provided the necessary signal levels at the multiplier inputs. In the second amplifiers in both channels the input noise got an additional amplification. However, with signal and noise present these amplifiers saturated very easily.

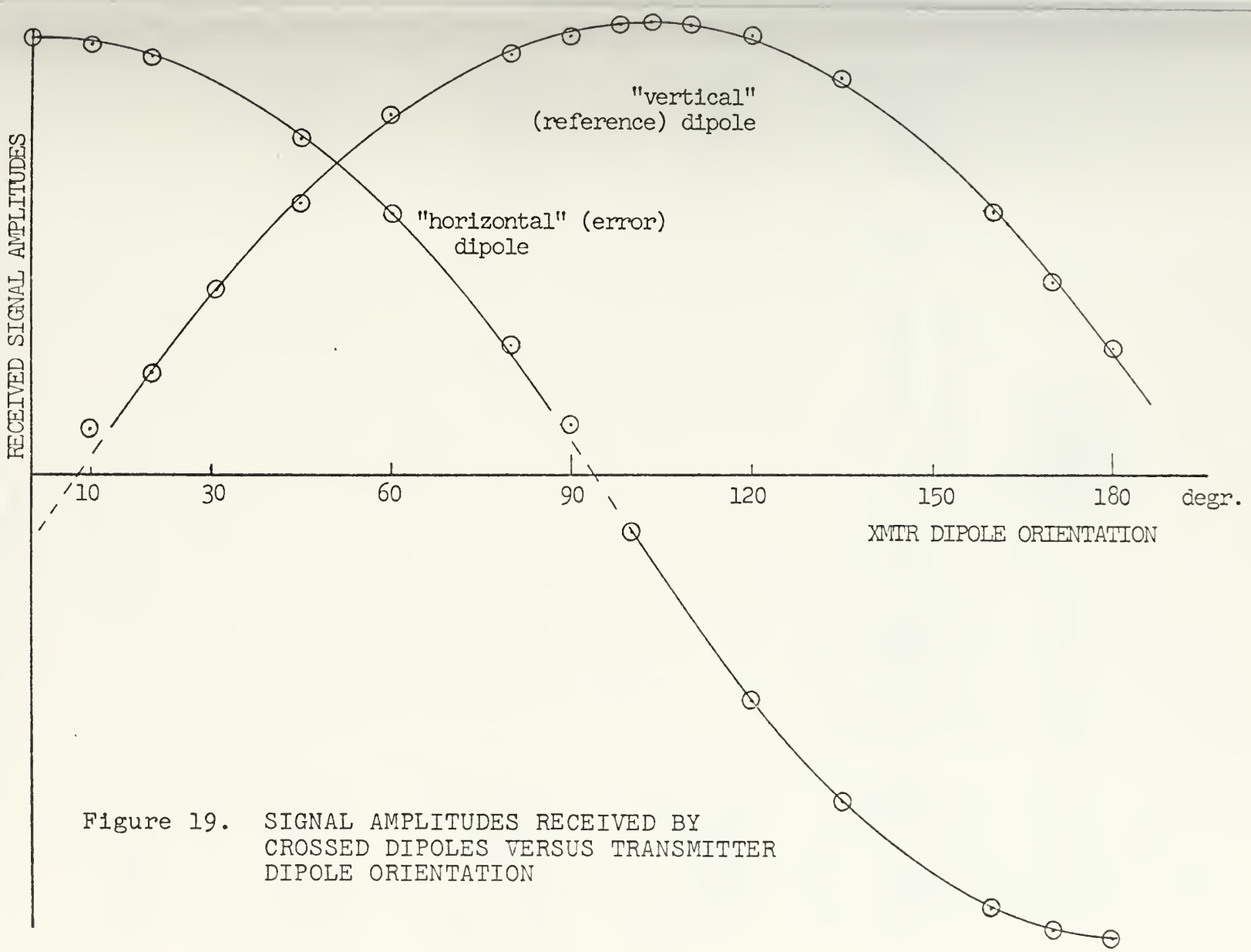

Figure 19. SIGNAL AMPLITUDES RECEIVED BY CROSSED DIPOLES VERSUS TRANSMITTER DIPOLE ORIENTATION

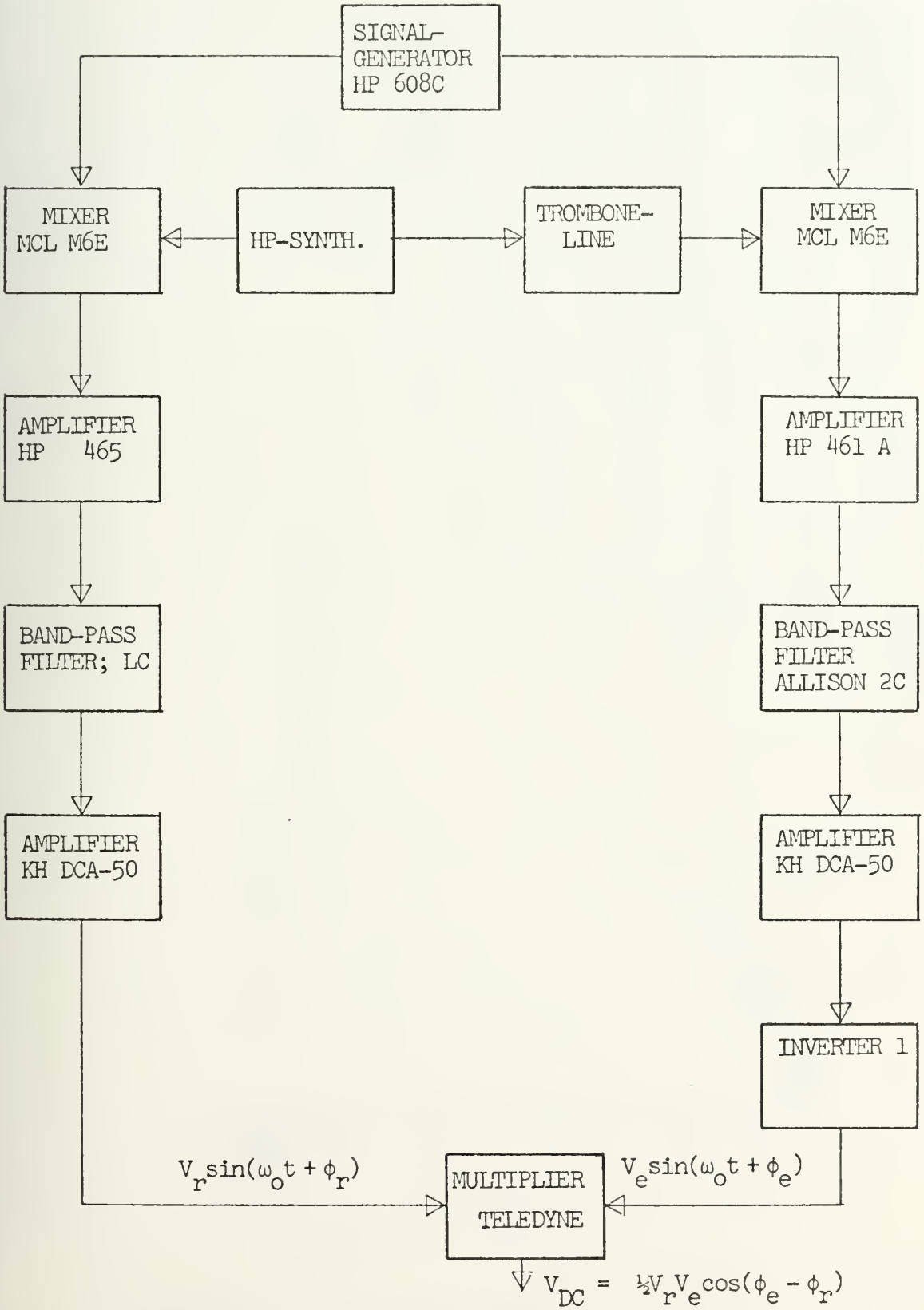

Figure 20. MULTIPLIER TEST SET-UP

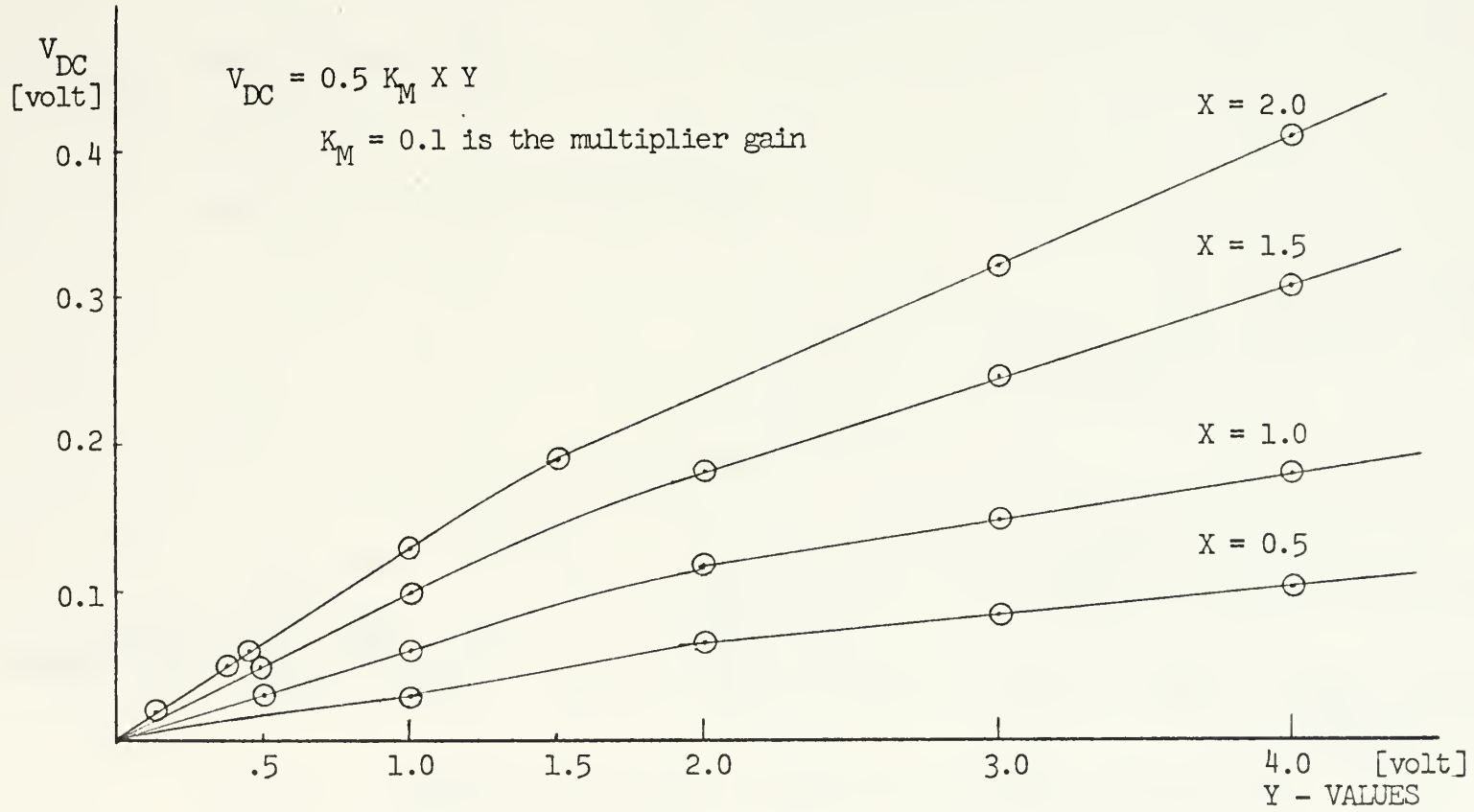

Figure 21. MULTIPLIER OUTPUT VOLTAGE FOR VARIOUS AMPLITUDES OF INPUT SIGNALS

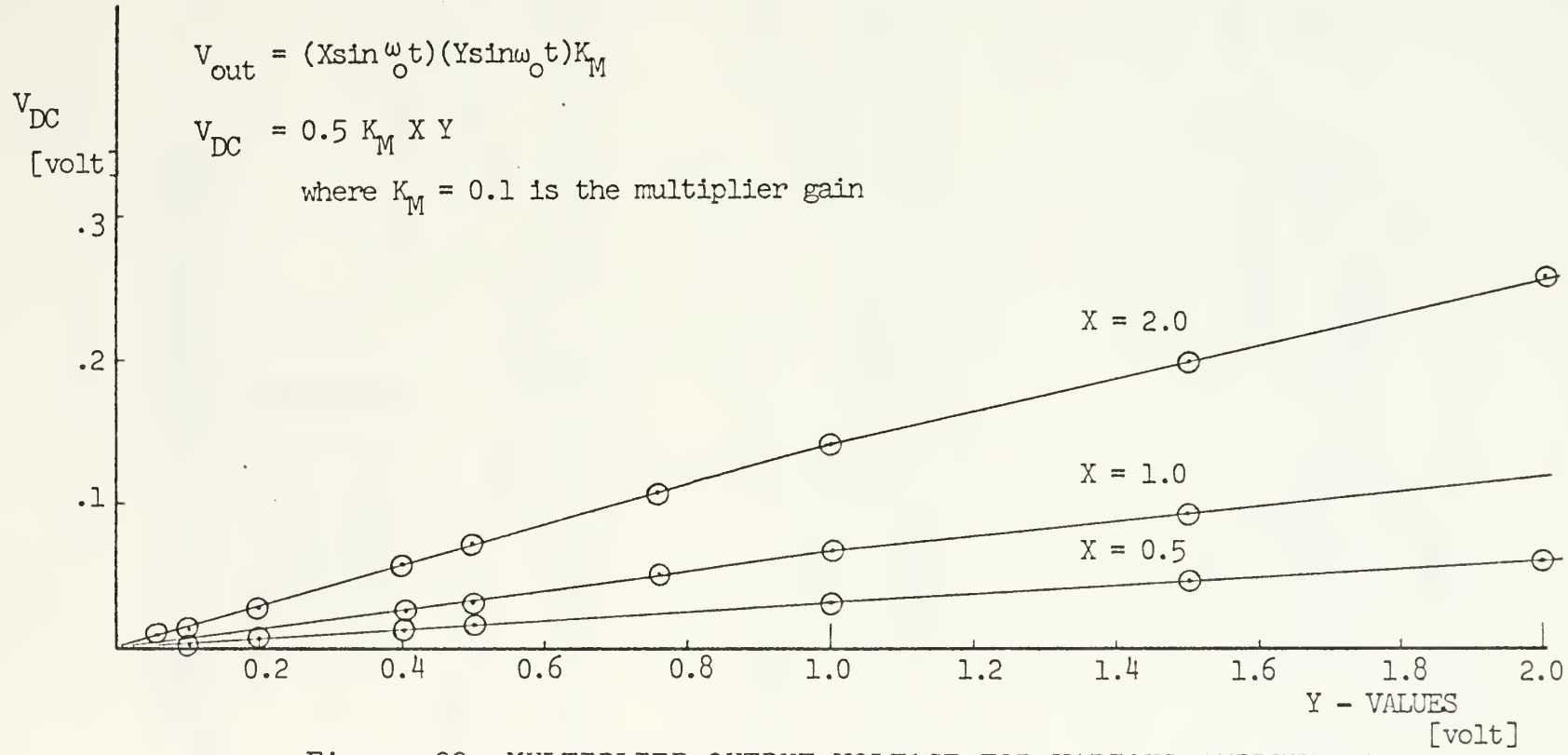

Figure 22 MULTIPLIER OUTPUT VOLTAGE FOR VARIOUS AMPLITUDES OF INPUT SIGNALS

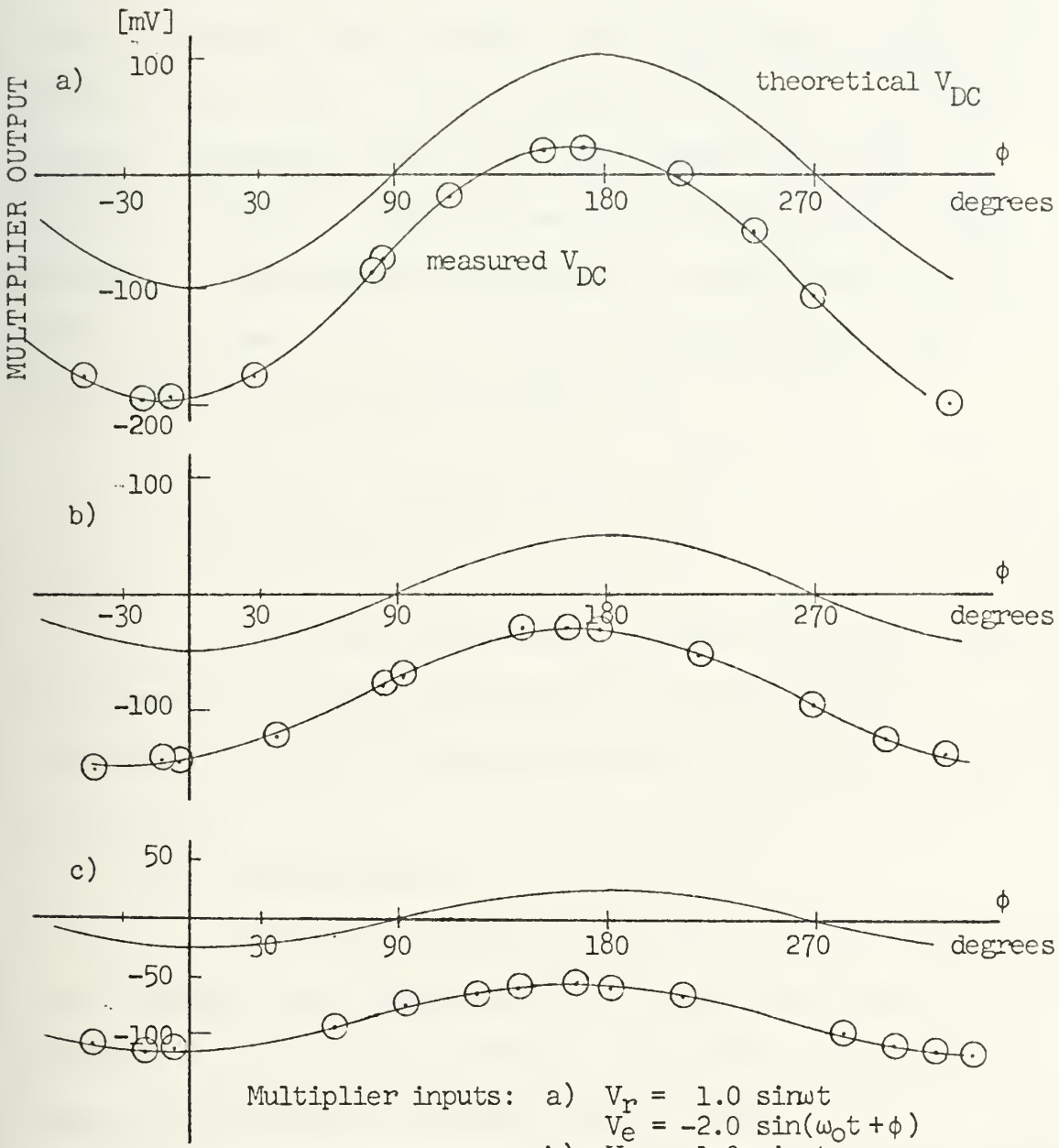

Multiplier inputs: a) $V_r = 1.0 \sin\omega t$
$V_e = -2.0 \sin(\omega_o t + \phi)$
b) $V_r = 1.0 \sin\omega t$
$V_e = -1.0 \sin(\omega_o t + \phi)$
c) $V_r = 1.0 \sin\omega t$
$V_e = -0.5 \sin(\omega_o t + \phi)$

Figure 23. MULTIPLIER OUTPUT VOLTAGE (DC) VERSUS PHASE DIFFERENCE OF INPUT SIGNALS

d. Filters

For both band-pass filters the frequency response curves, $|H(f)|$ and $|H(f)|^2$ and arg $H(f)$, were determined. They are shown in Fig. 24-29. The area under the $|H(f)|^2$ - curve is the value of the integral $\int_0^\infty |H(f)|^2 \cdot df$ which is needed to determine the noise power spectral density in front of the filter from the measured rms noise voltage behind it. Becuase the frequency response curves of the BPF's are known, the noise spectral densities in front of either filter can be calculated from

$$\sigma_n^2 = N_o \int_{-\infty}^{\infty} |H(f)|^2 \, df \qquad (91)$$

Over the narrow band of the BPF's the noise can be assumed to be white with the double-sided spectral density N_o. σ_n is the measured rms noise voltage behind the filters.

e. Servo-System

The servo-system used in the working model is the standard servo amplifier and DC-amplifier experiment package of the school's control laboratory. For block diagram and transfer function see Fig. 31.

The DC-amplifier did not give enough amplification to turn the motor with a very weak DC-input voltage. So small angles between the reference dipole and the polarization plane of the transmitted signal, for which the multiplier output and thus the servo input are close to zero

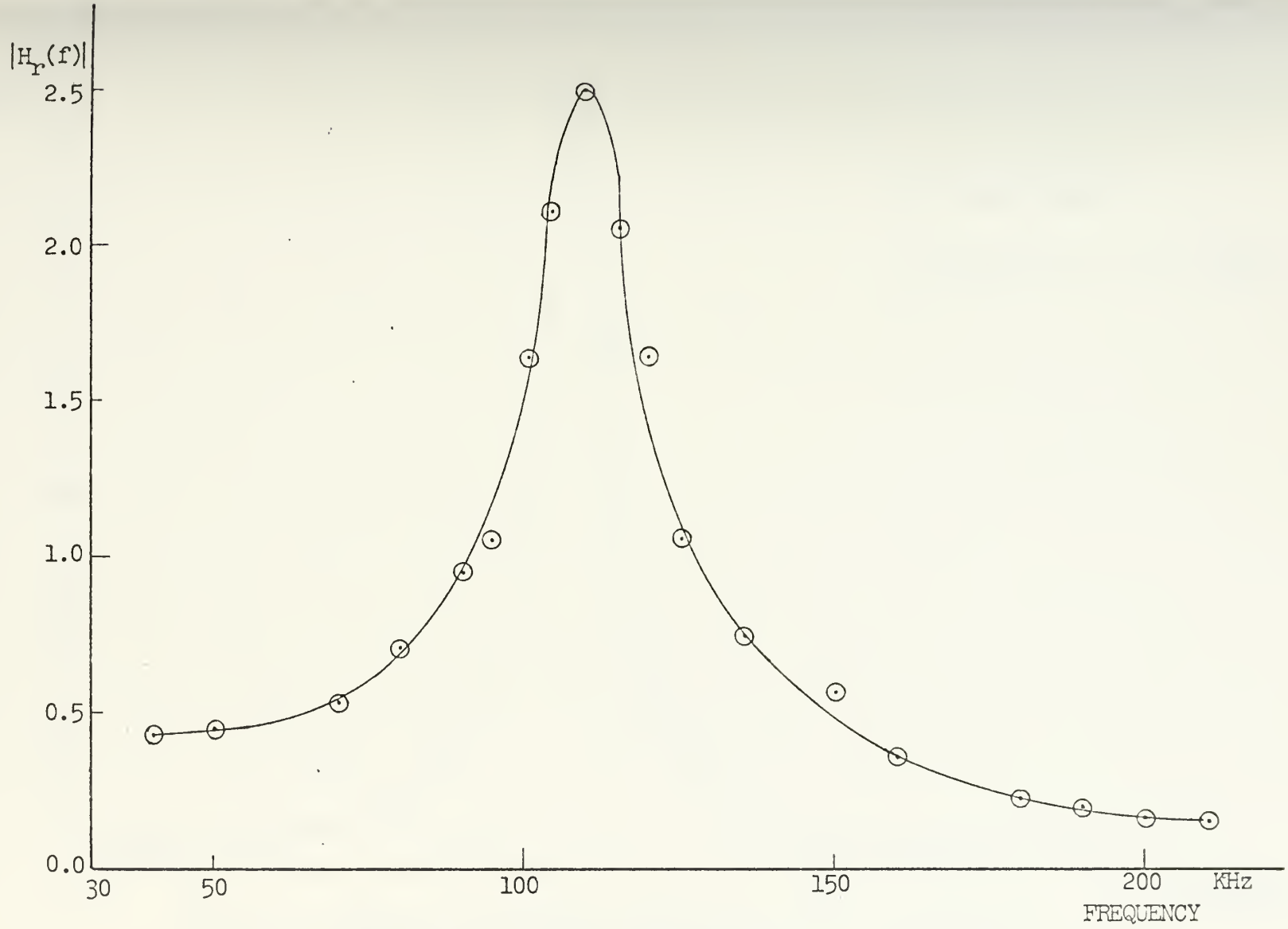

Figure 24 FREQUENCY RESPONSE (MAGNITUDE) OF REFERENCE CHANNEL BAND-PASS FILTER

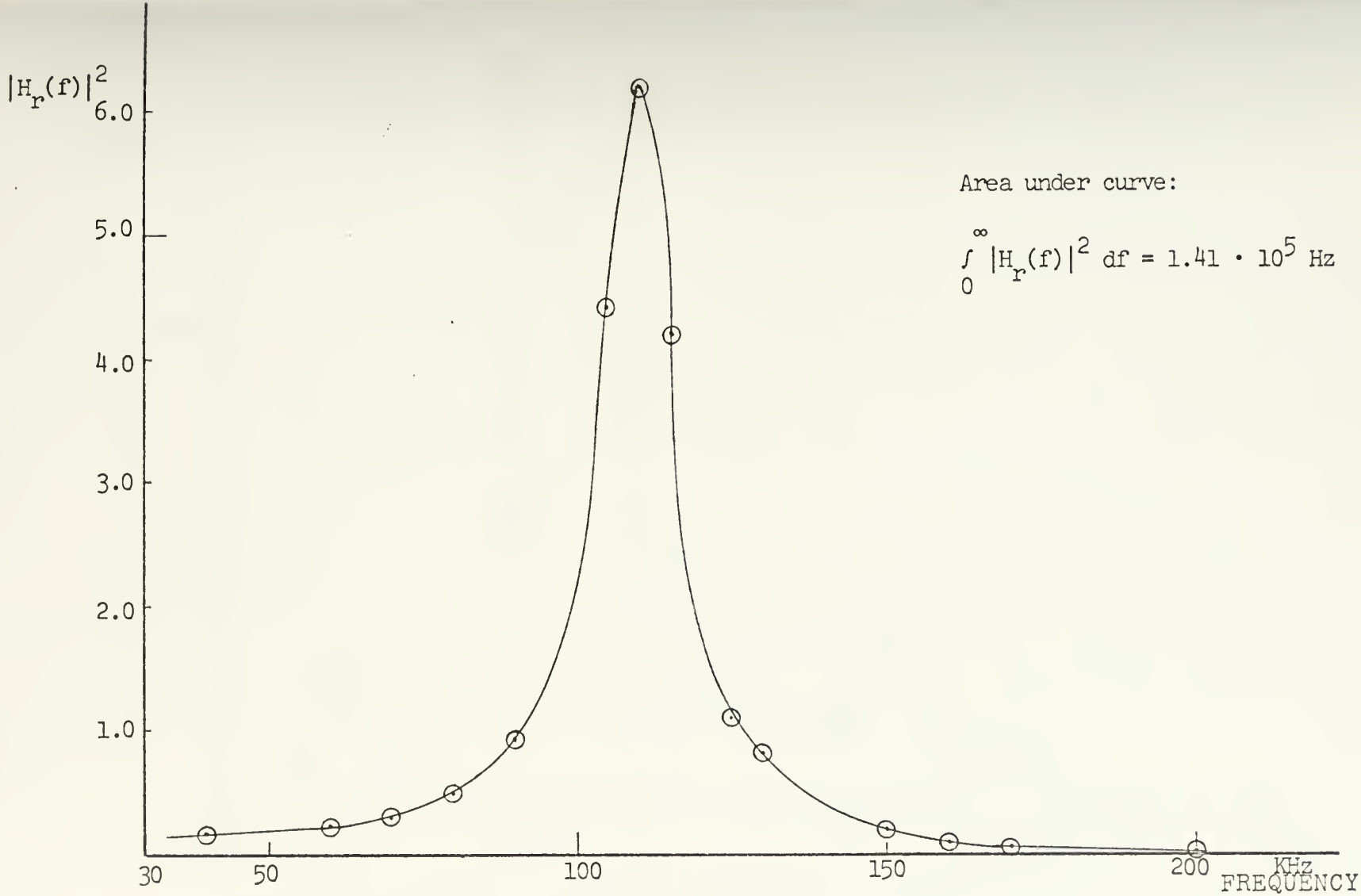

Figure 25 SQUARED MAGNITUDE RESPONSE OF BPF IN REFERENCE CHANNEL

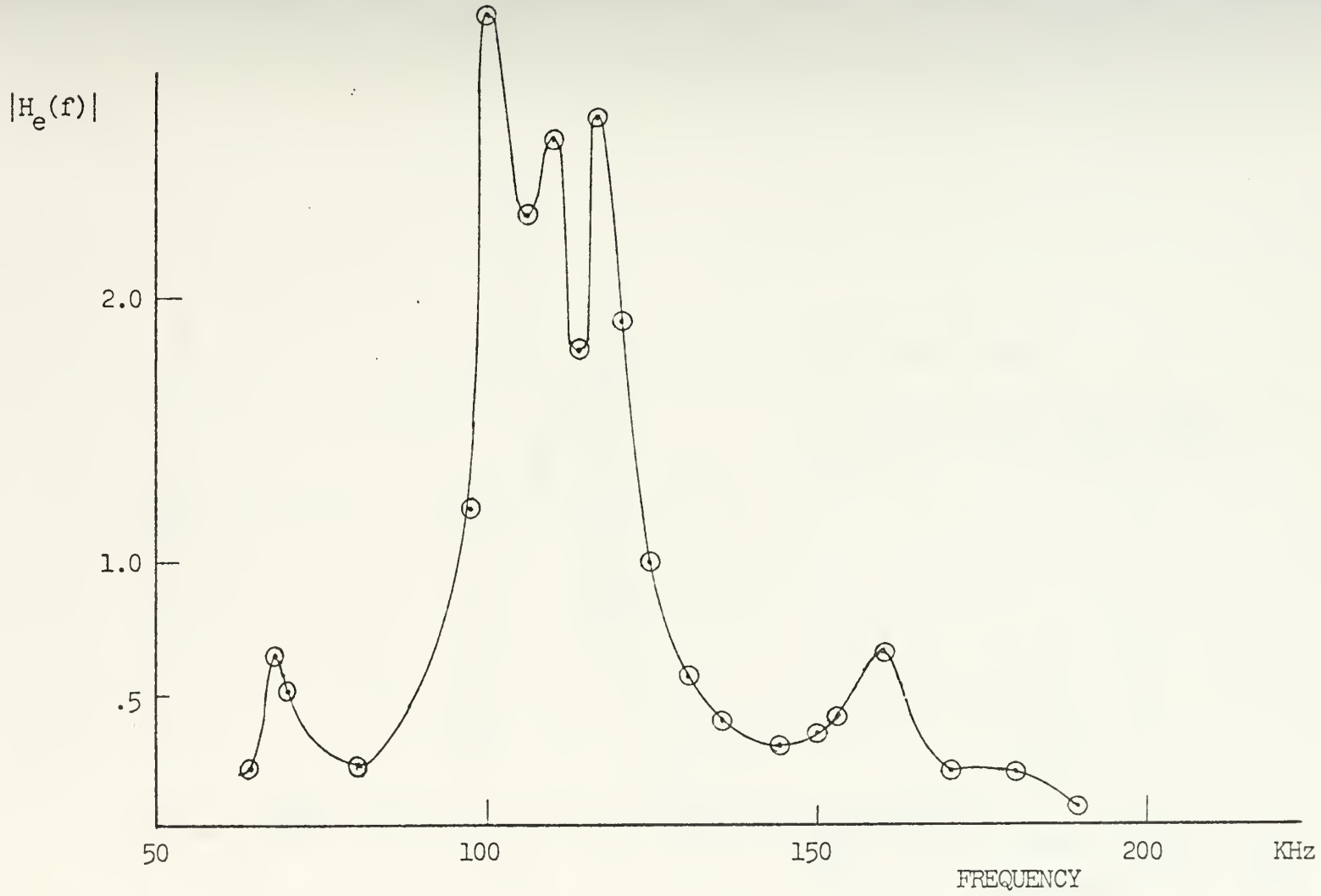

Figure 26 FREQUENCY RESPONSE (MAGNITUDE) OF ERROR CHANNEL BAND-PASS FILTER

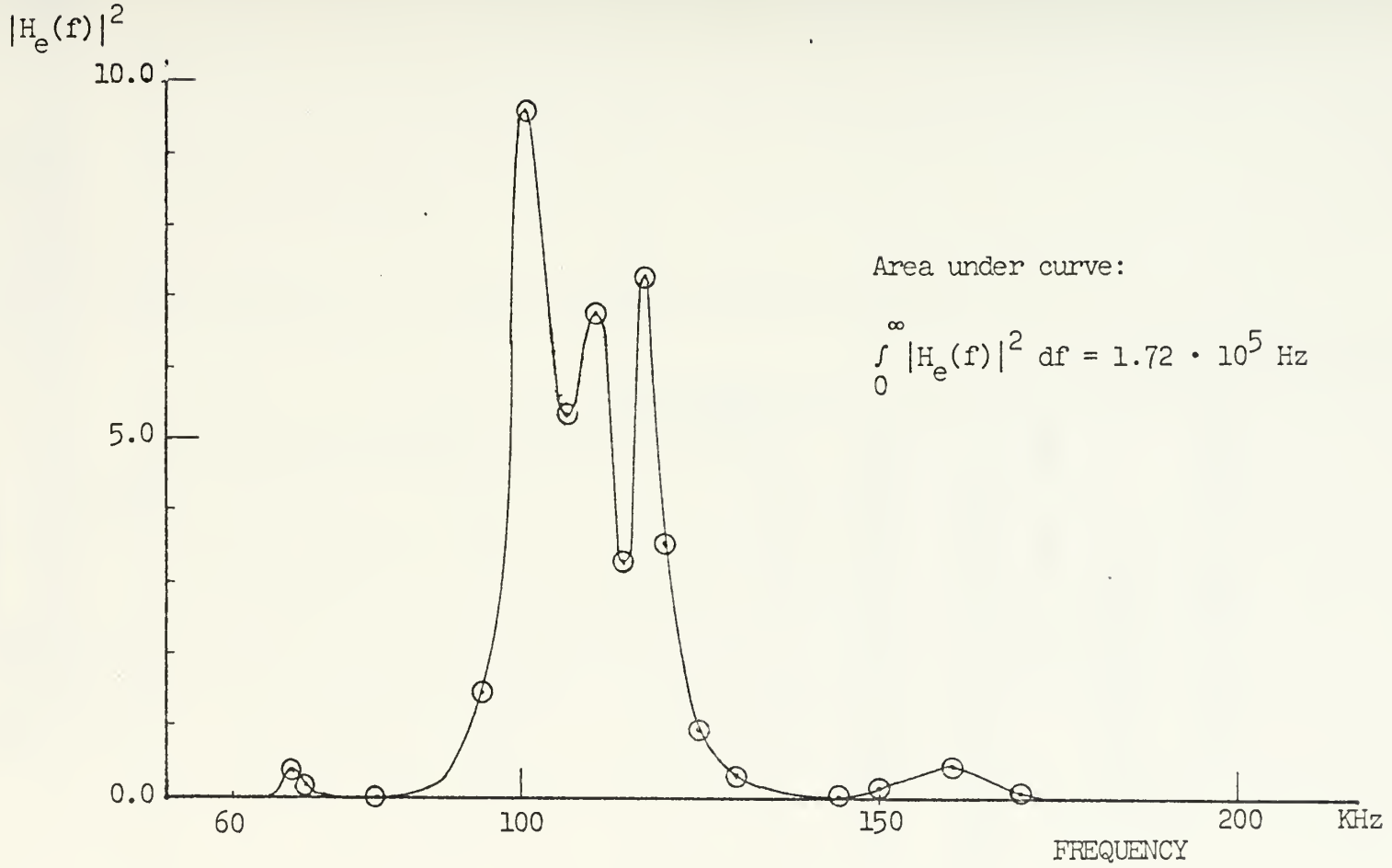

Figure 27 SQUARED MAGNITUDE RESPONSE OF BPF IN ERROR CHANNEL

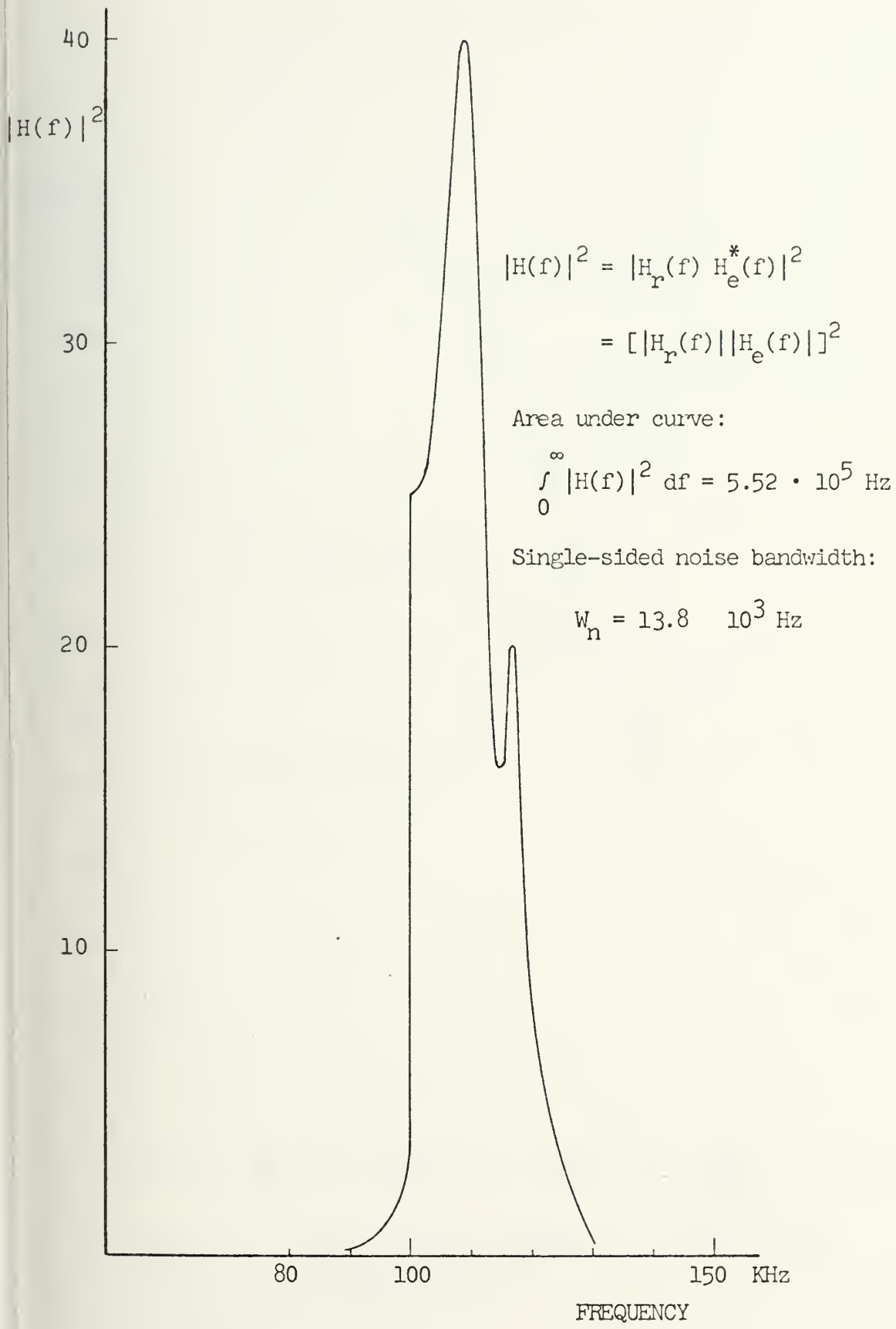

Figure 28 FREQUENCY RESPONSE (MAGNITUDE) OF THE PRODUCT $H_r(f)H_e^*(f)$

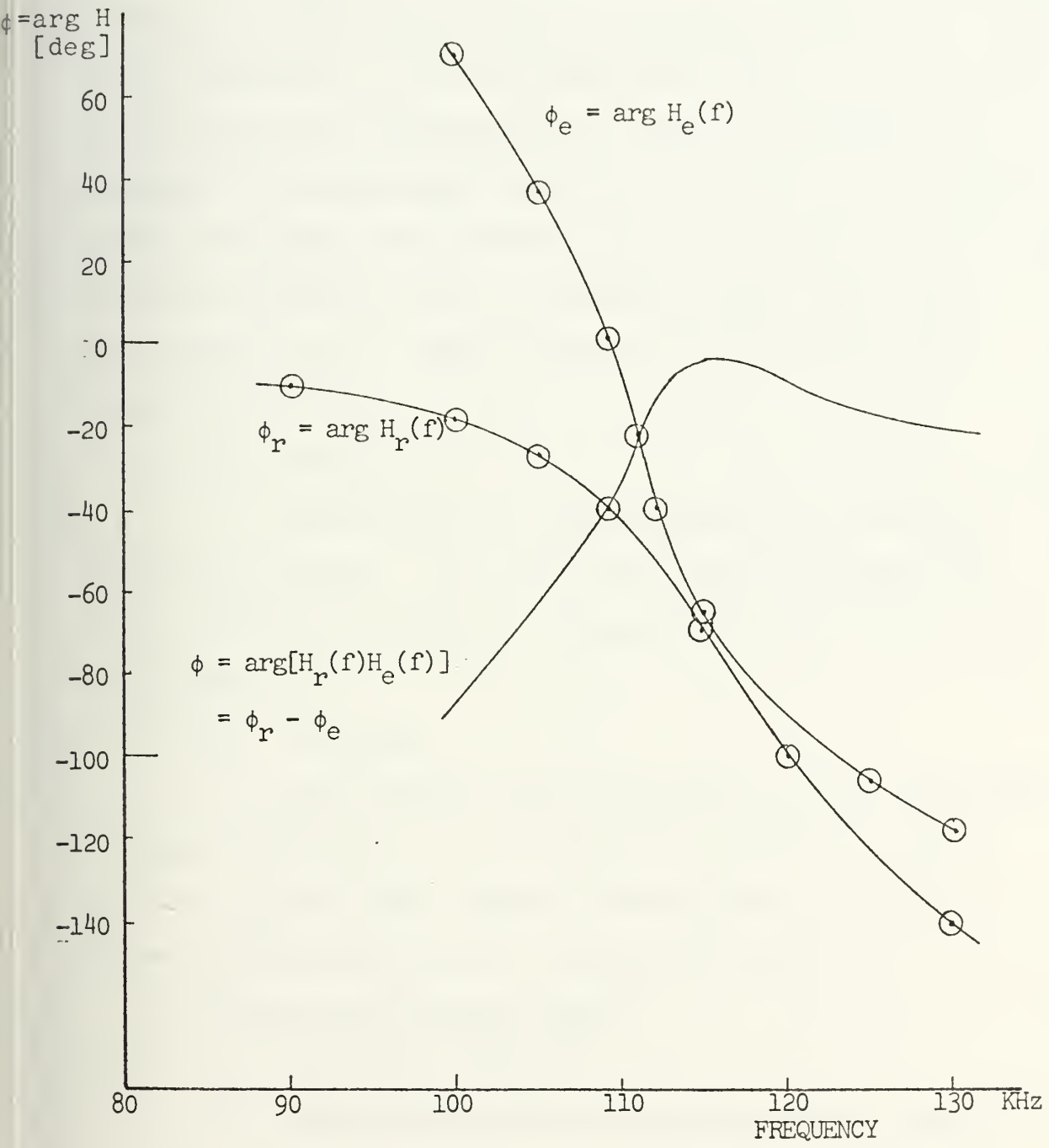

Figure 29 PHASE RESPONSE CURVES OF FILTERS AND OF THEIR PRODUCT

volts, could not have been corrected. In order to overcome this difficulty caused by the friction in the bearings of the motor and to get an overshooting system the DC-input voltage to the servo system was (1) applied directly to the input terminals of the servo-amplifier and (2) integrated and fed into the preamplifier of the servo-amplifier (a diagram of this amplifier is given in Fig. 30). With this scheme the servo motor turned, even with very low DC-voltage available, as soon as the integrator output had reached a high enough level. Modification of the servo system is shown in Fig. 32.

f. Integrator

The integrator could integrate positive and negative voltages. Its input level could be changed by means of an potentiometer. The maximum output voltage was ± 10 volts.

g. Inverters

The inverters were developed to give the proper voltage directions and to provide the abilities to feed into the system extra signals for adjustments like the offset cancellation in the multiplier output.

2. Testing the Working Model

a. Open Loop Operation

The working model was assembled and tested in an open loop configuration. That means the multiplier output was not connected to the integrator and the servo-amplifier.

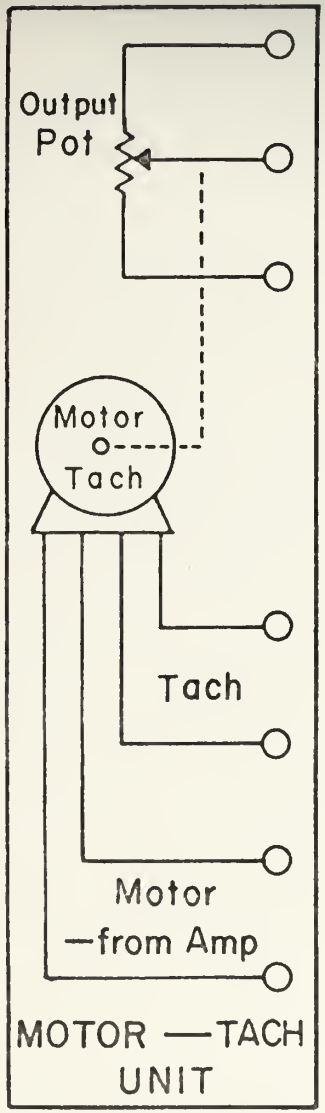

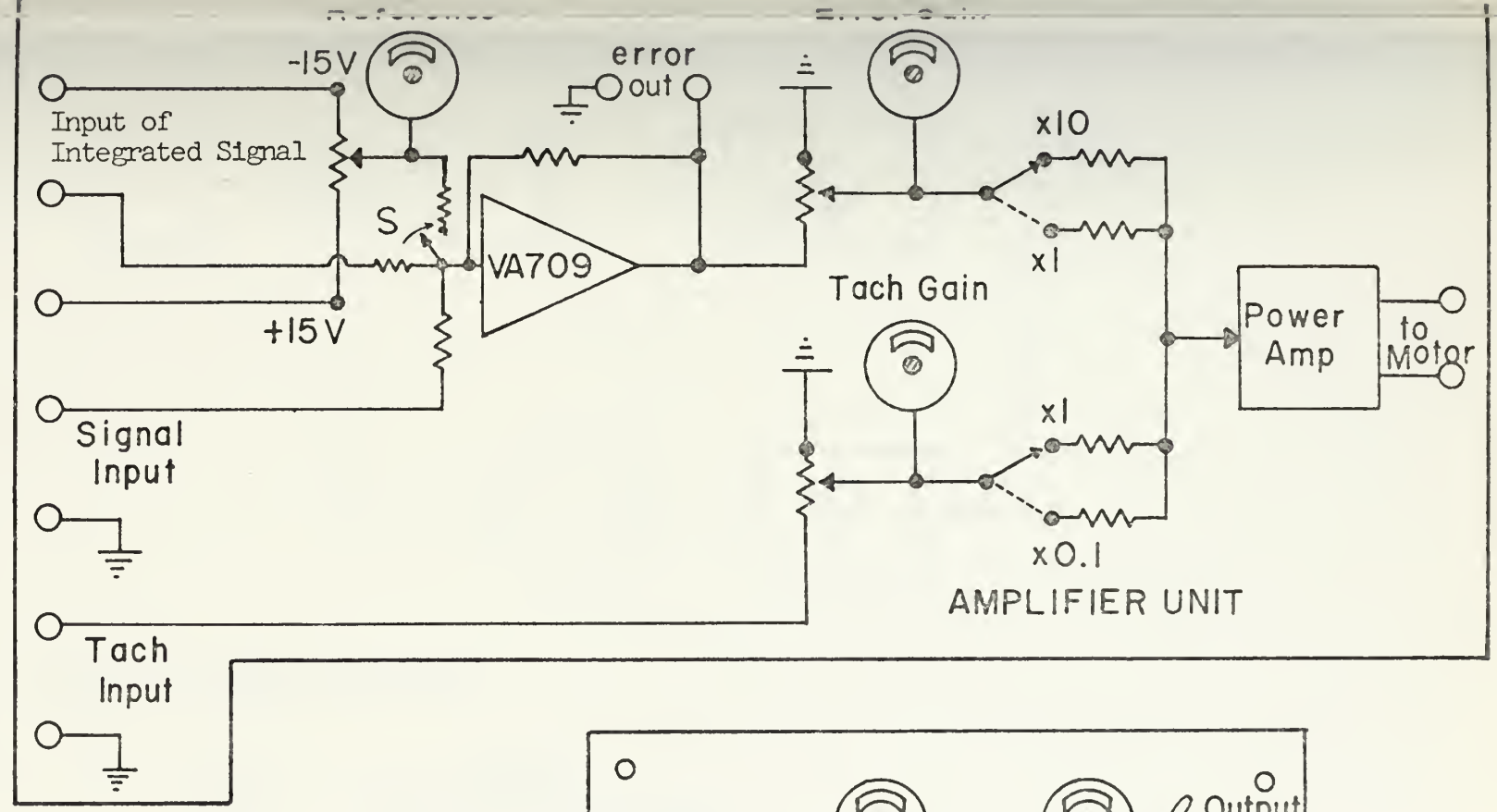

POWER
120 VAC
28 VDC

Switch S was open

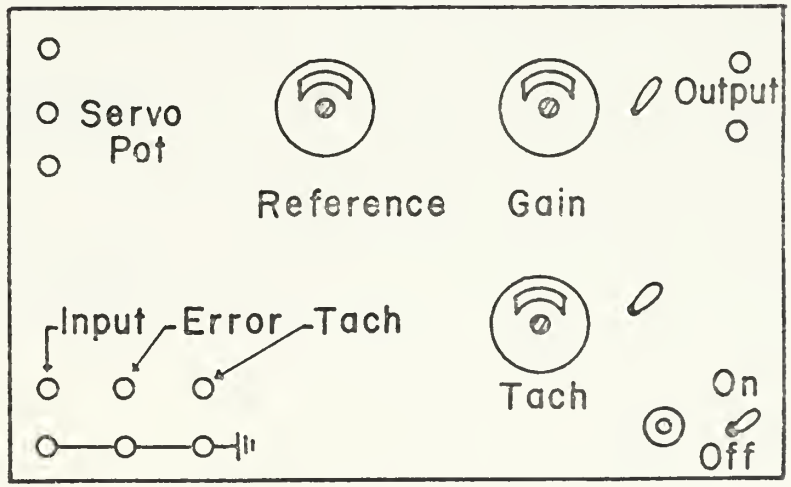

FRONT PANEL

BULLARD HALL DC SERVO

FIGURE 30

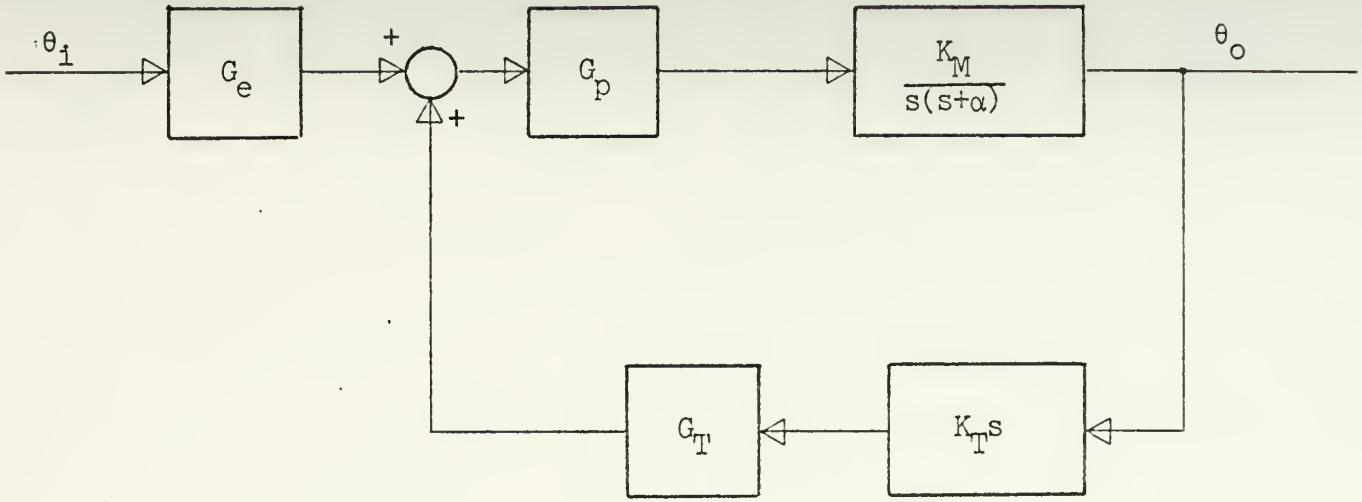

System Transfer Function:

$$\frac{\theta_o(s)}{\theta_i(s)} = \frac{G_p K_M G_e}{s^2 + s(\alpha - G_T G_p K_T K_M)}$$

Figure 31 SERVO SYSTEM

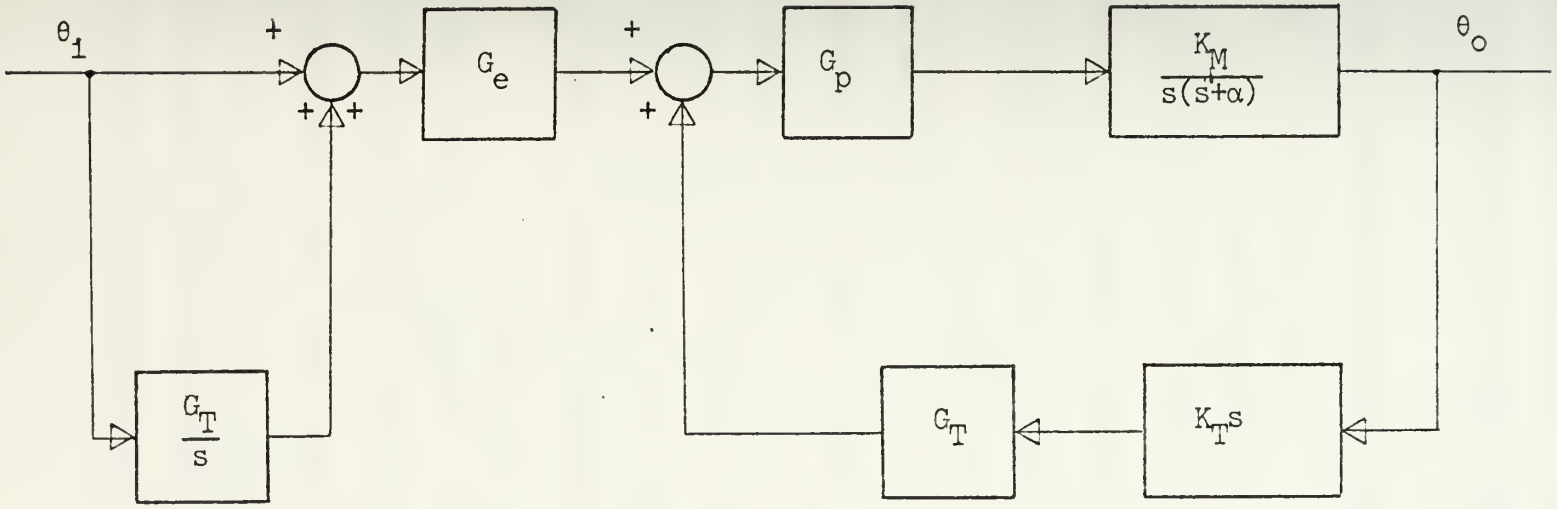

System Transfer Function:

$$\frac{\theta_o(s)}{\theta_i(s)} = \frac{G_e G_p K_M (s+1)}{s^3 + s^2(\alpha - G_T G_p K_T K_M)}$$

Figure 32 SERVO SYSTEM MODIFIED BY THE ADDITIONAL INTEGRATOR IN THE INPUT

The transmitting dipole radiated the 470 MHz signal. The crossed dipoles were rotated with constant speed and the DC output voltage of the multiplier was measured behind the inverter and recorded on a strip chart. Simultaneously the amplitude of the signal received by the reference dipole was measured with the vector-voltmeter and recorded as reference onto the same strip chart. The multiplier output had the sinusoidal shape as given by Equations (15) and (21). (See Fig. 33.)

The distortion of the curve's shape was caused (1) by the tension of the two coaxial cables coming from the dipole pair and running to the amplifiers and (2) by the imperfect dipole symmetry.

The signal received by the reference dipole was measured by a vector voltmeter which only indicated the signals magnitude. A sign change was not recorded. The imperfect symmetry of the reference dipole was the reason that the received signal's magnitude did not come close to zero when the dipole was positioned orthogonal to the polarization plane of the transmitted signal.

The significance of the Fig. 33 is the relative change of the multiplier output voltage with respect to the orientation of the crossed dipoles, here indicated by the variation of the amplitude of the signal received by the reference dipole, the absolute value of signal strength and multiplier output are unimportant for this test. Therefore scaling on the ordinate is not done.

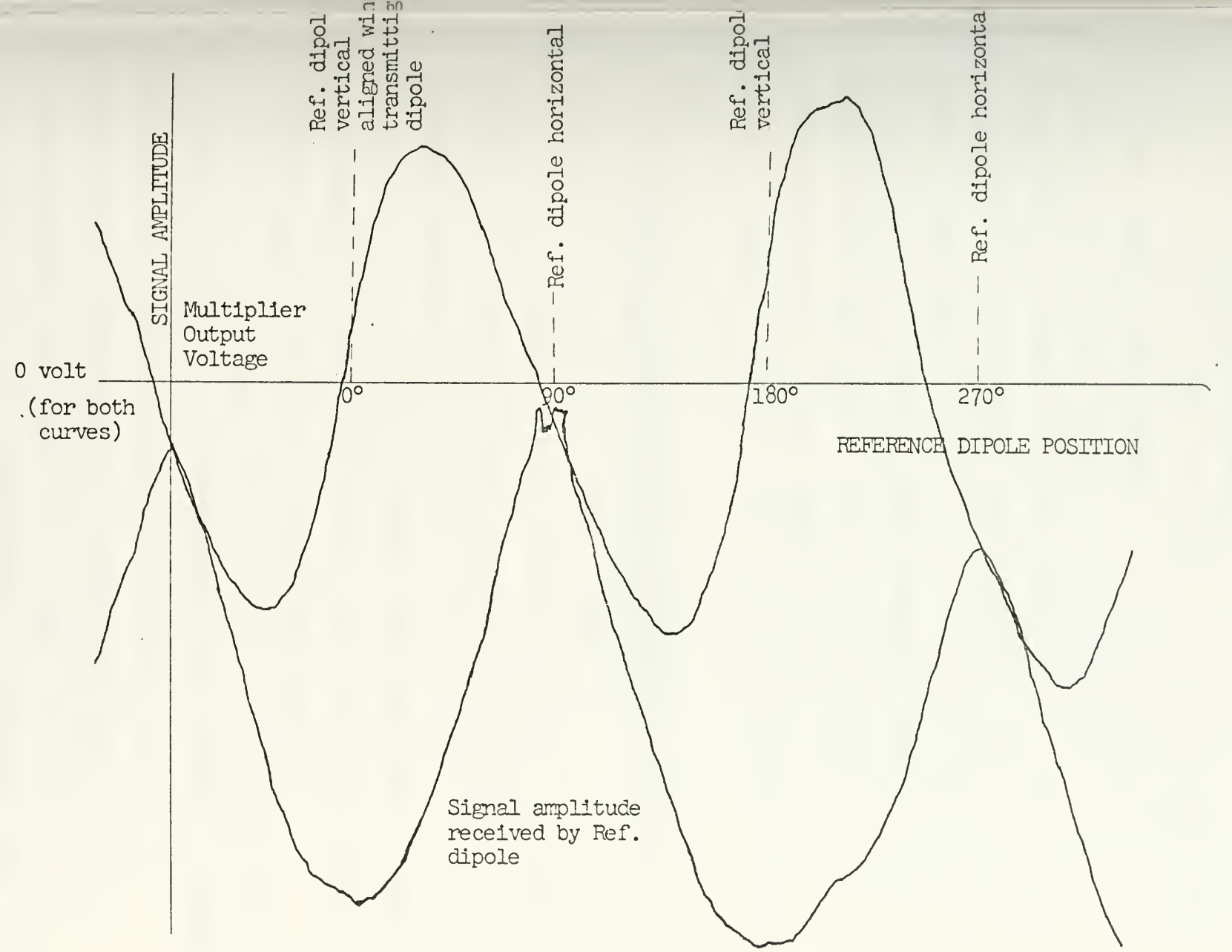

Figure 33 MULTIPLIER OUTPUT VOLTAGE (DC)
VERSUS REFERENCE DIPOLE ORIENTATION

b. Closed Loop Operation

Now the loop was closed. Without any noise fed into the channels the response of the system has been observed for different signal levels received and for various gain settings at the servo-amplifier. The system responded as a second order control system. The reference dipole of the crossed dipole pair was aligned with the transmitting one, and the system's response time was set by adjusting the input gain and the tachometer feedback gain of the servo-system. Small angular changes of the transmitting dipoles caused the proper reaction of the receiving end.

3. Methods of Measuring the Polarization Angle and Determination of the RMS Angle Error

a. Potentiometer on Motor Shaft

A constant voltage is applied across the potentiometer. The wiper moved by the motor shaft provided a voltage depending on its relative position with respect to the end-terminals of potentiometer, thus the output voltage was a measure of the orientation of motor shaft and crossed dipoles, θ_p, with respect to a reference position.

In the final test series the potentiometer had a positive voltage on one end-terminal and a negative voltage on the other, the potentiometer was mounted on the motor shaft so that the wiper was as close as possible in its center position with the reference dipole vertical, at 0°. Exact adjustment of the potentiometer to read zero volts for

this dipole position was done by changing the applied voltages slightly. During the tests the potentiometer output voltage was recorded by a strip chart recorder which was calibrated to record the actual angle of the polarizer in degrees. From these continuously taken readings the standard deviation of the angle due to the system noise could be approximately determined by using the fact that six standard deviations are measured between the two peak values of the recording.

b. Digital Shaft Angle Encoder

The polarization angle was read automatically with the DECITRAK shaft angle encoder and immediately analyzed in a calculator. Mean and standard deviation of the angle readings were shown on its display and printed on its printer (Fig. 34).

The equations used for these calculations are:

- mean

$$M = \frac{1}{n} \sum_{1}^{n} \theta_i \tag{92}$$

- variance

$$\sigma^2 = \frac{1}{n-1} \sum_{1}^{n} \theta_i^2 - M^2 \tag{93}$$

A clock was also available to set the time interval between the different readings and calculations. This was not used. The HP 9100A calculator was given the number of readings to

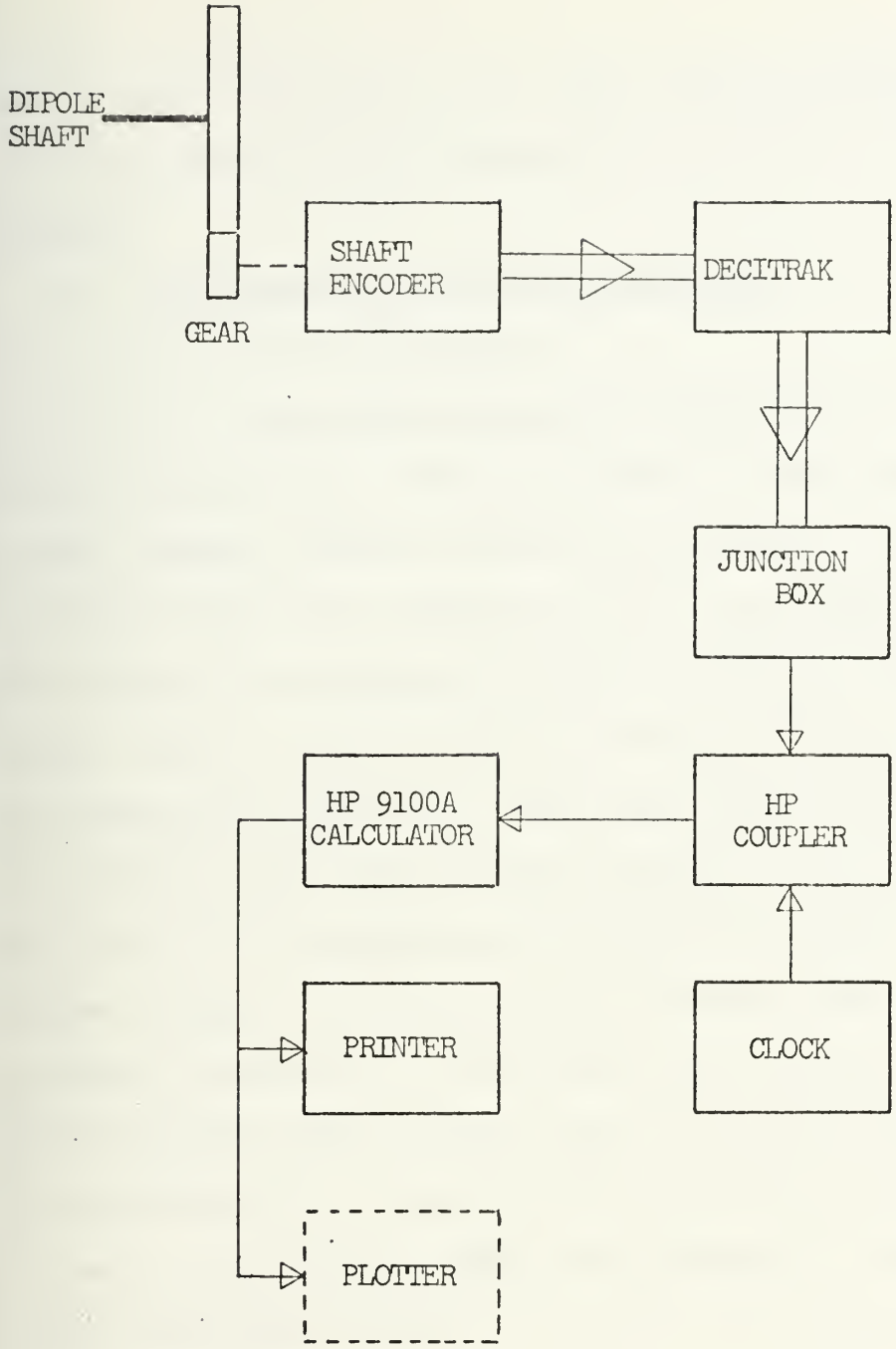

Figure 34 SET UP FOR POLARIZATION ANGLE MEASUREMENT

use for the calculation, the time interval between these was the time needed by the calculator to update the intermediate results.

4. Performance of the Working Model

a. Test Description

The working model was operating in the closed loop configuration. Noise of various levels was fed into either channel and into both simultaneously. The noise rms voltages behind the bandpass filters were measured, and also the signal rms voltages in front of these filter with the proper dipole aligned with the transmitting dipole and without noise were measured. The polarization angle was recorded on a strip chart using a potentiometer on the motor shaft and also it was automatically measured by the digital shaft angle encoder and fed into the HP 9100A, where mean and standard deviation of the polarization angle were calculated. Using Equation (48) the rms angle error was calculated for the measured rms voltages of the signal and the noise. The actually measured rms angle error then was compared with this theoretical value.

b. Calculations

(1) Rms Angle Error of Working Model

The performance of the correlation polarimeter is given by the rms angle error due to the system noise. In Section III.B it is derived. Because the filters used in the working model have a non-zero phase response the rms angle error is given by

$$\sigma_\theta^2 = \frac{2 W_S S_n(f)}{K^2} \tag{48}$$

$$= \frac{k T_e W_S}{K^2} \int_{-\infty}^{\infty} |H(f)|^2 (k T_r/2 + S_s(f))df \tag{94}$$

The transfer function of the combined filter is

$$H(f) = H_r(f) \cdot H_e^*(f) \tag{15a}$$

$$= |H_r(f)| \cdot |H_e(f)| \, e^{j(\phi_r(f)-\phi_e(f))} \tag{95}$$

In the test series with the working model a sine-wave was received by the crossed dipoles. Thus

$$s(t) = 2 V \sin \omega_0 t \tag{96}$$

and the signal spectrum is

$$S_s(f) = \frac{1}{2} V^2 [\delta(f-f_0) + \delta(f+f_0)] \tag{97}$$

where V is the rms signal voltage.

The input signals of the reference channel band-pass filter is

$$s_r(t) = 2 V_r \sin \omega_0 t \tag{98}$$

with a spectrum

$$S_r(f) = 1/2\ V_r^2\ [\delta(f-f_0) + \delta(f-f_0)] \qquad (99)$$

The band-pass filter in the error channel has as input

$$s_e(t) = 2\ V_e \sin \omega_0\ t \qquad (100)$$

with a spectrum

$$S_e(f) = 1/2\ V_e^2\ [\delta(f-f_0) + \delta(f-f_0)] \qquad (101)$$

In above equations

$$V_r = G_r\ V \qquad (102)$$

and

$$V_e = G_e\ V \qquad (103)$$

where G_r and G_e are the total gains in the reference and error channel in front of the band-pass filters, and f_0 is the mixer output frequency.

The two channel input noises are affected by the two gains too. That means the noise spectral densities in front of the filters are

$$N_e' = G_e^2 N_e \tag{104}$$

and

$$N_r' = G_r^2 N_r \tag{105}$$

Using these equations, (63) can be written as

$$\sigma_\theta^2 = \frac{k T_e W_S G_r^2 G_e^2 \int_{-\infty}^{\infty} |H_e(f)|^2 |H_r(f)|^2 (N_r + S_s(f)) \, df}{G_r^2 G_e^2 \left\{ \int_{-\infty}^{\infty} |H_r(f)||H_e(f)| \cos \phi(f) \, S_s(f) \, df \right\}^2} \tag{106}$$

which then can be expressed as

$$\sigma_\theta^2 = 2 W_S N_e' \frac{2 N_r' \int_{-\infty}^{\infty} |H_r(f)|^2 |H_e(f)|^2 df + G_r^2 V^2 |H_r(f_0)|^2 |H_e(f_0)|^2}{G_r^2 G_e^2 |H(f_0)|^2 |H_e(f_0)|^2 \cos \phi(f_0) V^2}$$

Substituting into this equation the definition of the noise bandwidth of the band-pass filter (44) and rearranging the expression the rms angle error for the working model finally is given by

$$\sigma_\theta^2 = \frac{k T_e W_S}{V_e^2 \cos^2 \phi(f_0)} \left(1 + \frac{k T_r W_n}{V_r^2}\right) \tag{107}$$

where

$$\frac{k\,T_e}{2} = N_e' = \frac{\sigma_{N_e}^2}{2\int_0^\infty |H_e(f)|^2\,df} \tag{108}$$

$$\frac{k\,T_r}{2} = N_r' = \frac{\sigma_{N_r}^2}{2\int_0^\infty |H_r(f)|^2\,df} \tag{109}$$

$$\int_0^\infty |H_r(f)|^2\,df = 1.41 \cdot 10^5 \text{ Hz} \quad \text{(from Fig. 25)}$$

$$\int_0^\infty |H_e(f)|^2\,df = 1.73 \cdot 10^5 \text{ Hz} \quad \text{(from Fig. 27)}$$

σ_{N_r} = rms noise voltage in reference channel

σ_{N_e} = rms noise voltage in error channel

V_r = rms signal voltage in reference channel

V_e = rms signal voltage in error channel

$\phi(f_0) = \phi_r(f_0) - \phi_e(f_0)$, this is (from Fig. 29) about 45°, however the signal phases in both channels were matched at signal frequency of 110 KHz by the trombone line. However even small frequency variations due to the drift in the signal generator cause relatively large angle changes.

With both channels phased up

$$\sigma_\theta^2 = \frac{h\ T_e\ W_S}{V_e^2}\left(1 + \frac{k\ T_r\ W_n}{V_r^2}\right) \tag{107a}$$

The rms angle error in degrees is

$$\sigma^2_{\theta_{degr}} = (57.3\ \sigma_{\theta_{rad}})^2 \tag{110}$$

(2) Servo Bandwidth

(a) Second-Order Loop. The transfer function of the servo system is of third order (Fig. 32). However, from the strip chart recordings it can be seen that the system behaved like an underdamped second-order system. In the analysis of the measurement it was treated as such.

The single-sided noise bandwidth of a second-order system with the transfer function F(s) is [3]

$$W_S = \frac{\int_0^\infty |F(f)|^2\ df}{|F(f_0)|^2} = \frac{\omega_0}{8\zeta} \tag{111}$$

For an overshooting system ($\zeta < 1$) in response to an unit step input the time τ(defined as response time) to first crossing of unit output is related to W_S by

$$\tau\ W_S = \frac{\pi - \tan^{-1}\left(\frac{\sqrt{1-\zeta^2}}{\zeta}\right)}{8\ \zeta\sqrt{1-\zeta^2}} = Q \tag{112}$$

In the above equations,

ζ = damping ratio

ω_0 = natural frequency

Q = system quality factor

For a second order system we have further the following relationships [9]:

- the peak value of the output occurs at time

$$t_p = \frac{\pi}{\omega_0 \sqrt{1 - \zeta^2}} \tag{113}$$

- the damped frequency

$$\omega_d = \omega_0 \sqrt{1 - \zeta^2} \tag{114}$$

- the ratio of the maximum output value (overshoot) and the final output value (steady state value)

$$M_{pt} = 1 + \exp \frac{-\zeta \pi}{\sqrt{1 - \zeta^2}} \tag{115}$$

M_{pt} and $\omega_0 t_p$ are plotted versus the damping ratio ζ in Fig. 35 and 36. Using the above relationships the system's noise bandwidth becomes

$$W_S = \frac{\pi}{8 \zeta t_p \sqrt{1 - \zeta^2}} \tag{116}$$

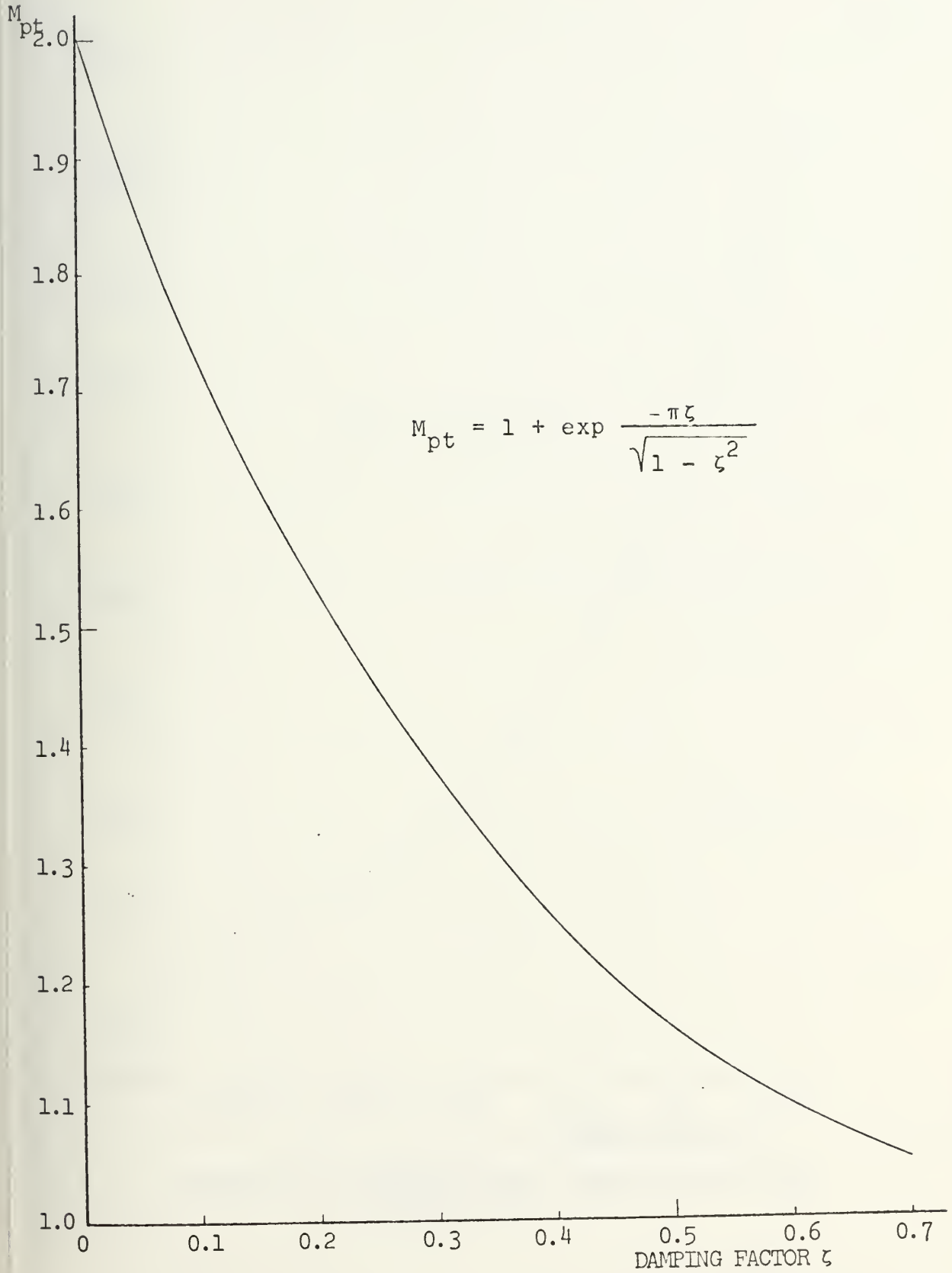

Figure 35 SECOND-ORDER LINEAR SYSTEM STEP RESPONSE [9]

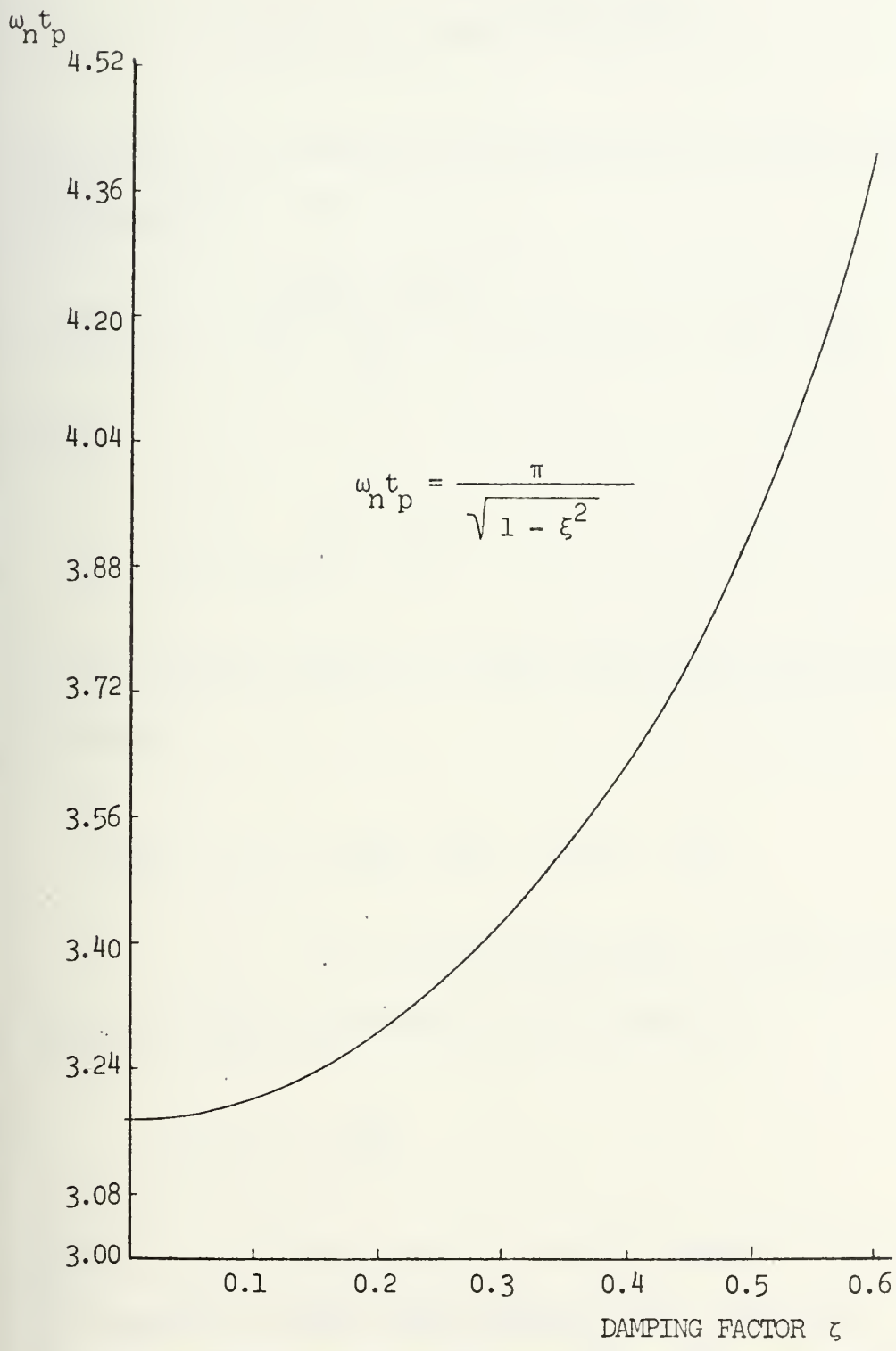

Figure 36 SECOND-ORDER LINEAR SYSTEM STEP RESPONSE [9]

and the time of the unit output crossing is

$$\tau = t_p - t_p \tan^{-1} \left\{ \frac{\sqrt{1 - \zeta^2}}{\zeta} \right\} \qquad (117)$$

The unit step response of a second-order system with a damping factor ζ is

$$y(t) = 1 - \frac{\omega_0 \exp(-t/\tau)}{\omega_d} \sin(\omega_d t + \tan^{-1} \tau\omega_d) \qquad (118)$$

with

$$\omega_d \equiv \omega_0 \sqrt{1 - \zeta^2}$$

If the damping factor is unity this unit step response becomes

$$y(t) = 1 - \exp\left(-\frac{t}{\tau}\right) - \frac{t}{\tau} \exp\left(-\frac{t}{\tau}\right) \qquad (119)$$

(b) First-Order Loop. For a first-order loop the noise bandwidth was determined as

$$W_S = \frac{1}{4\tau} \qquad (89)$$

where τ is the time constant of the system, the time when the system's output has reached 63% of its final value. This time constant can be found from the output curves of the system.

For the first-order system the unit step response is

$$y(t) = 1 - e^{-\frac{t}{\tau}} \qquad (120)$$

Both response curves are plotted in Fig. 37 with respect to the normalized time $\omega_n t$ which is for $\zeta = 1$ equal to $\frac{t}{\tau}$ [10]. From here it can be seen that the time t/τ of the second-order system is approximately the time of the first zero crossing of the unit output for systems with a damping factor $0.2 < \zeta < 0.5$. And this time is about twice the time constant τ of the first-order system (needed in equation (82), (87)). Thus, as the time constant τ in (82), (87), half the time for the unit output crossing of the second-order system, read from the strip chart recordings, was taken.

c. Test Results

(1) No Noise in Reference Channel. For both system approximations (see Section IV.B.4.b) the theoretical rms angle errors are calculated assuming a perfect phase match. These and the measured values are plotted with respect to the factor $k\, T_e\, W_S / V_e^2$ in Fig. 38-41. The measured and calculated values disagree by a factor of about two which is a reasonable agreement.

The ellipticity of the transmitting dipole and of the receiving dipole pair undoubtedly contributed to

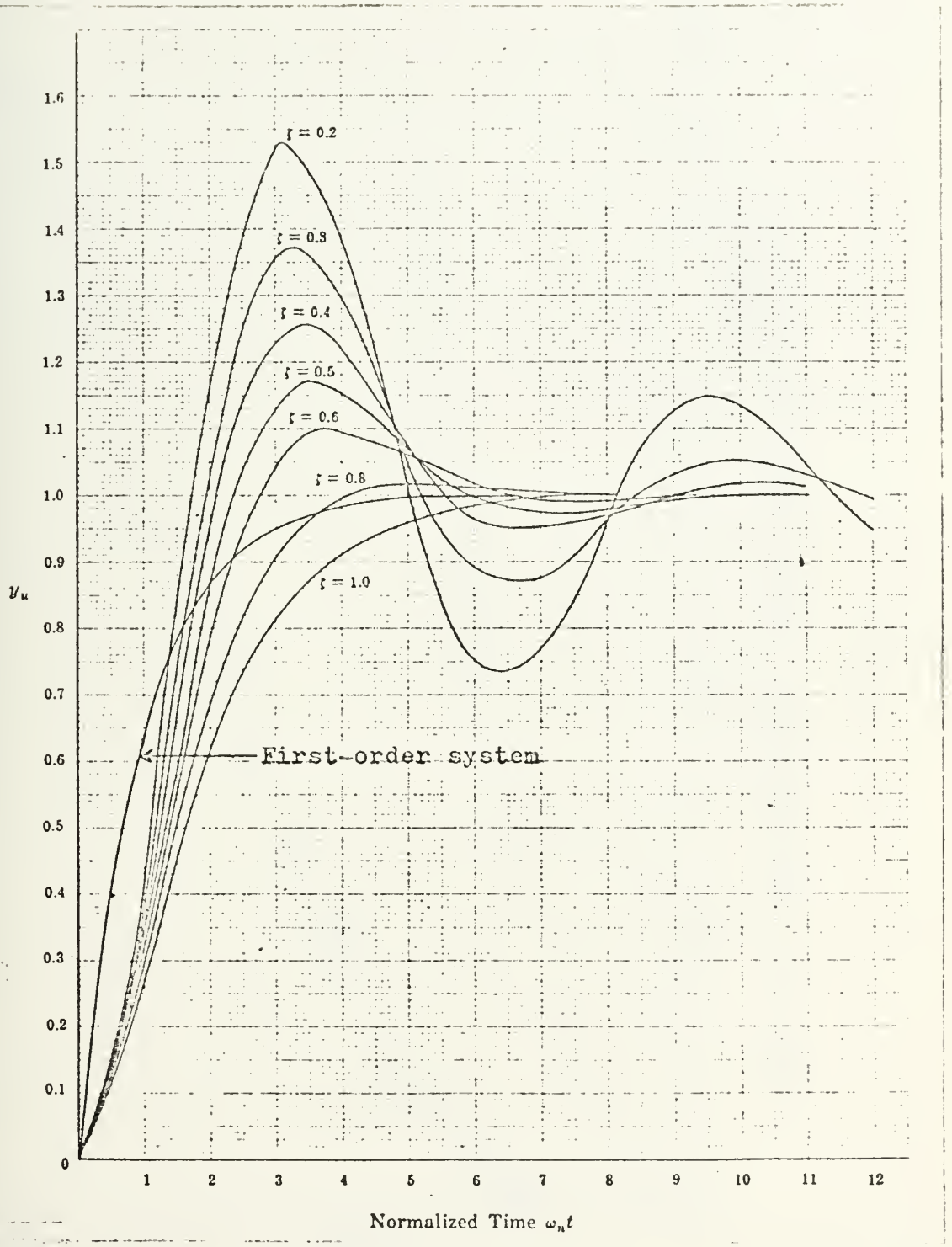

Figure 37 UNIT STEP RESPONSE
(Second-order system curves are defined by the damping ratio ζ).

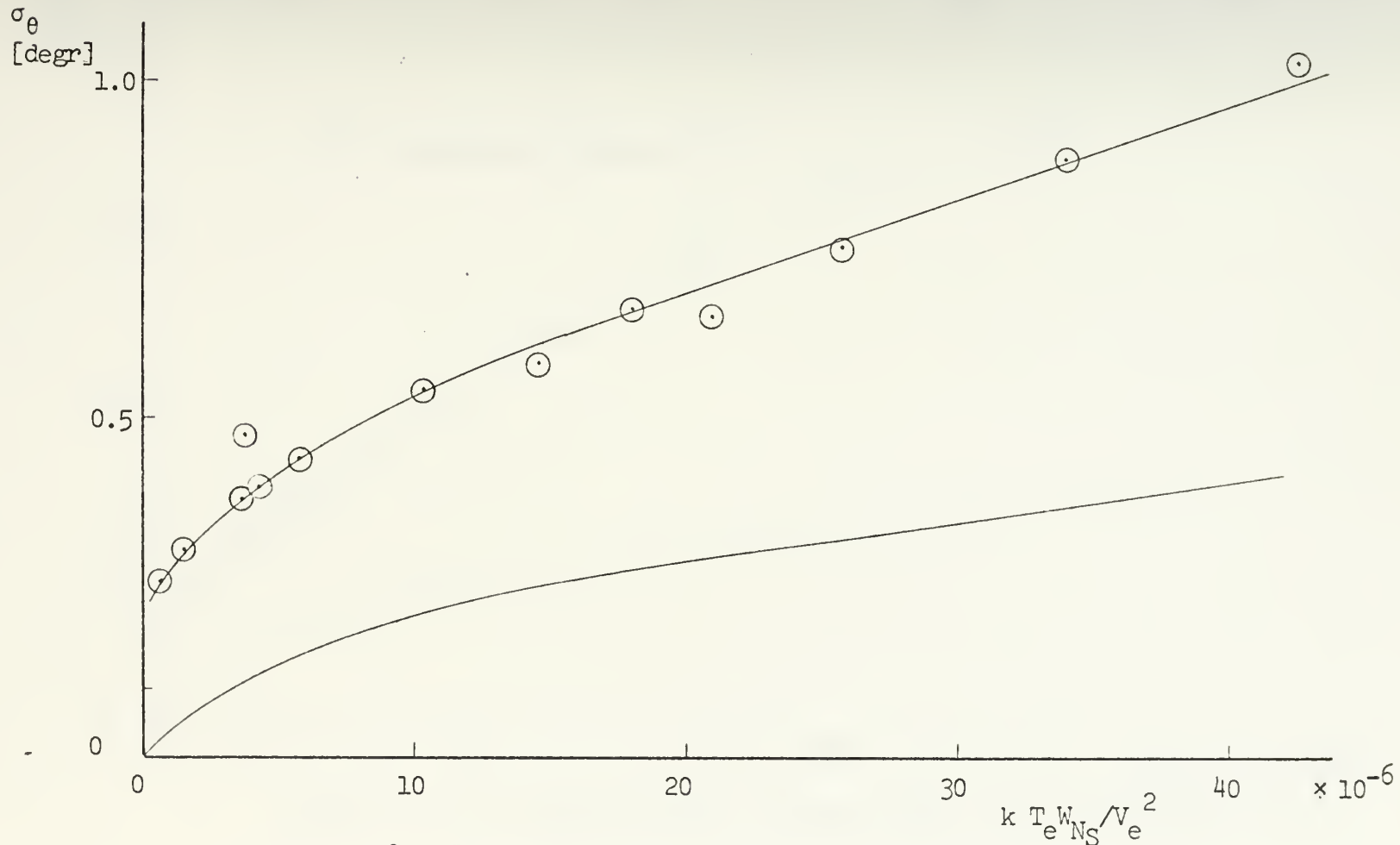

Figure 38 RMS ANGLE ERROR (SECOND-ORDER APPROXIMATION)

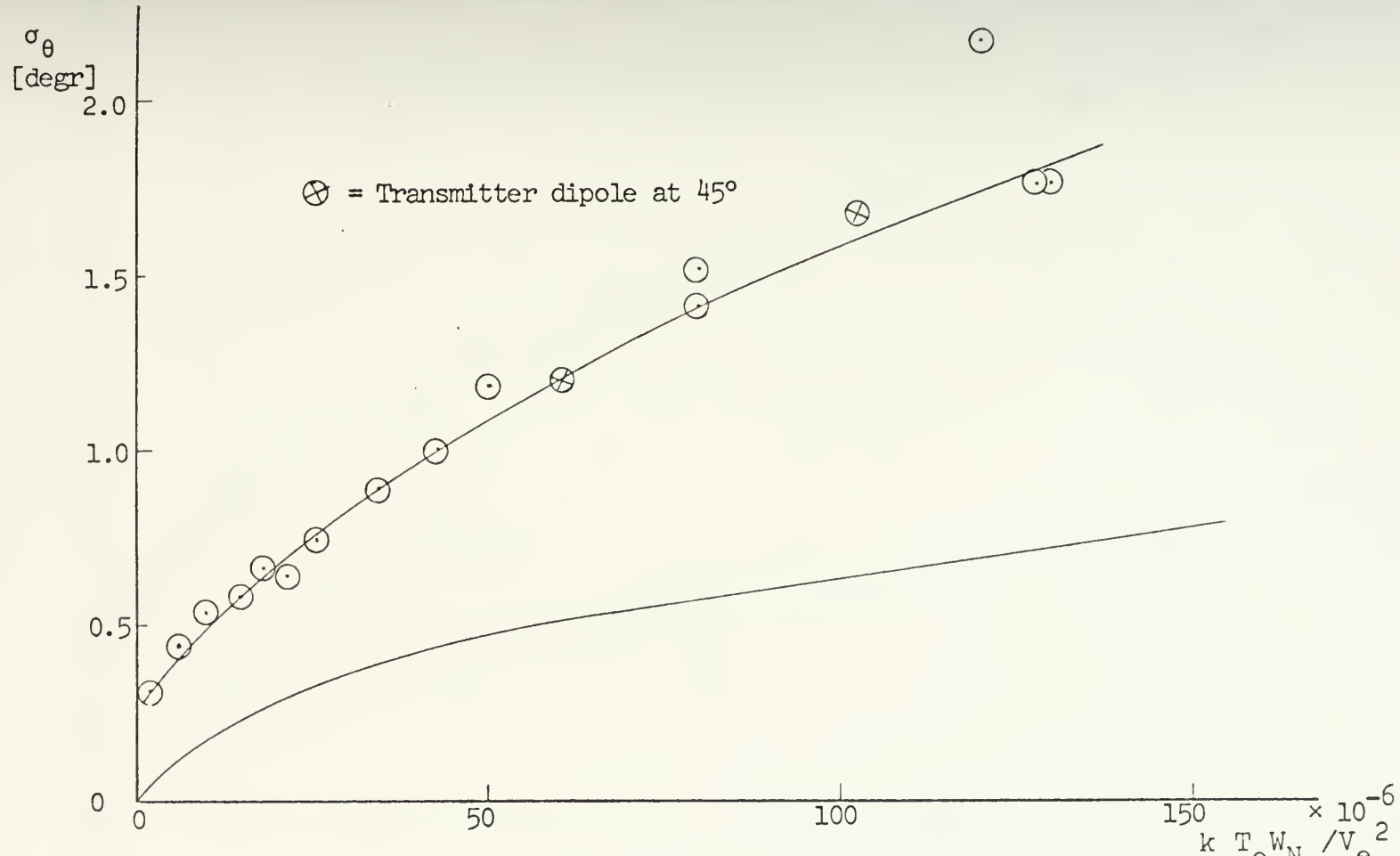

Figure 39 RMS ANGLE ERROR (SECOND-ORDER APPROXIMATION)

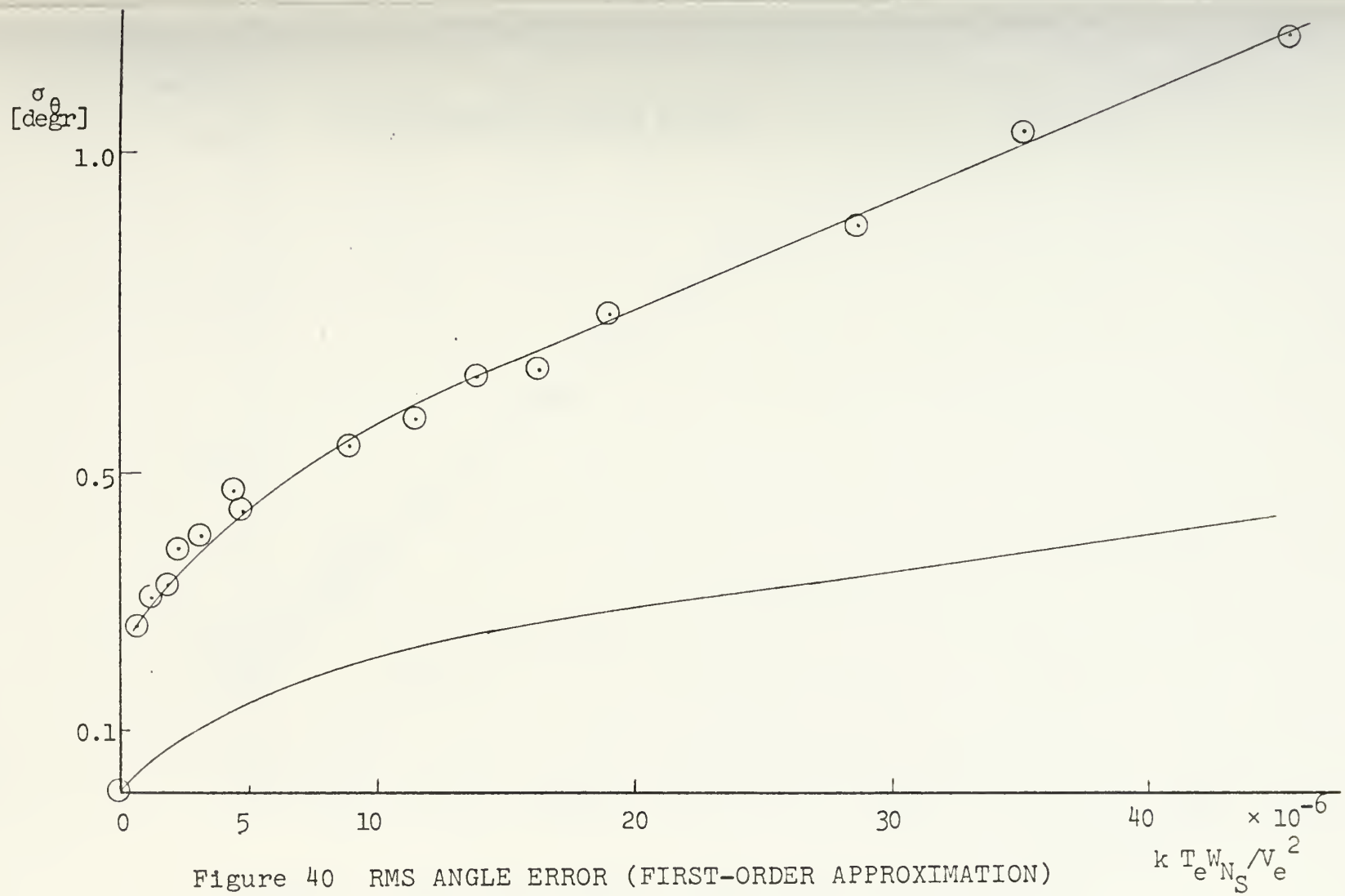

Figure 40 RMS ANGLE ERROR (FIRST-ORDER APPROXIMATION)

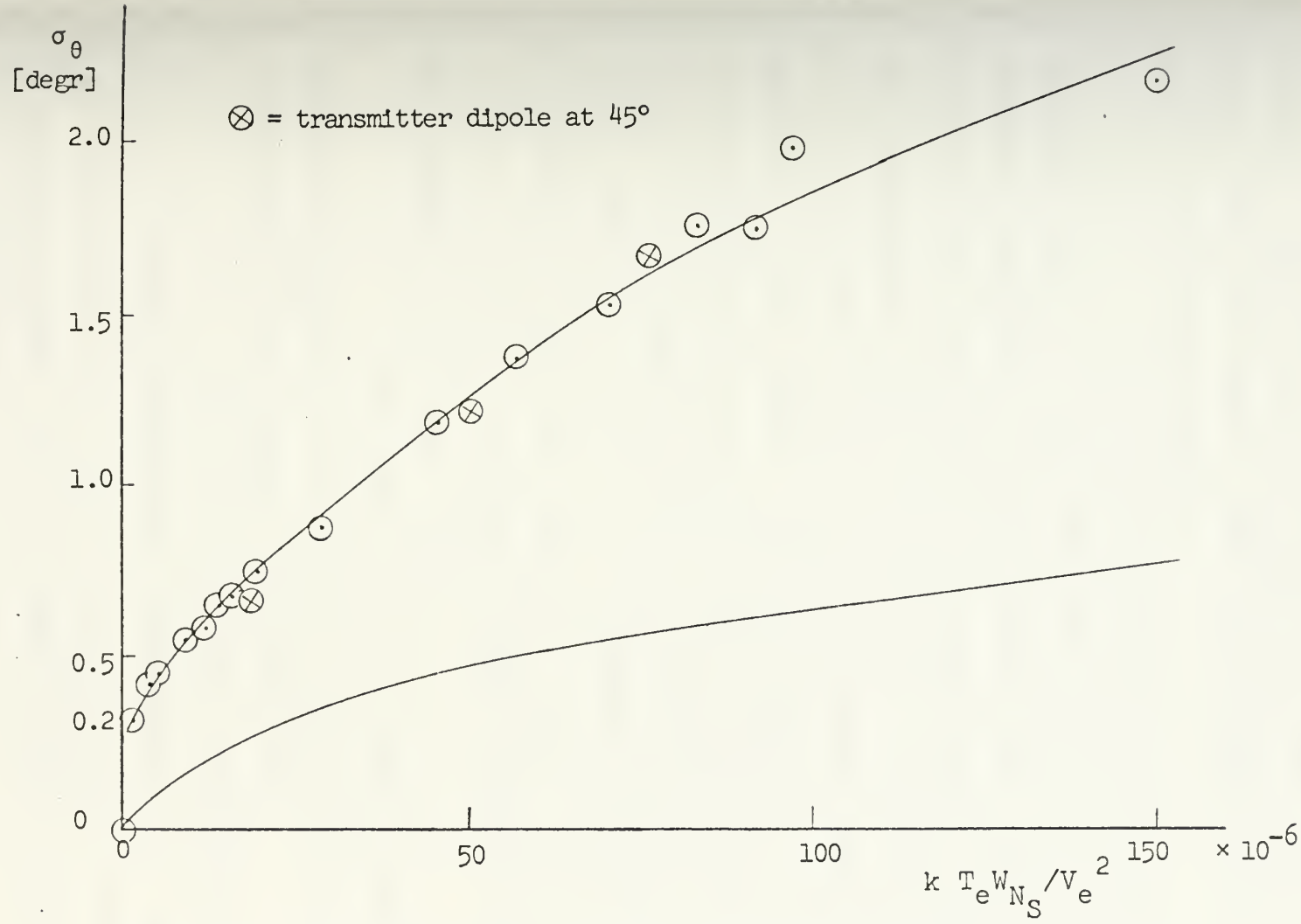

Figure 41 RMS ANGLE ERROR (FIRST-ORDER APPROXIMATION)

the increase of the rms angle error over theory. With the reference dipole perfectly aligned with the transmitting dipole there was always a small out-of-phase signal component in the error channel.

Due to the instability of the signal generator used as a local oscillator for the two mixers, amplitude variations of the multiplier input signals were observed which, especially at low noise levels, resulted in a significant offset in angle error. Simultaneously, a frequency drift caused a phase difference between the multiplier input signals. They were adjusted to be equal at the signal frequency of 110 KHz in front of the multiplier, but a frequency drift of 1 KHz would result in a phase difference of about 10°. Frequency variations between 108 KHz and 112 KHz were observed. Because σ_θ^2 is proportional to $1/\cos^2\phi$ an increase in phase difference will cause an increase in rms angle error.

The mixers in the two channels were not physically separated so that their crosstalk at 470 MHz contributed to the measured rms angle error.

These three problems, ellipticity of feed system, crosstalk between the two channels, and instability in frequency will not exist in an operational correlation polarimeter system, and it is expected that it will match the theory better.

(2) Noise in Reference Channel. The noise in the reference channel was only effective in increasing the rms angle error when noise was present in the error channel. For both system approximations the ratio of σ_θ^2 with reference channel noise and σ_θ^2 without it have been calculated and have been plotted in Fig. 42a and b versus the degradation factor F_D of the reference channel, which is in theory the value of the ratio. The σ_θ^2 values were picked for the same values of $k\, T_e\, W_{N_S}/V_e^2$. The measured and the theoretical results agree closely.

(3) Comment. An error source in the analysis of the measurements might have been the difficulty in reading the time values from the strip chart recordings accurately. Small errors here cause errors in system noise bandwidth and σ_θ^2.

In summary the working model proved the theory to be correct. It performed as predicted. Even with high noise levels in both channels the reference dipole of the receiving end became aligned with the transmitting dipole, i.e. plane of polarization of the transmitted signal. It followed changes in the orientation of the plane of polarization like an underdamped second-order system.

The working model also can be thought of as a realization of a "wireless servo system", the reference input to this is angle information given by the plane of polarization of the transmitted signal. The receiving end

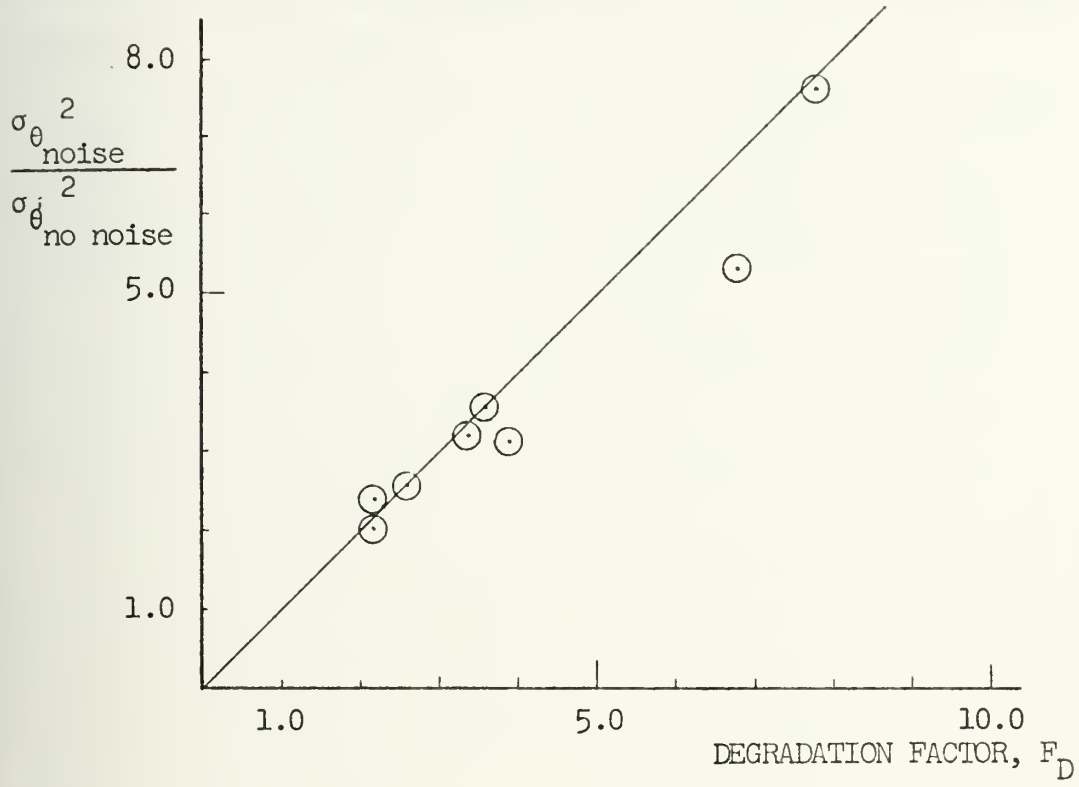

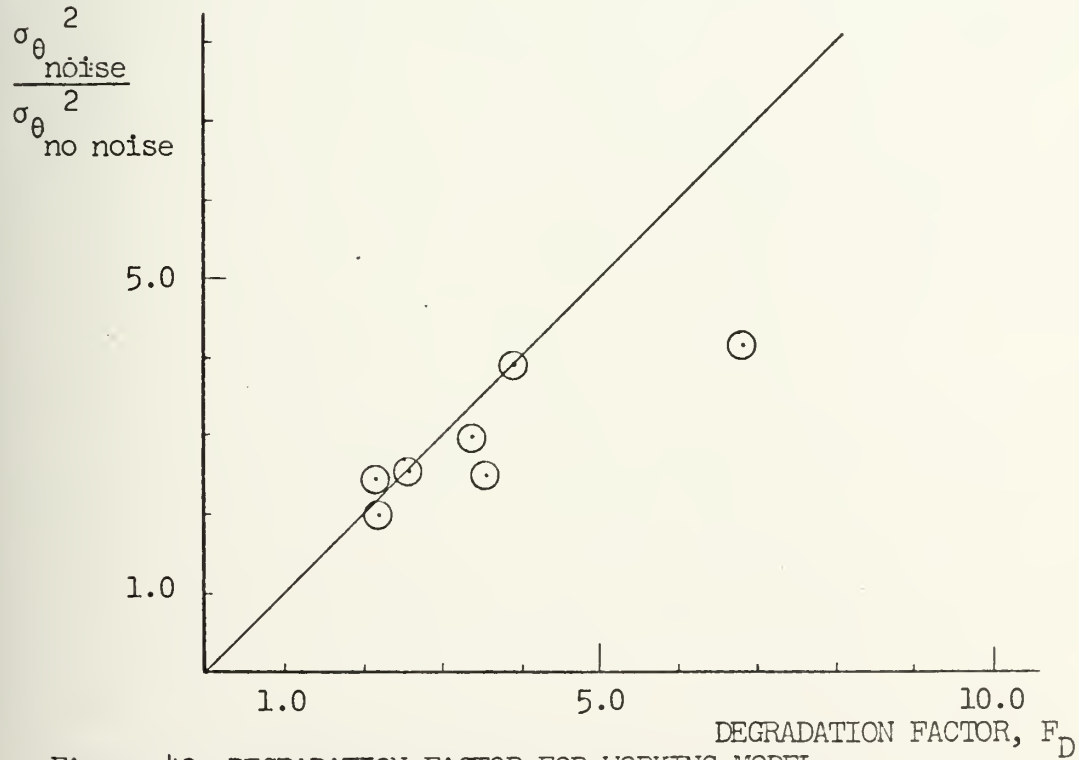

Figure 42 DEGRADATION FACTOR FOR WORKING MODEL
a) FIRST-ORDER APPROXIMATION b) SECOND-ORDER APPPROXIMATION

is forced by its closed loop response to align the reference dipole of the crossed dipole pair with the transmitter dipole.

V. CORRELATION POLARIMETER FOR THE JPL-DEEP SPACE STATION

A. SYSTEM DEVELOPMENT

A correlation polarimeter for the NASA/JPL 64-meter fully steerable parabolic dish antenna located in the Mojave Desert at Goldstone, California was developed. It was desired to use as much as possible of the present coherent polarimeter in the new system to minimize costs and to allow easy switching between the coherent scheme and the correlation scheme.

In Fig. 43 and 44 the rotatable feed system and the phase-locked-loop receiver of the coherent polarimeter as presently used in the JPL Deep Space Station at Goldstone are shown. Both are described in detail in Ref. 3. The feed system (polarizer) is used by the correlation polarimeter without any changes. Comparing Fig. 45 and 44, one can see the changes in the receiver necessary to realize the practical correlation polarimeter shown in Fig. 4. The part "correlation polarimeter chassis" drawn in detail in Fig. 46 was integrated in the Goldstone receiver system [11] by proper cable connections [12].

In the development of the correlation polarimeter for the Goldstone system five major changes of the scheme of the polarimeter as shown in Fig. 4 were necessary: (1) To minimize costs for the narrow band-pass filters, a frequency range had to be selected where low-priced filters with the desired bandwidths were available. As center frequency 250 Hz

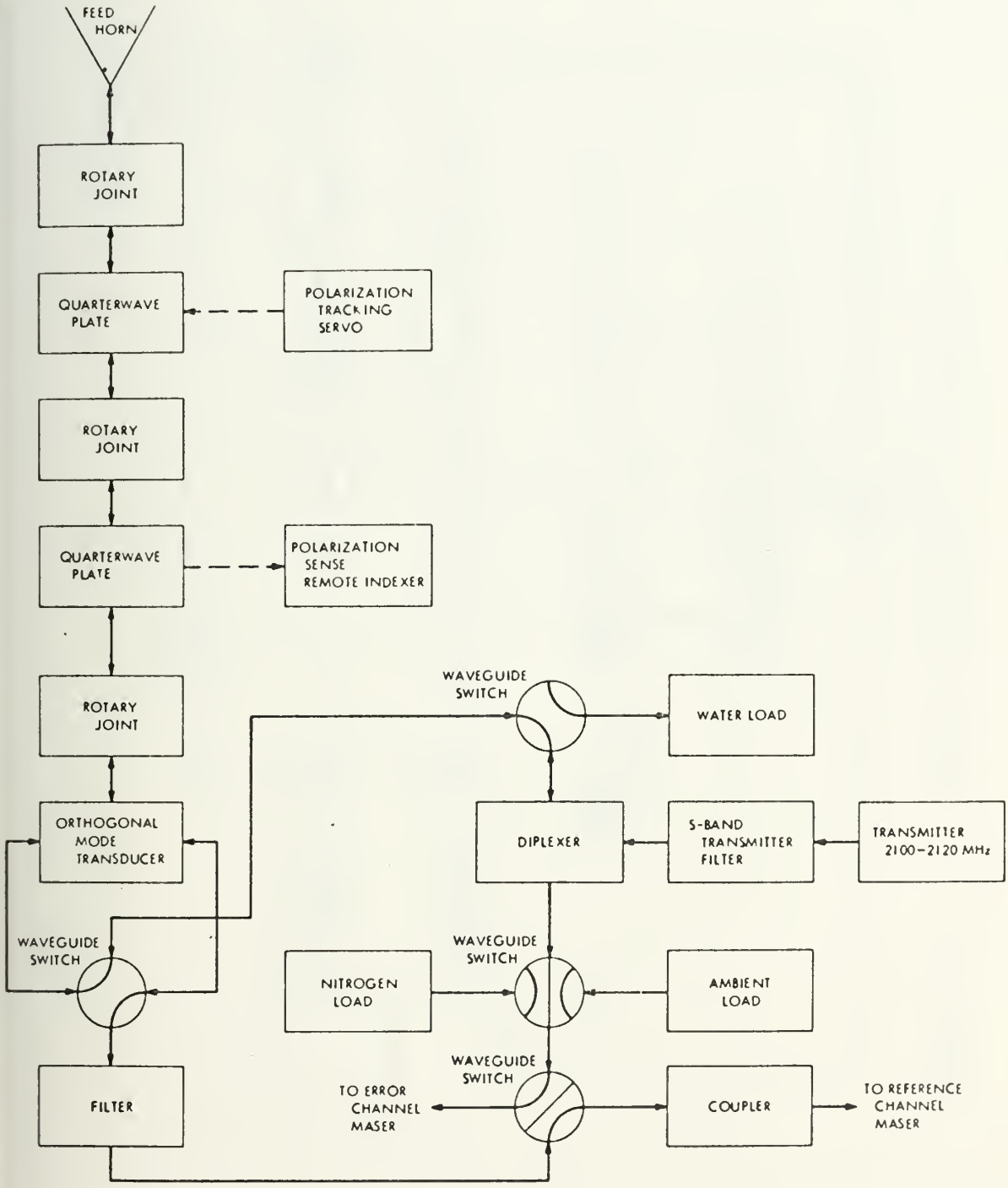

Figure 43 ROTATABLE FEED SYSTEM AT GTS, [3]

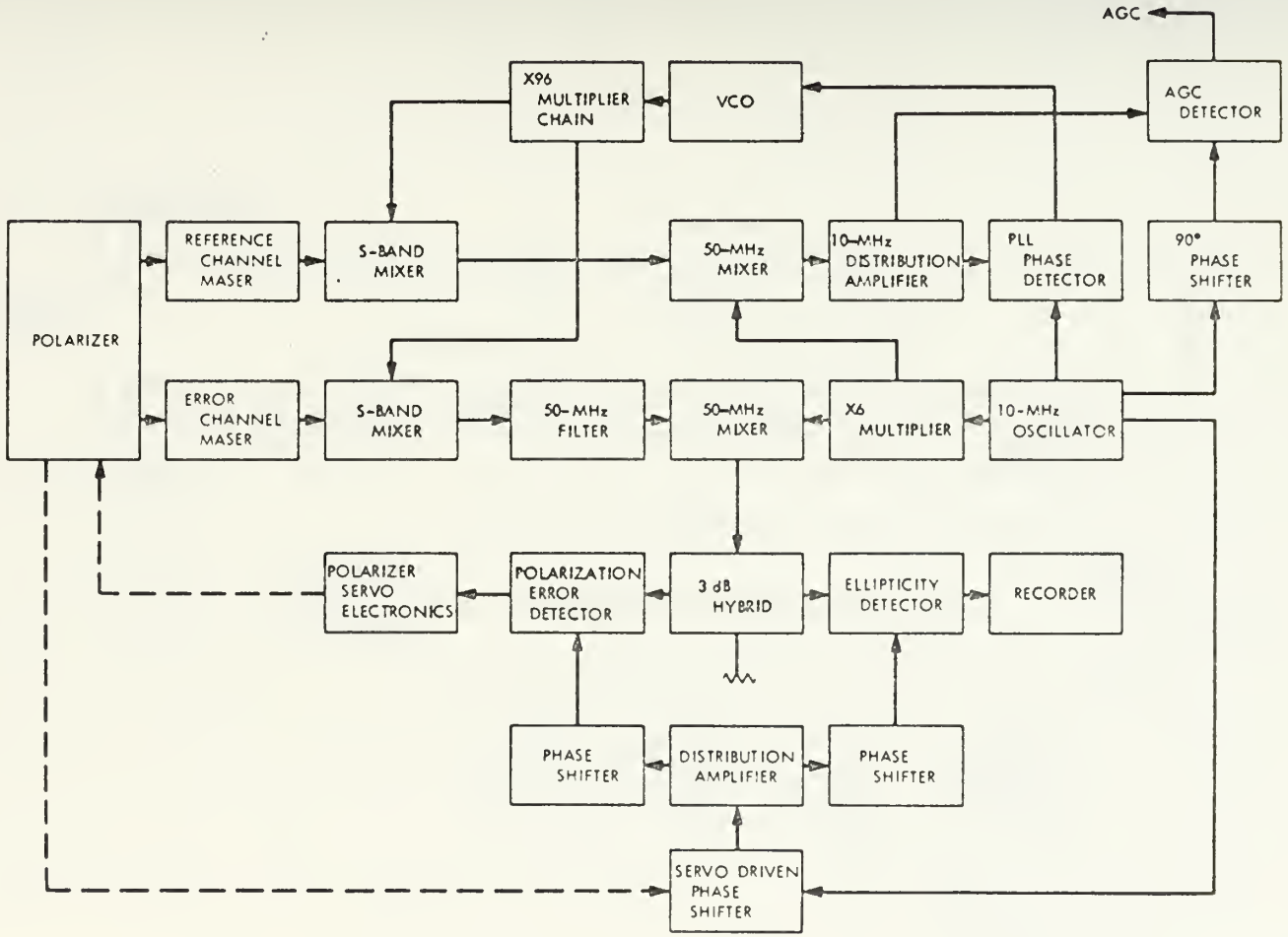

Figure 44 COHERENT POLARIMETER AT GTS, [3]

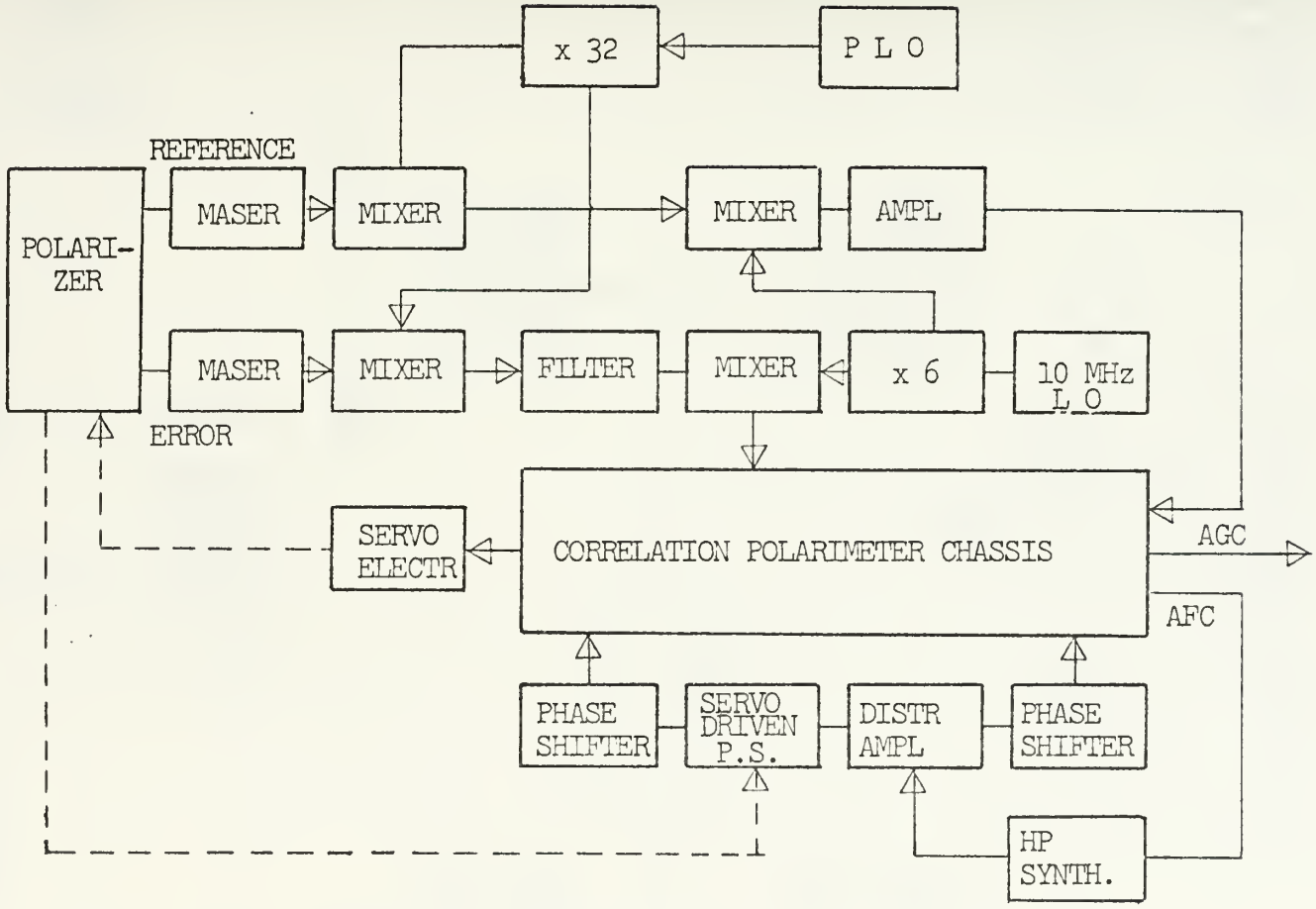

Figure 45 CORRELATION POLARIMETER FOR DEEP SPACE STATION

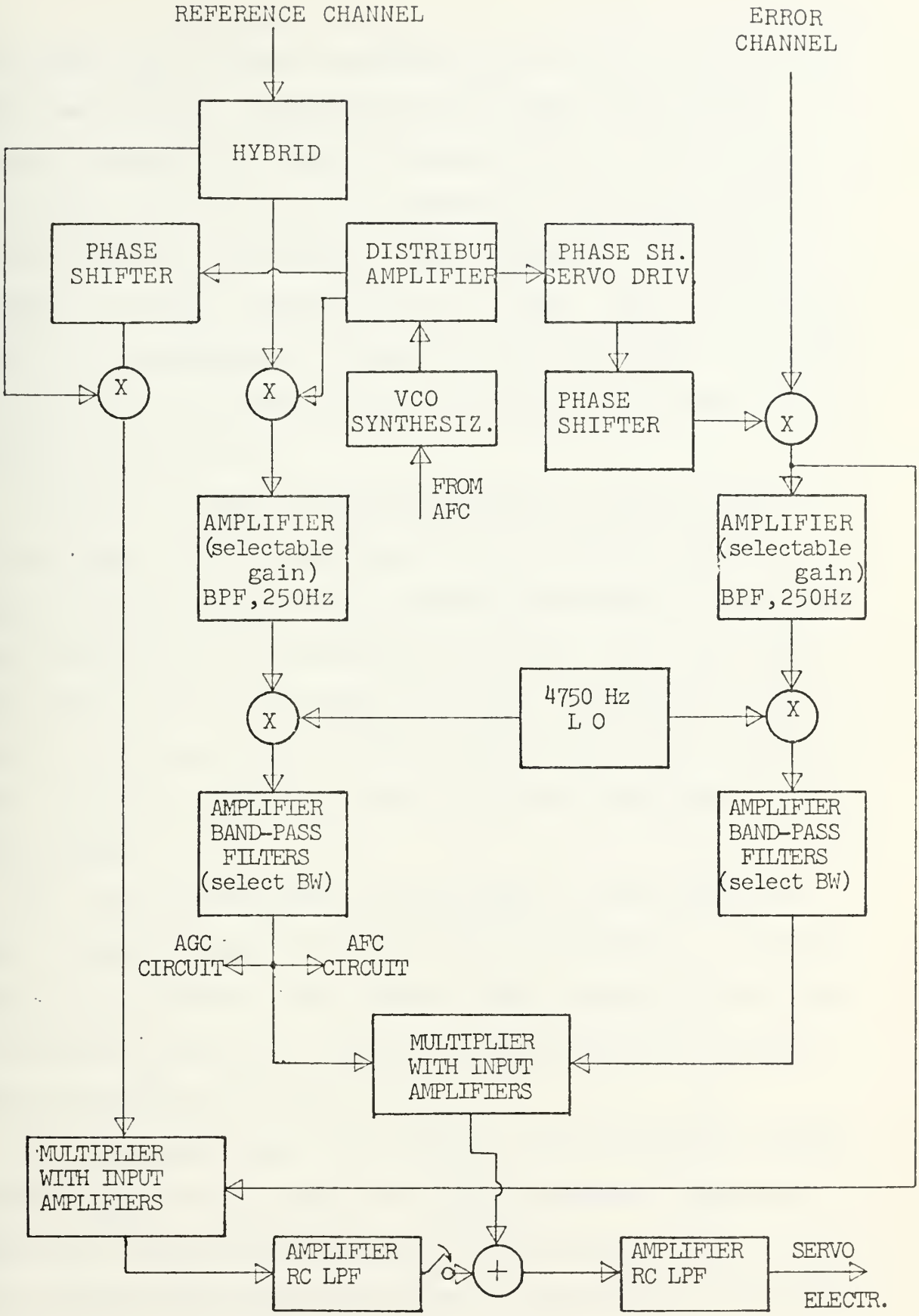

Figure 46 CORRELATION POLARIMETER CHASSIS

was chosen. The filter bandwidths are 5 Hz, 12.5 Hz, 25 Hz, 50 Hz, and 125 Hz. To prevent noise images which would occur by mixing the 10-MHz IF directly down to 250 Hz, an additional mixer stage and an additional band-pass filter are included in each channel. The 10-MHz IF, with noise bandwidth 2200 Hz, is mixed down to 5 KHz. Then in the BPF with 250 Hz bandwidth at center frequency of 5 KHz the noise is bandlimited once more. Then the 5-KHz IF is mixed down to the desired 250 Hz.

In order to have the operation point of the AFC loop in the center of the linear part of its response (zero output voltage at 260 Hz) the center frequencies of the band pass filters had to be adjusted to 260 Hz. This means the 9.995 MHz LO had to be offset by 10 Hz. If desired in the future to go back to the desired 250 Hz a low-pass filter with a cut-off frequency of about 240 Hz is required in the AFC circuit.

(2) For the additional mixer stage a local oscillator with an output frequency of 4750 Hz is necessary. A crystal oscillator provides a very stable 2-MHz frequency which then is divided by means of a digital IC-circuit by 421 to give the desired 4750 Hz (Fig. 47).

(3) To ensure that the signals in both channels undergo matched phase shifts across the system bandwidth identical band-pass filters are necessary. Only constant phase differences between the two channels can be cancelled by the phase shifters.

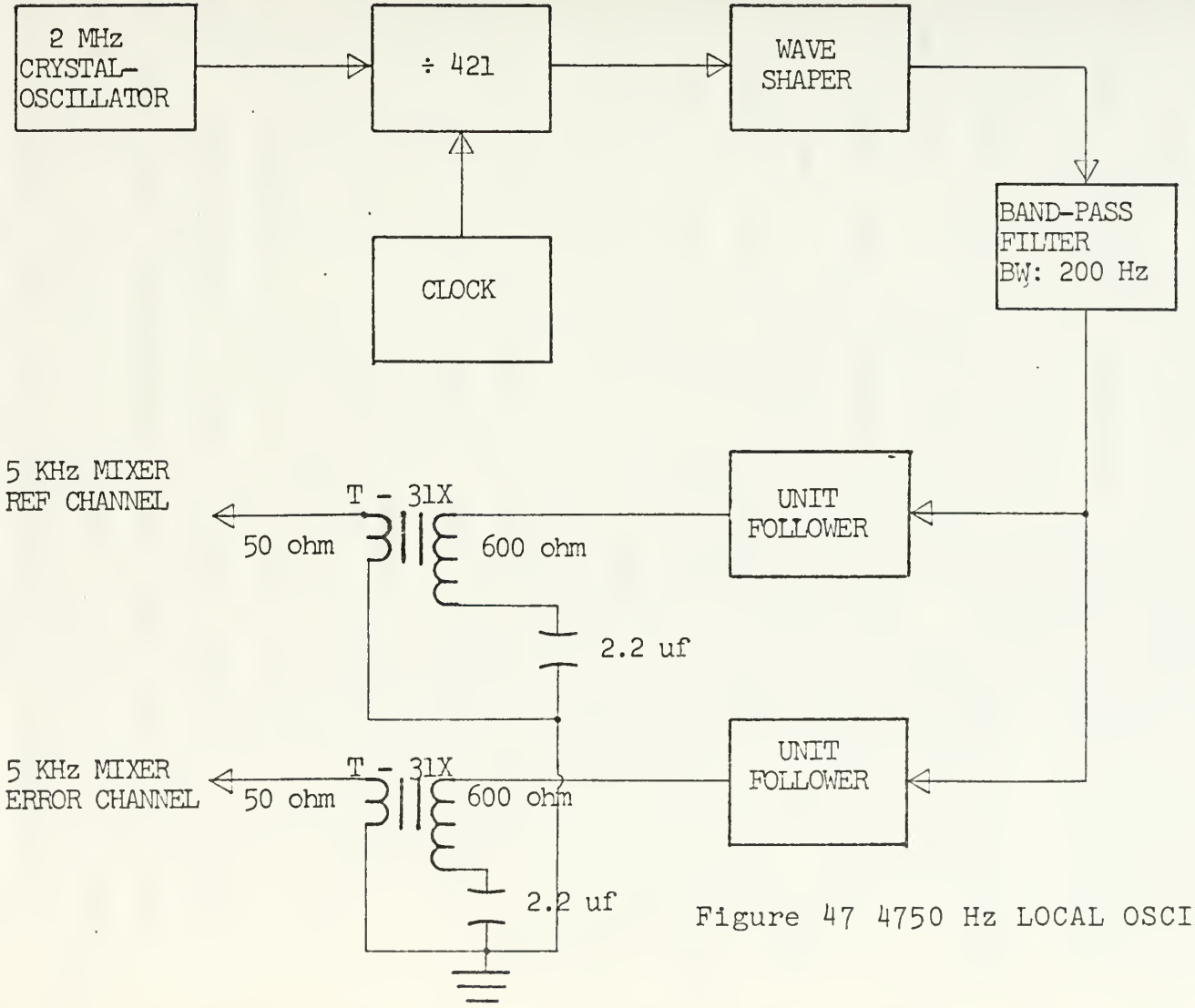

Figure 47 4750 Hz LOCAL OSCILLATOR

(4) In the inner loop the reference input of the multiplier is hard-limited. This provides a high drive for the multiplier even for a low signal level and thus better performance because the effect of DC-drift in the multiplier output is reduced. Also it prevents exceeding the dynamic range of the multiplier. However, due to this hard-limiter the multiplier now acts as a phase detector.

It is known that the sun emits little linearly polarized noise compared to the unpolarized noise. The polarized noise level into the multiplier of the inner loop from the reference channel is affected by the spacecraft signal level in the reference channel due to the hard-limiter. However, if the signal to total noise power ratio is greater than 0 dB then the amount of polarized noise (which is much smaller than the total noise) must have negligible effect on tracking and the outer loop (designed to eliminate the effects of the polarized noise) is not needed. When the signal to total noise ratio is below 0 dB then, however, the polarized noise component could become appreciable compared to the signal and a tracking offset due to this noise will be generated. Now the hard-limiter in the reference channel of the inner loop is dominated by the total noise and the polarized noise component is "linear" through the hard-limiter.

Due to the fact that the polarized noise strength is much smaller than that of the unpolarized noise a hard-limiter in the reference channel of the outer loop is always dominated by the latter since in addition the signal component

has negligible effect in the wide band of the outer loop (2.2 KHz). And again the polarized noise component can be assumed to be "linear" through the hard-limiter as far as correlation with the error channel input is concerned.

Thus the reference channel in both loops is hard-limited. For low signal to total noise ratios the offset in tracking due to the polarized noise can be eliminated by subtraction of the DC-output voltage of the multiplier of the outer loop from that of the inner loop. Block diagrams for both multiplier circuits are shown in Fig. 48 and 49.

(5) The discriminator of the AFC loop is realized with a low-pass filter, a detector, a subtractor, and a DC reference voltage. The block diagram is shown in Fig. 50. Since the cut-off frequency of the filter is 250 Hz offsets in the signal frequency about this point will cause amplitude variations of the filter output and thus will result in different output voltages behind the detector. These then are compared against the DC-reference voltage which is so adjusted to give to provide a zero output for a 260 Hz input frequency.[1]

B. SYSTEM DESCRIPTION

The system operates as described in Section II, with the above mentioned changes taken into account. The wide

---

[1]This is the new center frequency of the band-pass filters. The frequency change was necessary in order to have the AFC circuit operate in the linear region of its response.

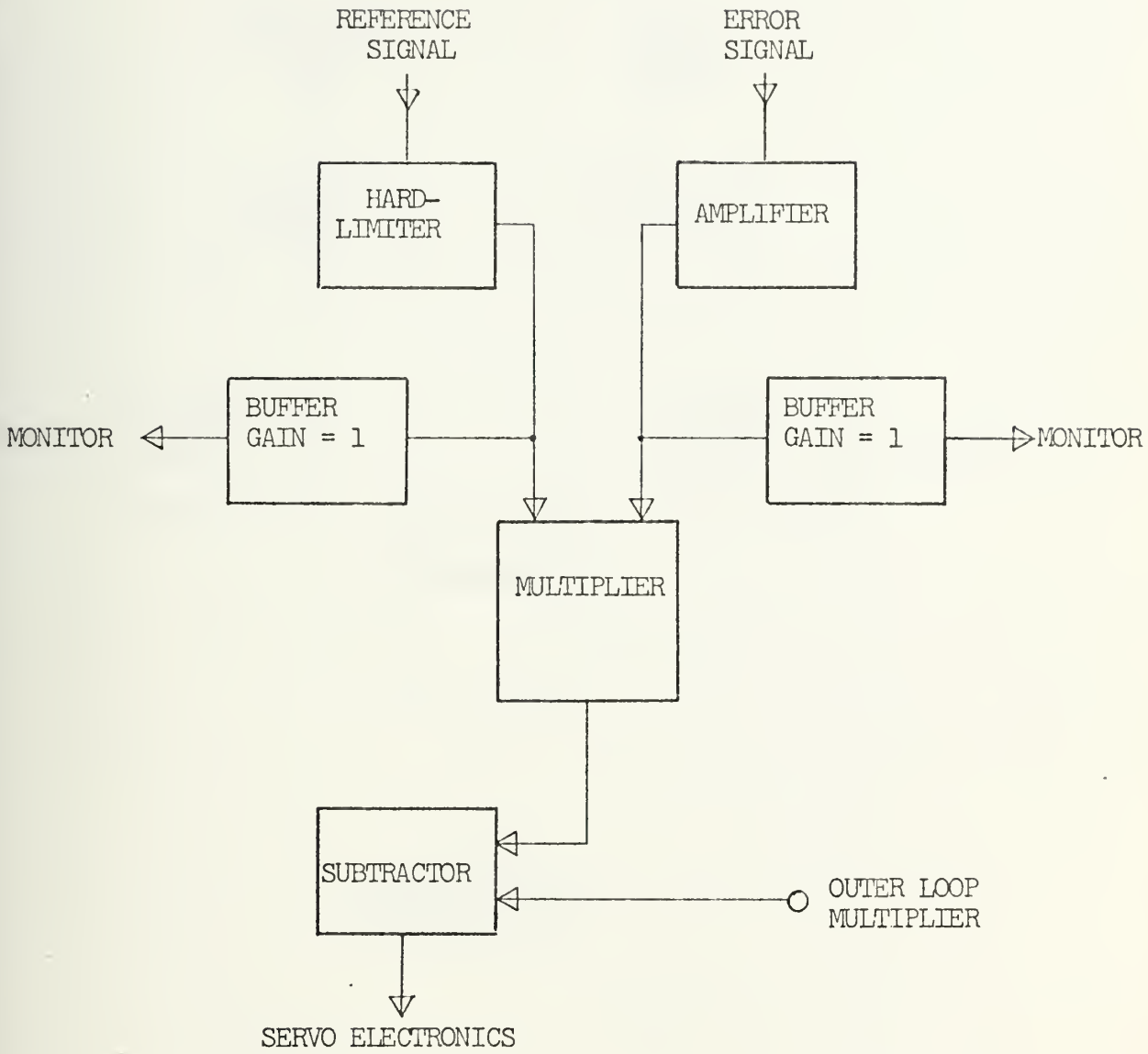

Figure 48 MULTIPLIER BOARD OF THE INNER LOOP

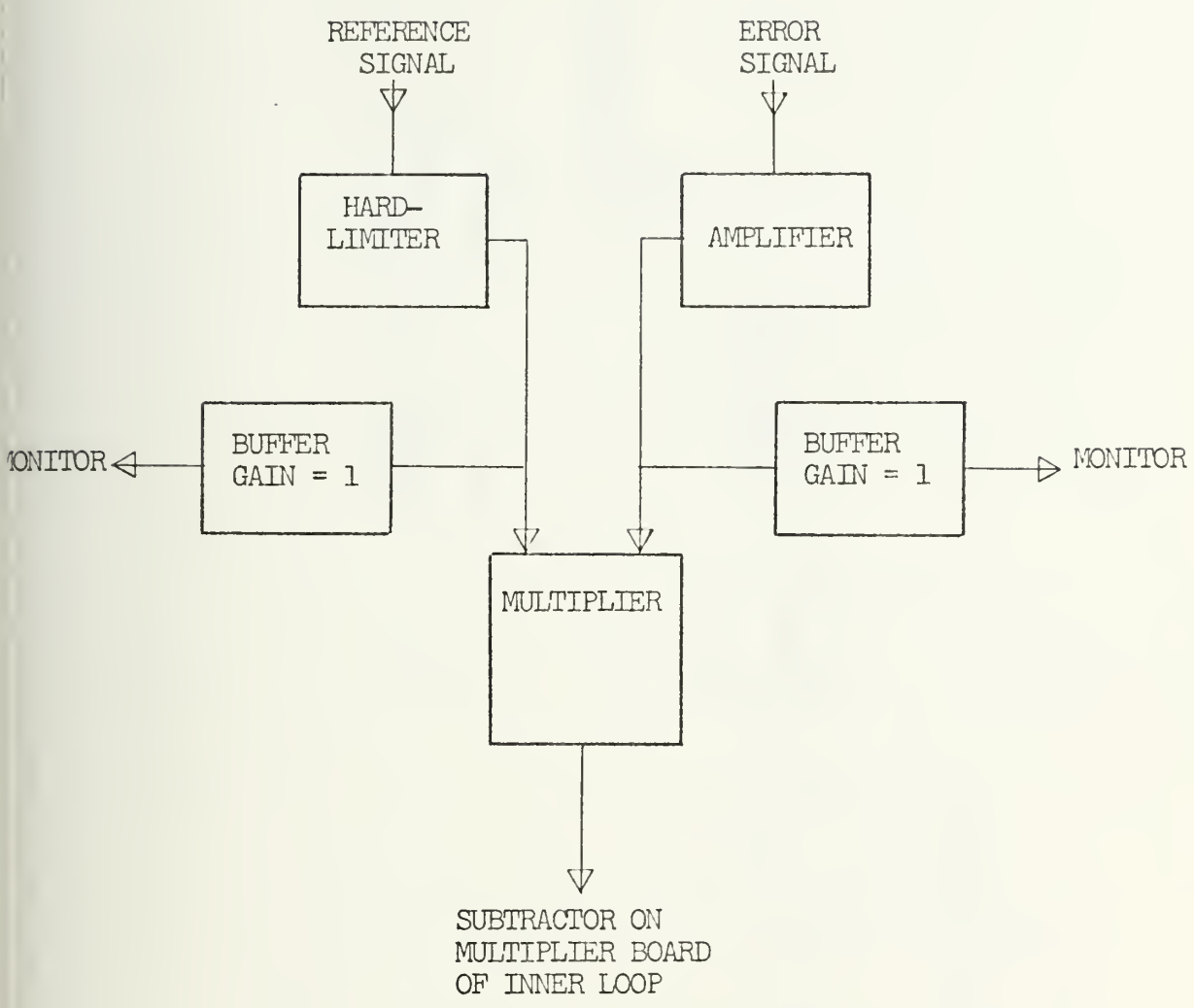

Figure 49 MULTIPLIER BOARD OF OUTER LOOP

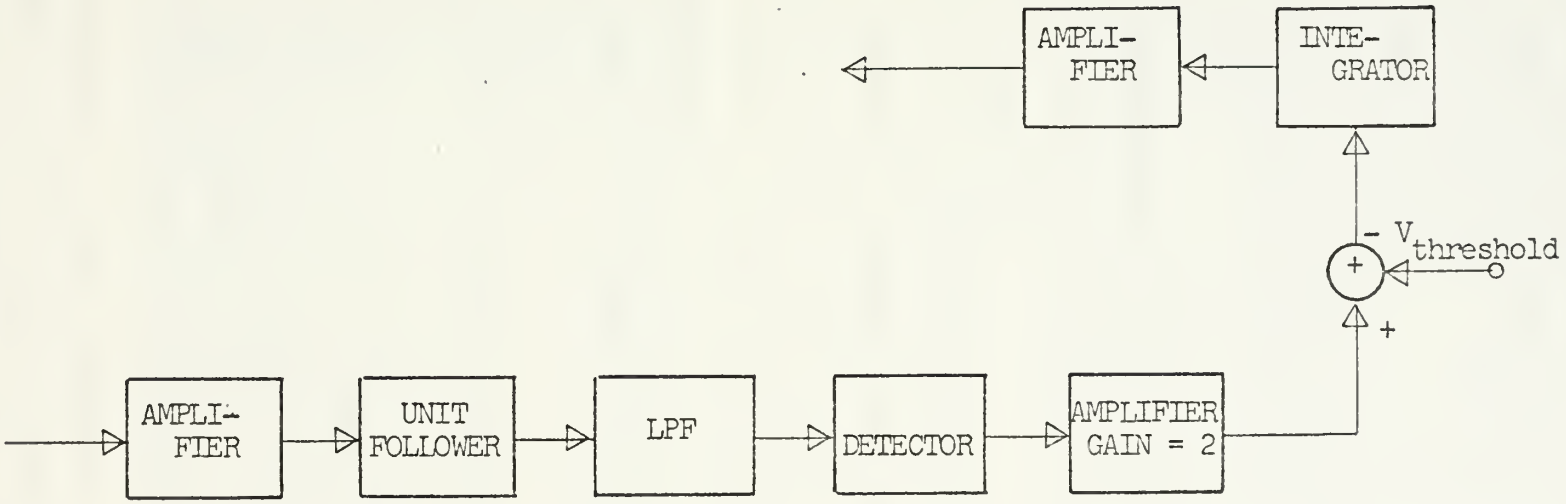

Figure 50 AFC CIRCUIT

band-pass filters for the outer loop are realized by the 10 MHz filter amplifiers with their 2.2 KHz bandwidth.

The front panel of the correlation polarimeter is shown on the photograph (Fig. 51). From left to right one sees:

- the power switch
- the switches and potentiometers for gain adjustment and the selection of amplifier stages in both channels
- the potentiometers to set the gains of the outer loop amplifier, of the AGC circuit and of the servo amplifier
- the control potentiometers for AFC gain and for the reference voltage which sets the free running frequency in the VCO, the AFC on/off switch and the switch to reset the integrator of the AFC
- panel meter
- the selector switches for the band-pass filters in both channels
- the switch to connect different subsystems to the meter
- the switch to set the range of the meter
- the controls for zeroing the multiplier outputs in outer and inner loop
- and all the BNC connectors to connect external instruments to the subsystems

The photograph (Fig. 52) allows a view into the chassis: one sees the back of the front panel with all the different controls

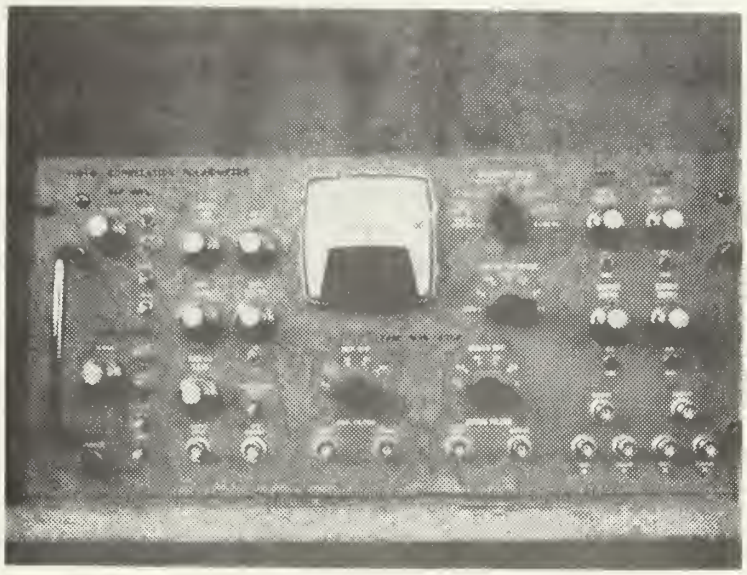

Figure 51 FRONT PANEL OF CORRELATION POLARIMETER CHASSIS

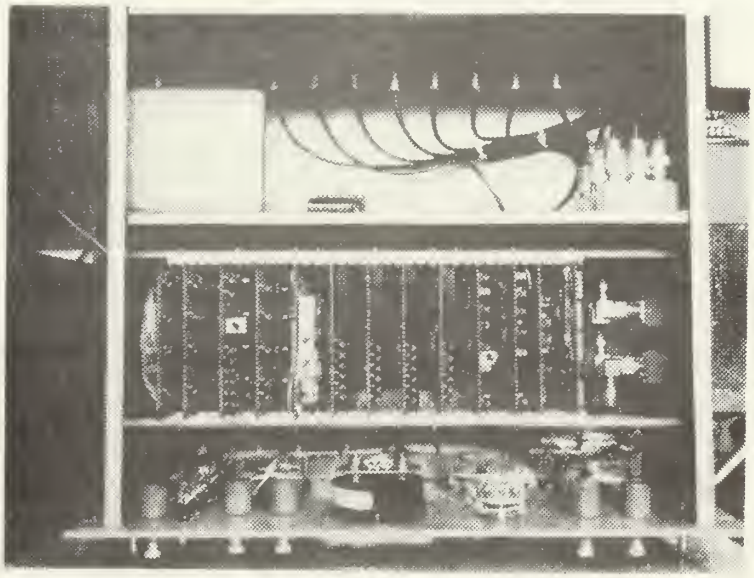

Figure 52 INSIDE VIEW OF CORRELATION POLARIMETER CHASSIS

- the rack with all circuit boards (listing from left to right is provided in Appendix C)
- behind the circuit boards in the left hand corner the system power supply
- on the right side the mixers
- the coaxial cables which run to TNC connector on the back panel

C. SYSTEM PERFORMANCE

The system analysis and the derivation of the performance of the correlation polarimeter described in Section III assume perfect multiplication of the reference and error channel signals in the correlator. Due to the hard-limiter in the reference channel of the actual correlation polarimeter the theoretical rms angle error which is the measure of the system's performance has to be modified by the degradation factor of the hard-limiter.

The hard-limiter is discussed in detail by Davenport [13] and Viterbi [14].

In the correlation polarimeter the output of the band-pass filter in the reference channel passes through a hard-limiter before it is correlated with the error channel signal in the multiplier. In the hard-limiter the SNR of the BPF-output is degradated or enhanced depending on the SNR at the input. The output power remains constant, i.e., the signal power and the noise power sum up to a constant value

$$S_{out} + N_{out} = P_{out} \tag{121}$$

Thus

$$S_{out} = \frac{P_{out}}{1 + SNR_{out}} \tag{122}$$

It is known that

$$SNR_{out} = \mu \, SNR_{in} \tag{123}$$

where μ is the degradation factor, it varies from 2 (+3.01 dB) for high SNR_{in} to $\pi/4$ (-1.05 dB) for low SNR_{in} [15].

The output signal power becomes

$$S_{out} = \frac{P_{out}}{1 + \frac{1}{\mu \, SNR_{in}}} \tag{124}$$

In the multiplier only the fundamental signal component of the hard-limiter output, its amplitude is $4/\pi$ - times the square wave amplitude provided by the hard-limiter, is correlated with the signal in the error channel to give the DC output voltage.

The rms angle error for a pure sine-wave as received signal by the polarizer feed is derived in Section IV.B.4.d. It is given with both channels phased up as

$$\sigma_\theta^2 = \frac{k \, T_e \, W_S}{V_e^2} \left(1 + \frac{k \, T_r \, W_n}{V_r^2}\right) \tag{107a}$$

The hard-limiter in the reference channel degrades the input SNR by μ to give its output SNR. Thus the rms angle error for the correlation polarimeter with hard-limited reference signal is

$$\sigma_\theta^2 = \frac{k\, T_e\, W_S}{V_e^2} \left(1 + \frac{k\, T_r\, W_n}{\mu\, V_r^2}\right) \qquad (125)$$

D. SIGNAL LEVEL CALCULATION

The design conditions for which the system should work are given as follows: The correlation polarimeter should be capable of tracking a -163 dBm signal at a system temperature of 1000° K.

The signal-to-noise ratios for the various bandwidths in the system are calculated as:

TABLE 1

SIGNAL-TO-NOISE RATIOS IN CORRELATION POLARIMETER SYSTEM

Bandwidth Hz	Bandwidth dB	kTB dBm	SNR dB	Voltage SNR
2200	33.4	- 135.2	- 27.8	0.0407
250	24.0	- 144.6	- 18.4	0.1202
125	21.0	- 147.6	- 15.4	0.1698
50	17.0	- 151.6	- 11.4	0.269
25	14.0	- 154.6	- 8.4	0.38
12.5	11.0	- 157.6	- 5.4	0.537
5	7.0	- 161.6	- 1.4	0.851

As reference an input signal to the correlation polarimeter chassis of - 26 dBm is taken. This signal level is provided by the Goldstone receiver system behind the 10 MHz IF amplifier.

Further it is assumed that all amplifiers in the correlation polarimeter will deliver an output of 10 volts peak without saturating. That means they will handle noise of 3.3 volts rms. The resulting signal levels are shown on the block diagram of the system (Fig. 53).

It may be possible to track a signal of - 163 dBm at a system temperature of 1000° K if the filter bandwidth is narrow, i.e. 5 - 25 Hz, but it is most unlikely that tracking will be possible under these conditions with wide filter bandwidths. Therefore the margin at the output of the error channel amplifier in front of the multiplier can be relaxed by a factor of 2 (6 dB). Thus the error input signal to the multiplier can have 1.1 volt rms when the polarizer is at 90°.

E. CALIBRATION OF SERVO INPUT VOLTAGE

For the coherent polarimeter system the servo input voltage required at a feed-system position of 45° is 3.0 VDC (using AGC). The error signal goes as the tangent of the polarizer angle, θ [3].

$$\text{servo input} = \varepsilon = 3.0 \frac{\tan \theta}{\tan 45°}$$

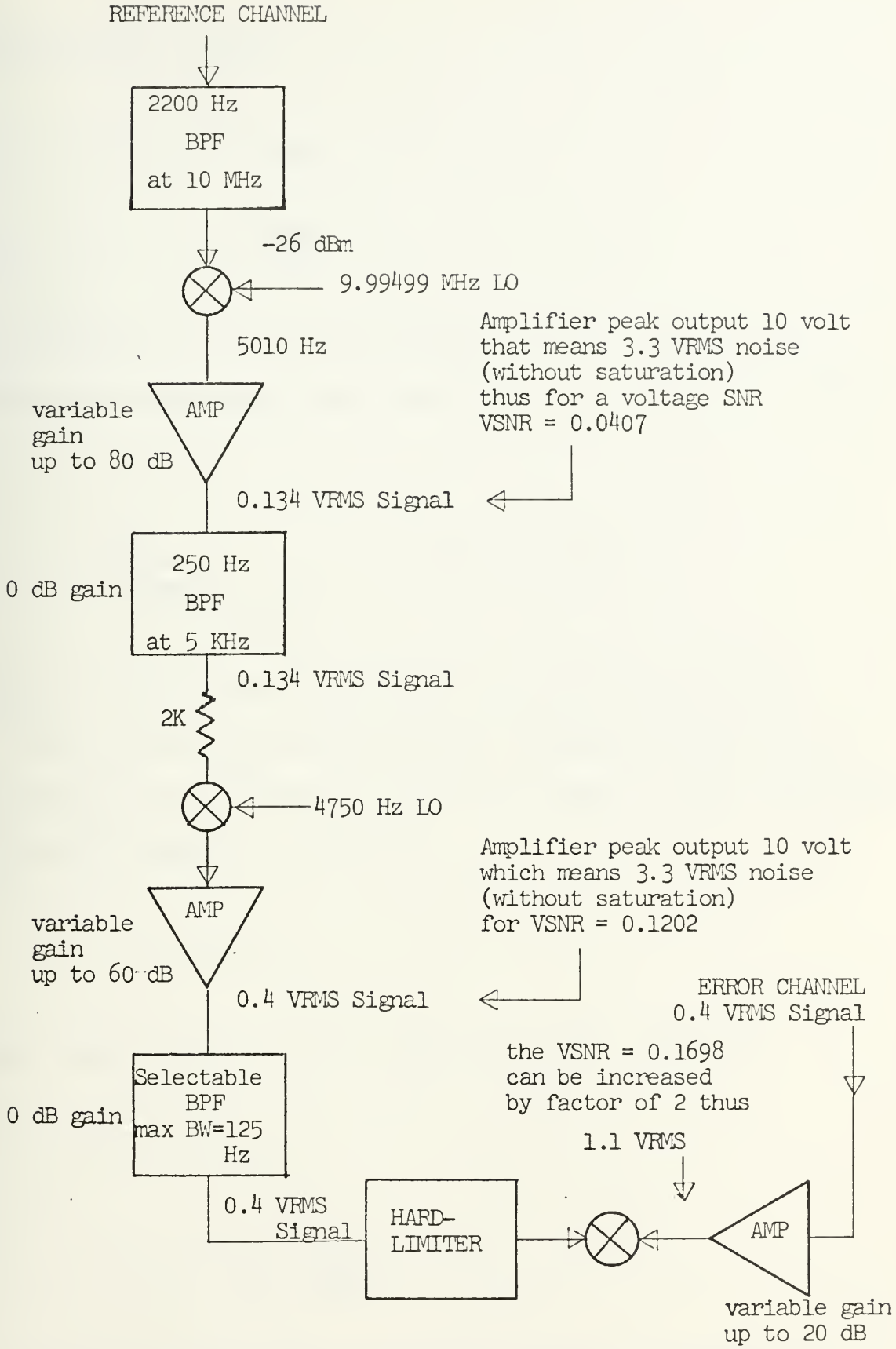

Figure 53 SIGNAL LEVELS IN CORRELATION POLARIMETER

Assuming small angles

$$\varepsilon = 3.0\ \theta_{rad}$$

$$\varepsilon = 3.0\ \frac{\theta_{deg}}{180^\circ}$$

The variation of the servo voltage with the angular position of the polarizer about the reference position, $\theta = 0^\circ$, is

$$\left.\frac{d\ \varepsilon}{d\ \theta_{deg}}\right|_{\theta_{deg}=0^\circ} = \pi/60 = 0.052$$

Rounded off, the variation is 50 millivolts per degree.

Due to the hard-limiter in the reference channel which is assumed to be noiseless the error signal in the correlation polarimeter system is given as

$$\varepsilon = K \sin \theta$$

which can be rewritten for small polarizer angles as

$$\varepsilon = K\ \theta_{rad}$$

$$\varepsilon = K\ \theta_{deg}\ \frac{\pi}{180}$$

To drive the servo motor properly a voltage variation of

0.05 volts per degree is desired. This means

$$\frac{d\,\varepsilon}{d\,\theta_{deg}} = 0.05 = K\,\frac{\pi}{180}$$

which results in a gain constant of K = 2.86.

Thus the error signal can be expressed as

$$\varepsilon = 2.86 \sin \theta$$

Now for a polarizer angle of 45° the error signal voltage to be fed to the servo system must be ε = 2.02 volts.

When the reference or the error channel is aligned with the polarizer reference position the signals in the BPF outputs are to be 0.4 volts rms, then when the polarizer is at 45° the signals will drop to 0.283 volts rms. At these levels the final amplifier in the correlation polarimeter chassis must provide a servo voltage of 2.0 volts.

VI. TEST-SERIES WITH THE CORRELATION POLARIMETER

A. CHECKING CIRCUIT BOARDS AND CHASSIS

1. Functional Performance of Circuit-Boards

a. Amplifier-Boards

Each amplifier stage was checked separately for desired amplification of 20 dB after the output offset was nulled by the 10 K-ohm trim pot for zero input. An offset would cause an unsymmetric amplification, i.e. different saturation levels for positive and negative inputs. The amplifiers are AC-coupled by RC high-pass filters to prevent DC flow.

b. Local Oscillator Board

The output frequency of the local oscillator is 4750 Hz. The band-pass filter in the output of the LO was adjusted to 4750 Hz as center frequency and its gain was set to give an output signal level of 0.5 volts rms across a 50 ohm load (the desired +7 dBm for the mixer LO-input) at both output terminals.

c. Band-Pass Filter Boards

(1) Stagger tuned BPF. For both filters with a bandwidth of 250 Hz at a center frequency of 5 KHz the frequency response and phase response curves were taken. (Figs. 54, 55) Both filters have the same response in magnitude and phase. Because the input signal to the system has a finite spread in frequency phase matching between both channels across the entire bandwidth of the filters is required.

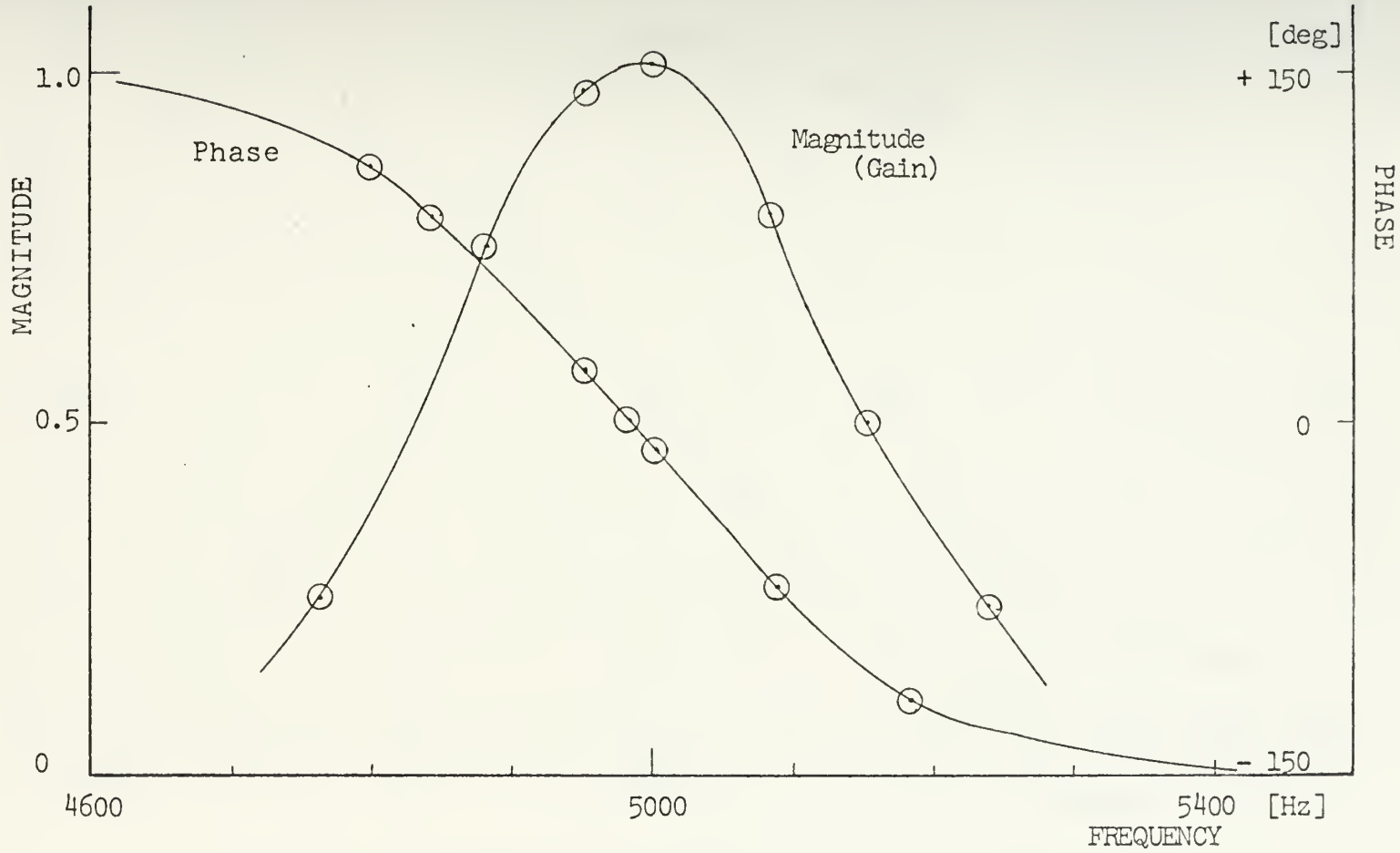

Figure 54 FREQUENCY RESPONSE OF 250 HZ BAND-PASS FILTER IN REFERENCE CHANNEL

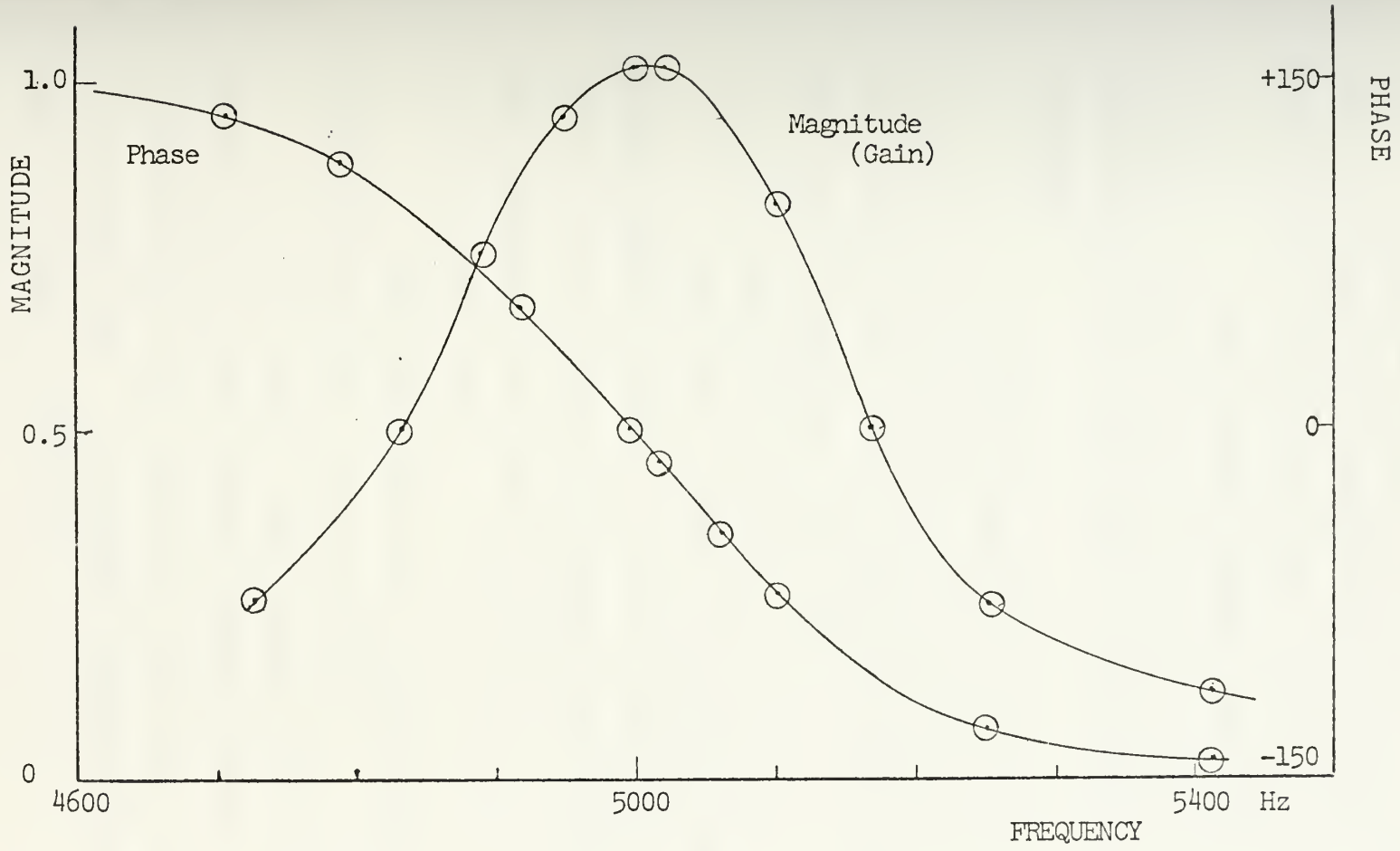

Figure 55 FREQUENCY RESPONSE OF 250 HZ BAND-PASS FILTER IN ERROR CHANNEL

(2) Single tuned BPF. The center frequency, f_c, for all filters was adjusted to 260 Hz by means of the 20 K trim pots (they are in series with 5 K fixed resistances). The frequency response and phase response curves were taken.

As for the stagger tuned BPF's matching of the phase response curves in the two channels is desired. This matching held true within a few degrees over the filter bandwidths.

Different gains of the filters do not affect the system operation because with the 500 ohm trim pots the filter input levels can be adjusted so that the filters give equal output amplitudes. (Fig. 56)

d. Multiplier Boards

The output offset of the amplifiers were nulled for zero input by means of the 10 K trim pots. Applied signals are AC-coupled by high-pass RC-filters so the multiplier inputs were multiplied properly.

e. AGC Board

The amplifier output offsets were nulled by means of the 10 K trim pots for zero inputs.

For various input signal levels (AC-coupled to prevent any DC input) the AGC output voltage was measured in front of the final amplifier whose gain can be adjusted on the front panel. The output voltage is plotted versus signal strength in Fig. 57.

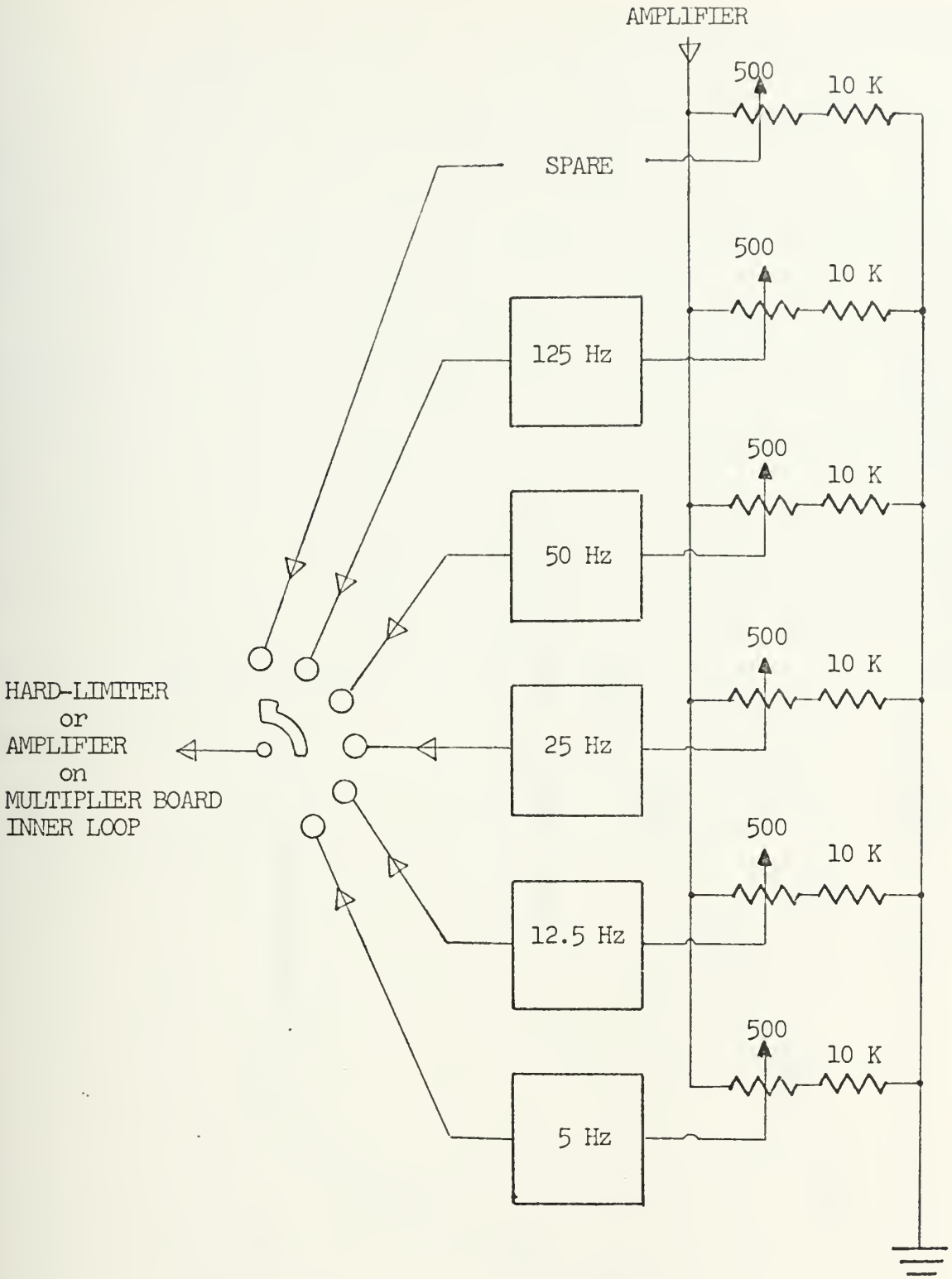

Figure 56 BAND-PASS FILTER SELECTION
AND INPUT ADJUSTMENT

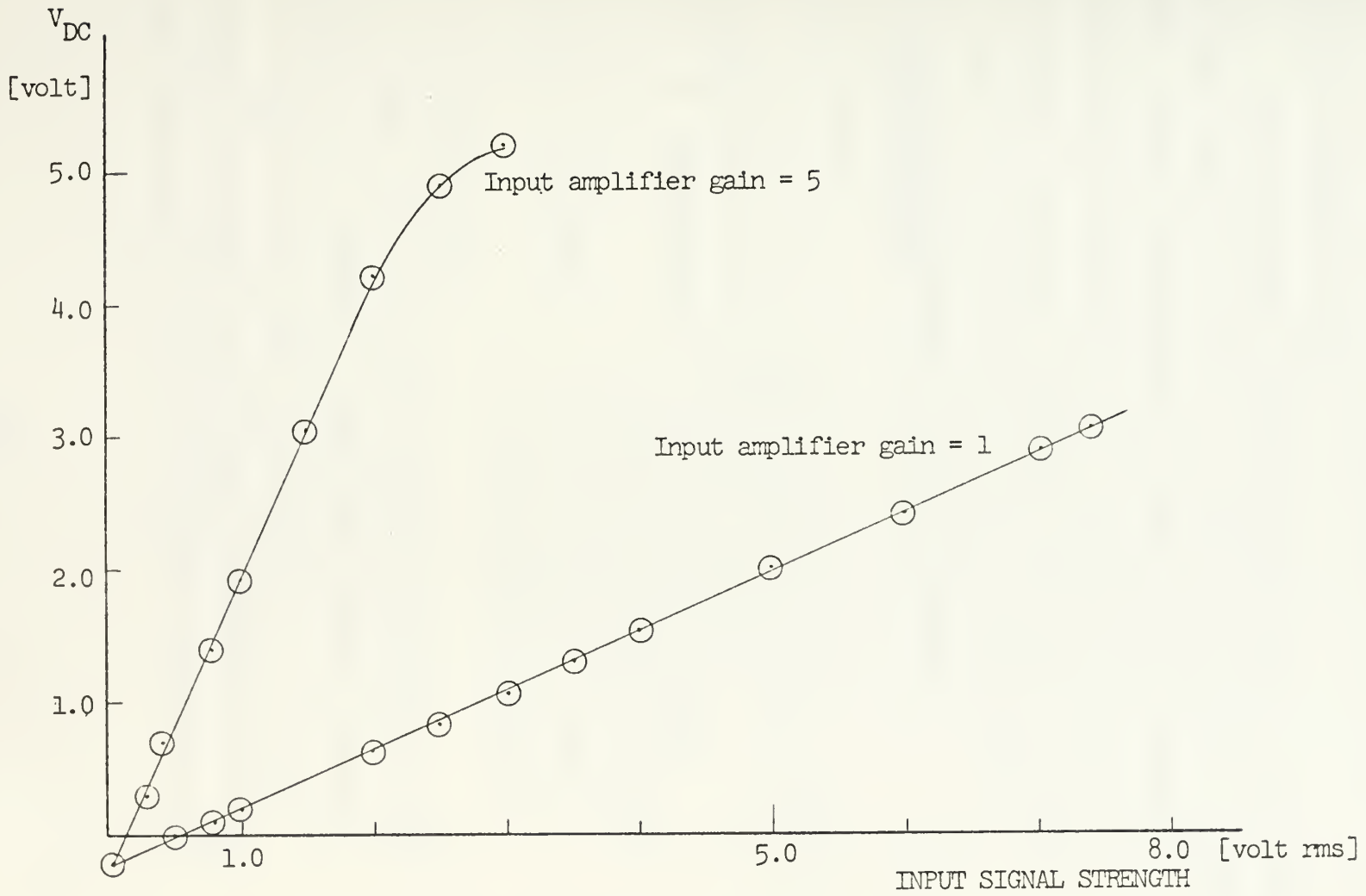

Figure 57 AGC OUTPUT VOLTAGE

f. AFC Board

The output offsets of the amplifiers were nulled. The integrator was inspected for proper functioning. The output offset of the low-pass filter with a cut-off frequency of 250 Hz was trimmed to zero.

The AFC output voltage was adjusted to zero volts for an input frequency of 260 Hz. Then the DC output voltage of the AFC circuit was measured in front of the integrator for various input frequencies and is plotted in Fig. 58. For this curve, the signal was applied directly to the AFC circuit and did not involve any of the preceding BPF's.

2. Functional Performance of the Components in the Chassis

a. Mixers

From external signal generators input signals to the L- and R-ports of the mixers were applied:

Mixers 1 - 3 (RELCOM-M6E): 10 MHz signal to R-port
9.99499 MHz signal to L-port

Mixers A - B (MCL-SRA6): 5.01 KHz signal to R-port
4.75 KHz signal to L-port

b. Panel Meter

The different meter ranges (selectable by the range switch) were checked by applying different voltage levels to a port of the meter input switch. It worked correctly in all ranges. The diodes in parallel with the meter give the desired protection against overdriving it.

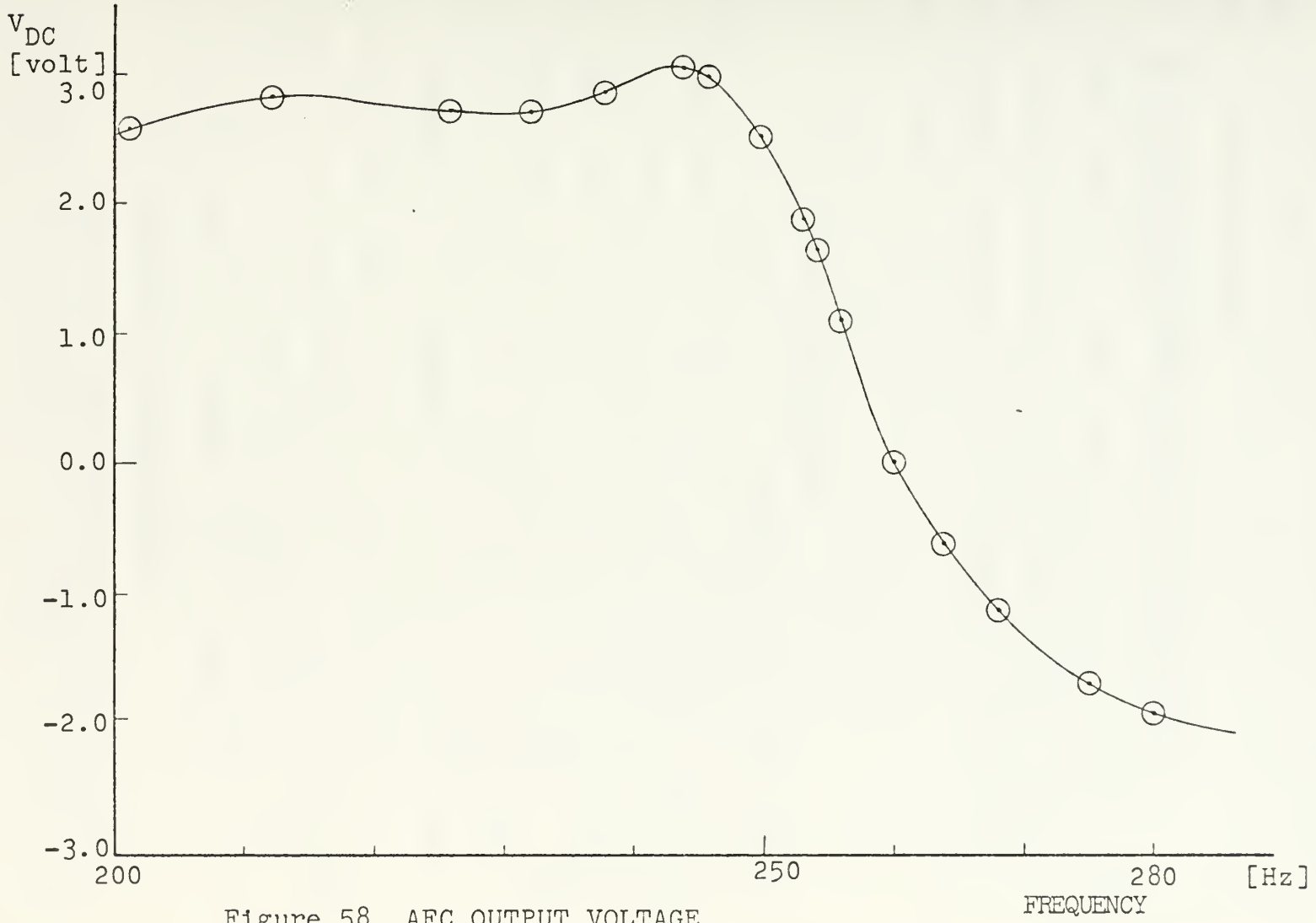

Figure 58 AFC OUTPUT VOLTAGE

c. Power Supply

The power supply delivers regulated undistorted voltages of +15 volts, -15 volts, and +5 volts, and can be checked by the panel meter.

3. Functional Performance of the Circuit Boards in the Chassis

Each board was tested separately in the chassis. Its supply voltage was delivered by the system's power supply. External signal generators (where necessary) and external meters and counters were used.

a. Amplifier Boards

(1) 5 KHz IF Amplifiers

By means of the switches on the front panel the different amplifier stages can be selected and also the gain of the first amplifier stage can be adjusted continuously in the range from $-\infty$ dB to 20 dB. Up to 80 dB of amplification are provided, since each stage has 20 dB of gain. This is fixed for the second thru fourth stage. The amplifiers can be selected in any combination. If they are switched in order the front panel labels on top of each switch indicates the total maximum gain used. If all switches are off (down) the four amplifiers are bypassed and the mixer output is fed directly to the BPF (250 Hz bandwidth).

(2) 250/260 Hz IF Amplifiers

These two amplifiers have a gain of 60 dB. The input level can be adjusted by a 1 K-ohm trim pot. To

filter out a little more of the 5 KHz a capacitor is put across the feedback resistor, although the amplifier by itself cuts off about 1 KHz.

b. Band-Pass Filter Boards

(1) Stagger tuned BPF's (f_c = 5 KHz). The two BPF's separated from each other worked properly. But on the board in the chassis there was crosstalk of up to 20 dB in each direction between them. This crosstalk of the 5010 Hz signal occured at their outputs. By encasing the filters in aluminum foil the effect could be reduced to about -40 dB but not completely eliminated. It is either a ground loop problem or case-to-case capacitive coupling. A physical separation on two boards would be more helpful.

(2) Single tubed BPF's (f_c = 260 Hz). The mixers A and B were connected to the BPF selector switches. For the mixer output signals of equal amplitude in both channels the outputs of all filters were adjusted to the same level by means of the 500 ohm trim pots in the input branches.

c. Multiplier Boards

(1) Inner Loop. The multiplier was calibrated as described in Section VI.B. Then a 260 Hz signal from an external siganl generator was fed into the BPF inputs (the 260 Hz IF amplifiers were removed) using the test set up shown in Fig. 59. The reference signal was adjusted to 0.4 volts rms at BPF input and the error signal strength was varied by means of the attenuator. The phase shifter in the

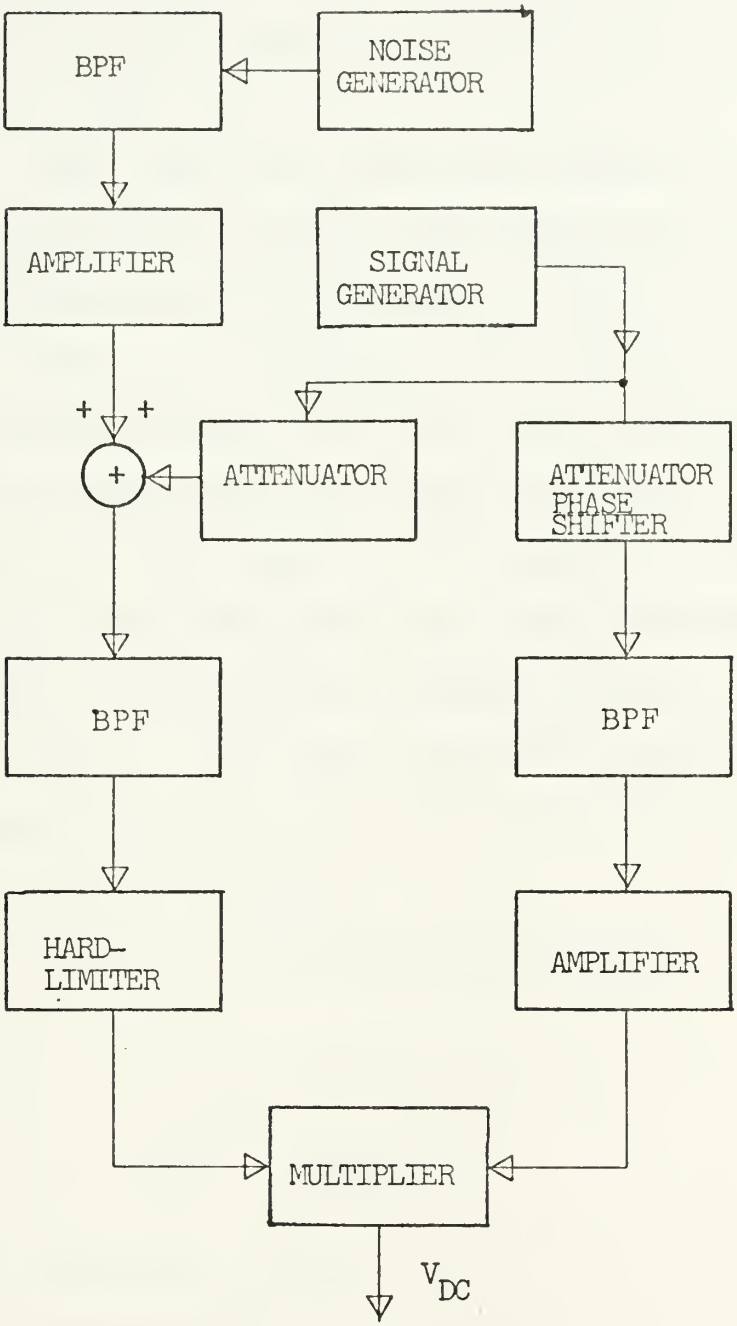

Figure 59 MULTIPLIER TEST SET-UP

error channel allowed setting the phases of reference and error signal to the same value and its also provided the possibility of a 180° flip of the error signal for a check. The multiplier DC output voltage is plotted versus error signal strength in Fig. 60.

Then signal and noise were applied to the BPF input in the reference channel (amplifier board, board #12 was removed) while the 260 Hz signal in the error channel was kept at 1.0 volt rms. The purpose of this error channel signal was to allow coherent detection of the reference channel effective amplitude out of the hard-limiter. For different signal-to-noise ratios in the reference channel the multiplier output voltage was measured. The normalized multiplier output voltage then was plotted versus the input signal-to-noise ratio. This curve shows the suppression factor of the hard-limiter in the reference channel with respect to the input SNR (Fig 61).

In Ref. 13 the suppression factor is given as

$$\gamma = \frac{1}{\sqrt{1 + \frac{1}{\mu \, SNR_{in}}}}$$

where $\mu = \pi/4$ for small SNR and

$\mu = 2$ for high SNR

(see [13], [14], and [15]).

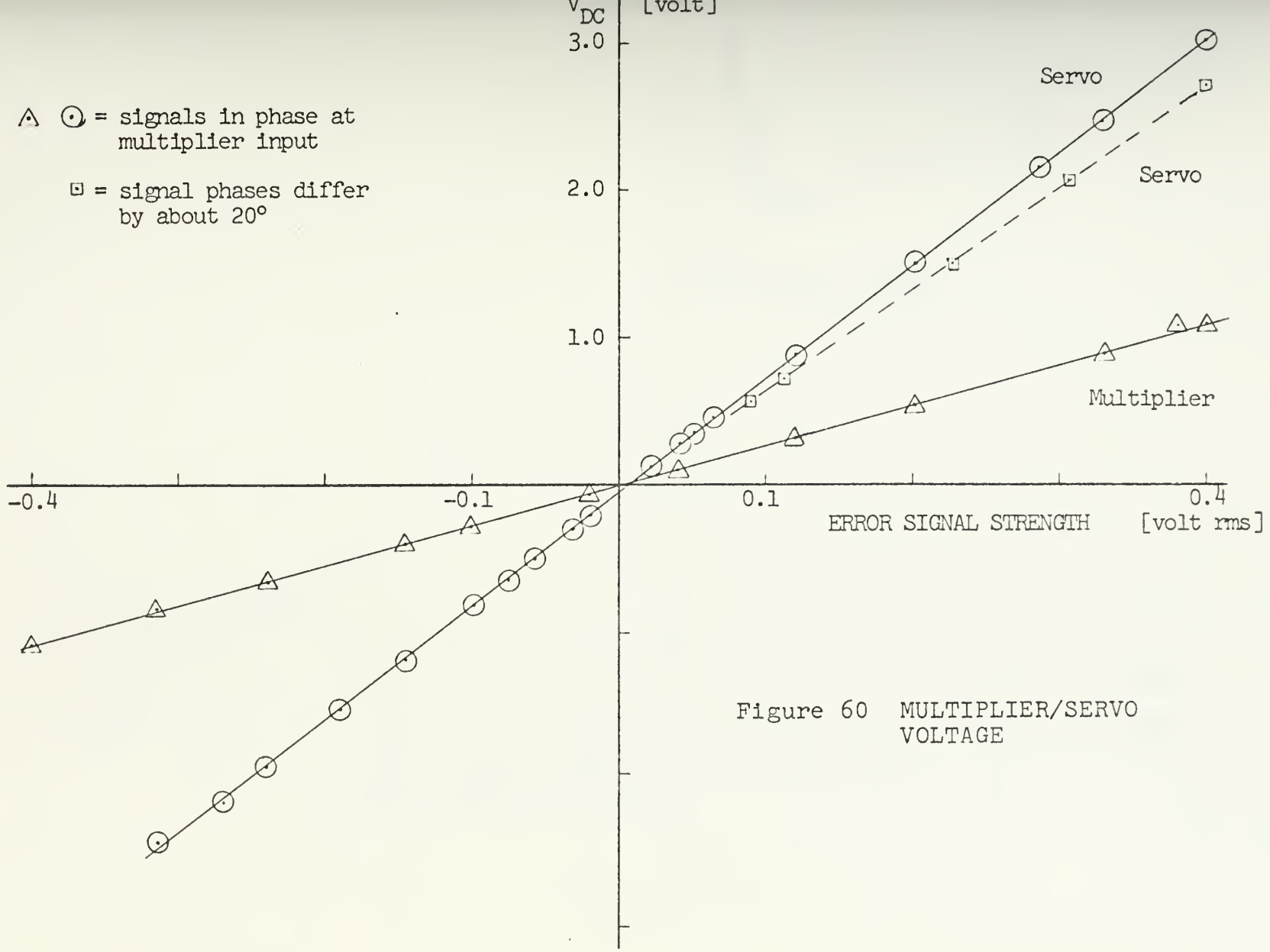

Figure 60 MULTIPLIER/SERVO VOLTAGE

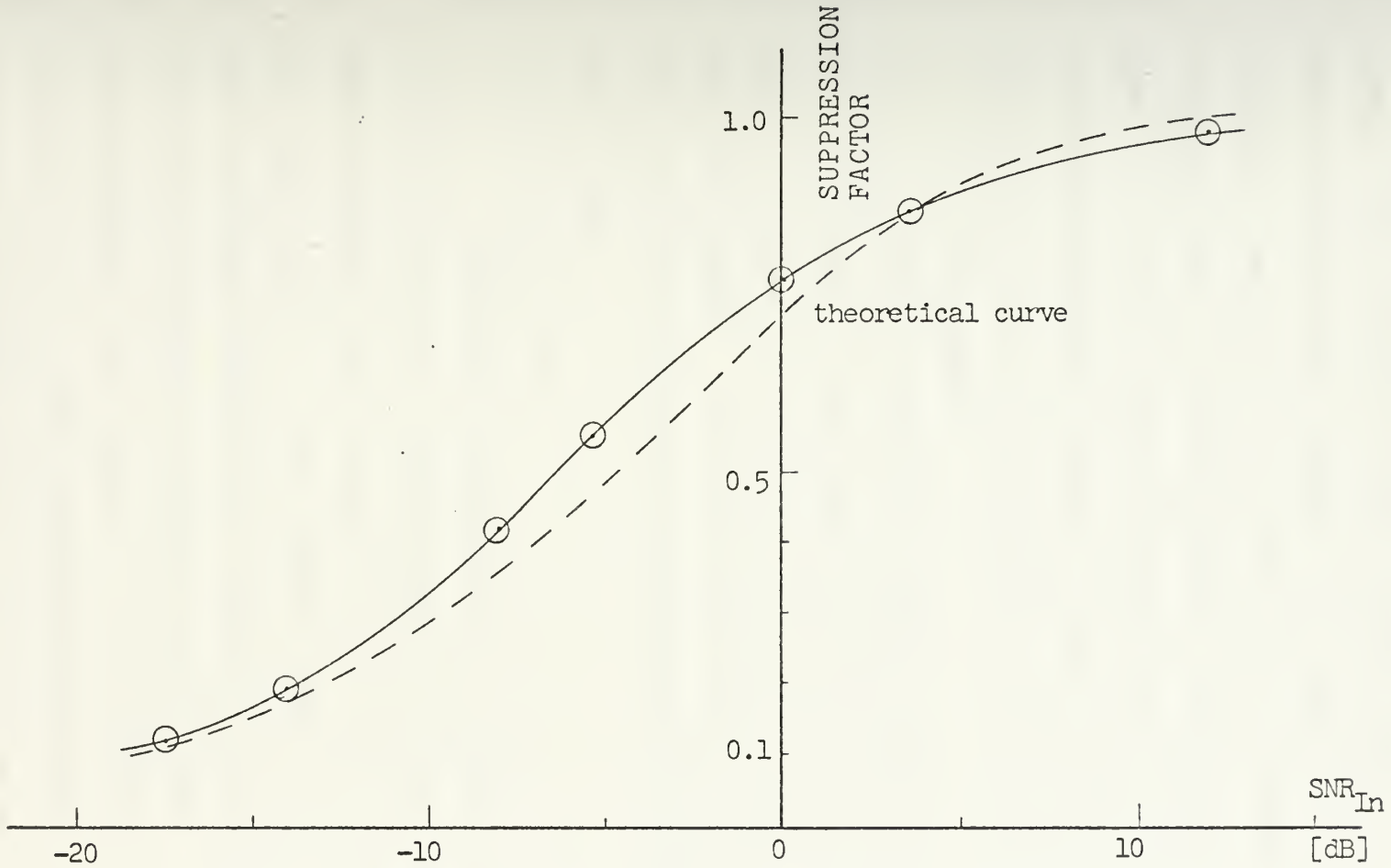

Figure 61 LIMITER SUPPRESSION FACTOR VERSUS INPUT SIGNAL-TO-NOISE RATIO

(2) Outer Loop. The outer loop multiplier was calibrated as described in Section VI.B. The output signals of the mixers 1 and 3 are AC-coupled to the amplifiers in both channel inputs. The amplified signal in the reference channel is hard-limited and AC-coupled to the reference input of the multiplier, the amplified error channel signal is directly fed to the error input of the multiplier via a AC-coupling RC filter. By means of the 50 K trim pots the input levels in both branches could be adjusted.

d. AGC Board

With a reference channel signal of 0.4 volt rms the input level of the input amplifier of the AGC circuit was set to give 1.1 volt rms before the diode – just as in the error channel – then the potentiometer "AGC Gain" on the front panel was adjusted to provide an AGC output voltage of + 1.0 volts.

e. AFC Board

Frequency changes of the reference signal (input to mixer 2) causing changes about the center frequency of the band-pass filters resulted in an AFC output voltage. This then was fed to the "Search" input of the HP-Synthesizer and its output frequency was adjusted automatically such that the mixer 2 provided a 5010 Hz output signal. With the V_{ref} potentiometer (front panel) the VCO frequency was set to 9994990 Hz for an AFC voltage equal to zero. The proper polarity of the AFC output voltage can be selected by means of the switch on the board.

4. Adjustments of the Assembled System

In order to allow testing of the assembled system without worrying about frequency drift the test set up shown in Fig. 91 was used. It provided stable signals and local oscillator frequencies.

The gains of the amplifiers throughout the system were set according to the signal level calculation. The 0.4 volt rms at the filter outputs were used during all tests as standard levels, i.e. the input amplifiers in the error and reference channels were adjusted by means of the switches and the potentiometers on the front panel to give this voltage for any applied signal.

The multipliers were calibrated as described in Section VI.B.

The phase shifter in the error channel local oscillator branch was set to give reference and error signal at the multiplier inputs equal phase, i.e. maximum DC output voltage of the multiplier. Then the frequency of the 5010 Hz generator was varied about this value which resulted in a variation of the fourth IF about the 260 Hz, the center frequency of the filters. With a digital phasemeter the phase difference between both channels was observed as the frequency varied. It remained for all practical purpose at a constant zero phase difference. The phase responses of the filters of equal bandwidth differed at center frequency by at most 2°.

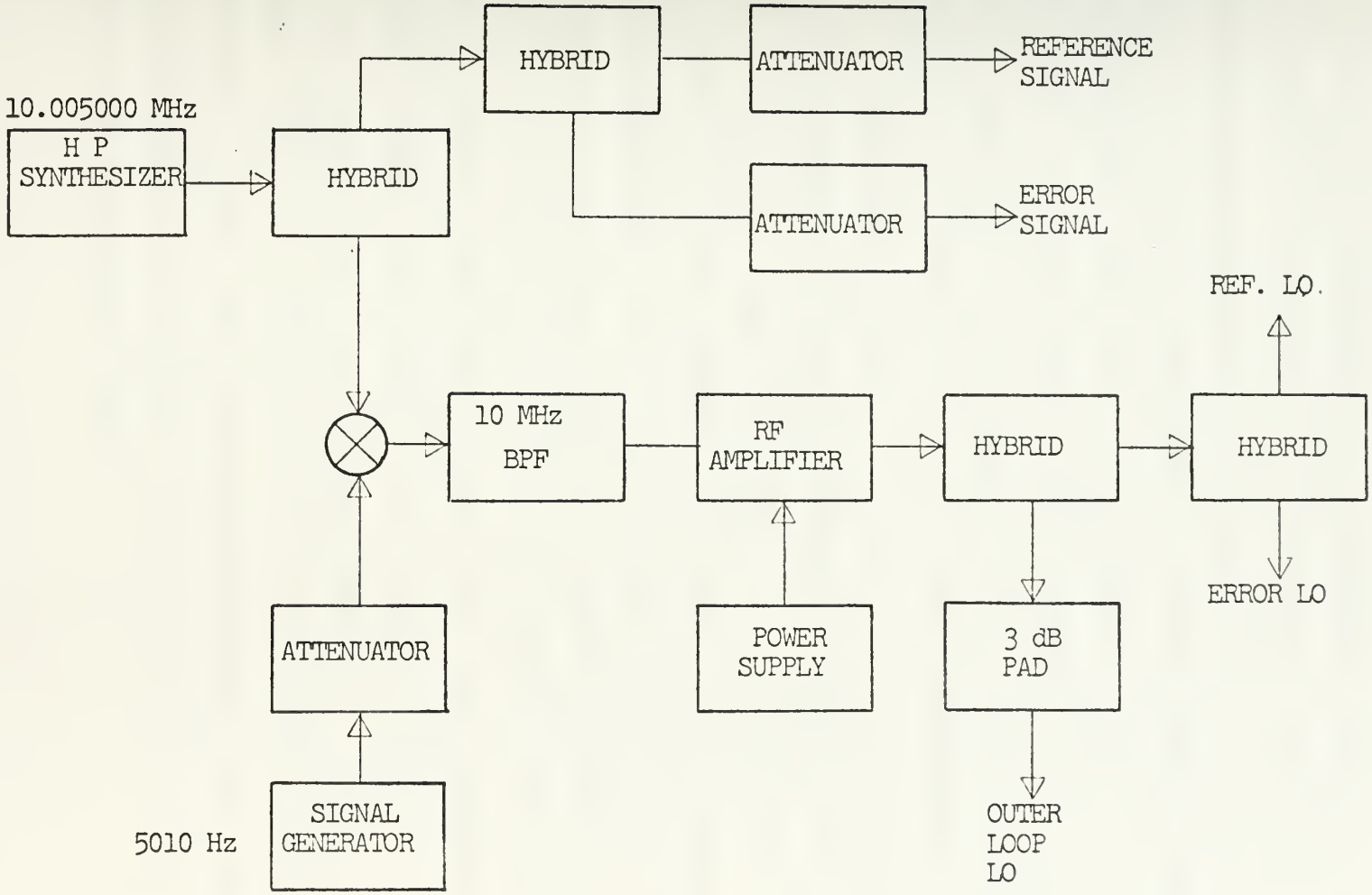

Figure 91 SIGNAL GENERATION FOR TEST SERIES

B. MULTIPLIER ZEROING

To zero the multipliers, the reference and error channels are connected to the signal sources, while leaving the reference signal high (0.4 volt rms at BPF output) the error signal is attenuated completely. With the potentiometer on the front panel "REF ZERO: the multiplier output is set to zero volts. Then the error signal is applied (0.4 volt rms at BPF output) and the multiplier output is made symmetric (using an oscilloscope) by means of the potentiometer "ERROR ZERO." The phase shifter in the local oscillator branches are then adjusted to give the reference and the error signal at the multiplier input equal phase, i.e. to maximize the multiplier DC output voltage. Then go back and attenuate error signal again and do final zeroing with the "REF ZERO".

With the error signal applied symmetry of multiplier output and its DC voltage can now be checked. Flipping the phase shifter by 180° should (and does) give a symmetric DC output voltage (same strength but opposite sign).

The idea in this calibration procedure is that the hard limited reference signal will always be present — even if due only to noise — so zeroing should be done with high reference signal level and it should not be set to zero when zeroing the multiplier output.

C. TESTS AT THE GOLDSTONE TRACKING STATION (GTS)

1. Connecting Correlation Polarimeter Chassis to GTS-Receiver

No.	Receiver Device	disconnected from	connected with
1	J 2 , 10-MHz IF amplifier in ref. channel (linear) (5A404)[2]	J 1 , 10-MHz phase detector (AGC)	Ref signal input of CPC[1]
2	J 2 , 10-MHz IF ampl. in angle channel (5A105)	J 1 , 10-MHz phase detector	Error signal input of CPC
3	J 4 , 50-MHz IF ampl and mixer (5A102)	J 1 , 500 Hz band-pass filter (special)	J 1 , variable attenuator (5A104)
4	J 2 , 500-Hz band-pass filter (special)	J 1 , variable attenuator (5A104)	
5	J 2 , 10-MHz distrib. ampl (5A114)	50 ohm termination	Ref channel LO of CPC
6	J 1 , 10-MHz distrib. ampl (5A114)	BP 2 , servo driven phase sh. (5A113)	VCO output (AFC loop of CPC) connected externally (HP Synth.)
7	J 2 , 10-MHz phase shifter (5A110)	J 2 , 10-MHz phase detector (5A106)	BP 1 , servo driven phase sh. (5A113)
8	BP 2 , servo driven phase sh. (5A113)	J 1 , 10-MHz distrib. ampl. (5A114)	Error channel LO of CPC

---

[1]CPC stands for Correlation Polarimeter Chassis.

[2]Referes to module position in receiver [11].

No.	Receiver Device	disconnected from	connected with
9	J 2 , 10-MHz phase shifter (5A109)	J 2 , 10-MHz phase detector (5A117)	Outer loop LO of CPC
10	J1 and J2 , AGC amplifier (5A305)	J3 and J4 , 10-MHz phase detector (5A406)	AGC output of CPC
11	Servo electronics	J3 and J4 , 10-MHz phase detector in angle channel (5A117)	Servo input of CPC
12	VCO search input (HP Synthesizer)		AFC output of CPC
13	Low voltage power supply		In-lock-relay to go on, so polarizer servo can go into track

The connection of the correlation polarimeter chassis to the GTS receiver system (Fig. 64) and the servo system of the coherent polarimeter is shown also in the blockdiagrams, Fig. 62 and Fig. 63.

2. Signal Generation

A test transmitter generated a signal of 19.10030800 MHz which then was multiplied by 120 to give the desired S-band signal. This was injected by means of two probes into the feed horn of the 64 meter antenna. This linearly polarized signal travelled down the waveguide system to the front-end amplifiers (maser) and in coaxial cables to the 50-MHz and 10-MHz mixer/amplifiers. These 10-MHz signals then were fed into the correlation polarimeter chassis.

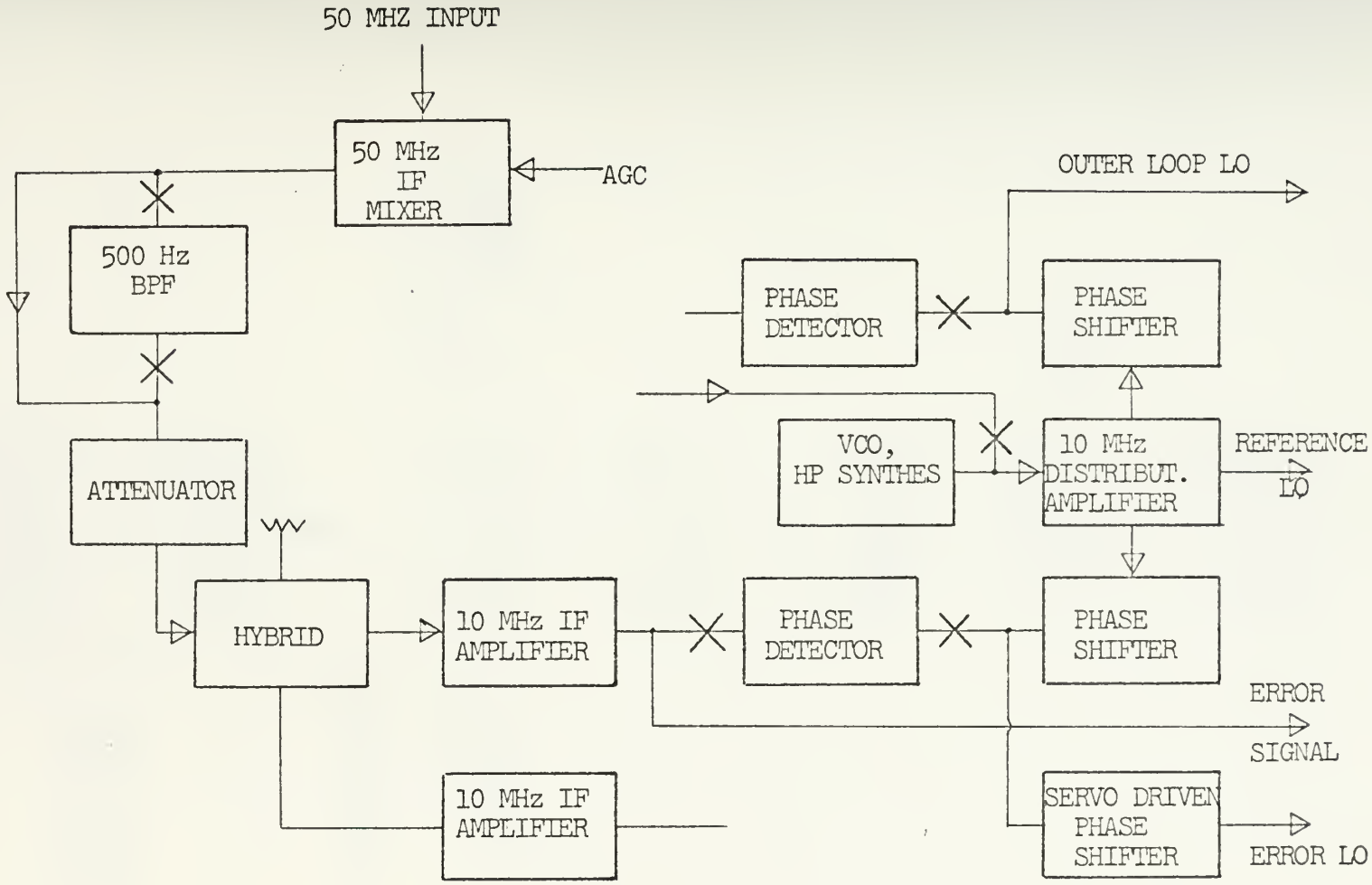

Figure 62 CONNECTION OF CORRELATION POLARIMETER CHASSIS TO ANGLE CHANNEL OF RECEIVER 1

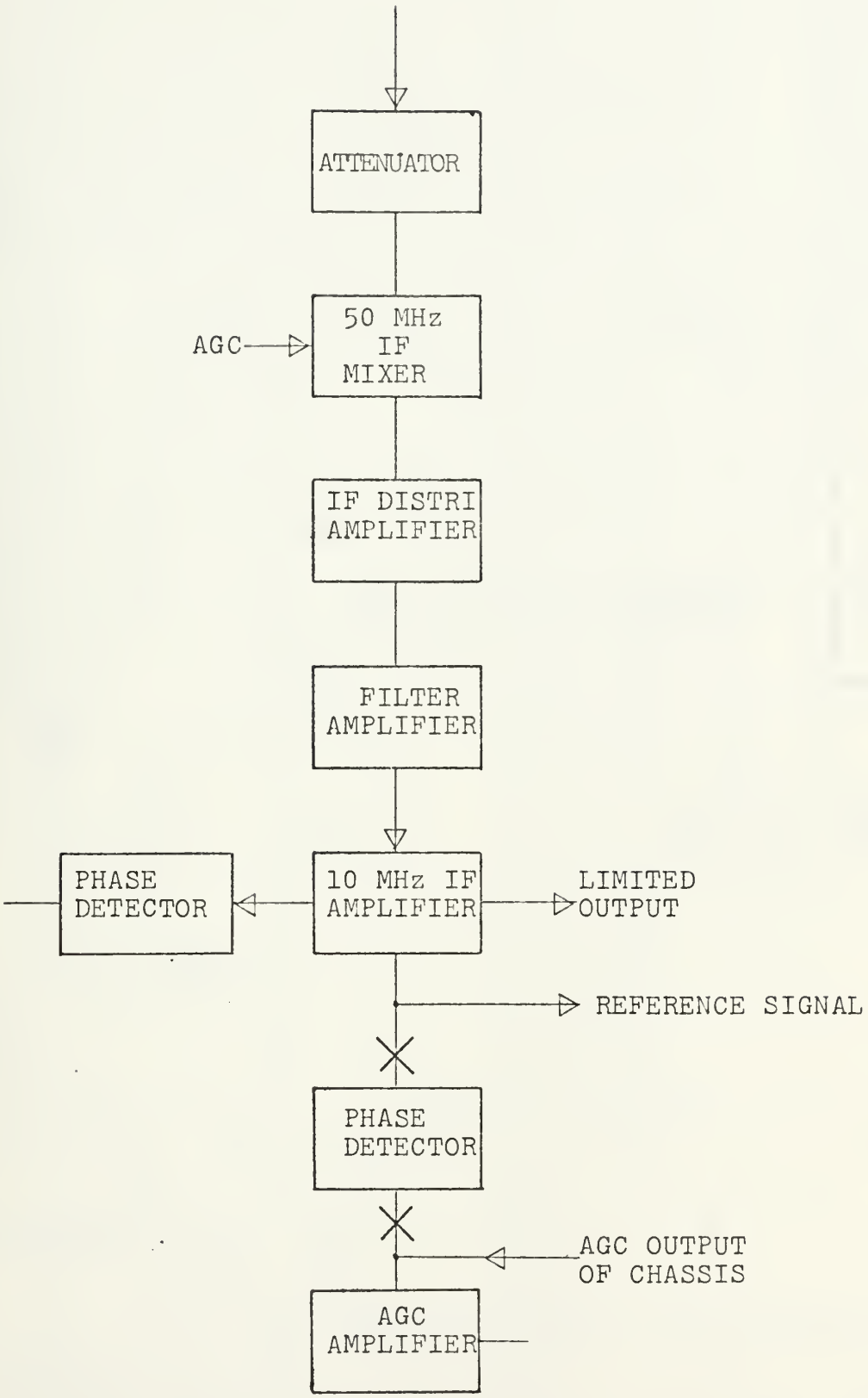

Figure 63 CONNECTION OF CORRELATION POLARIMETER CHASSIS TO REFERENCE CHANNEL OF RECEIVER 1

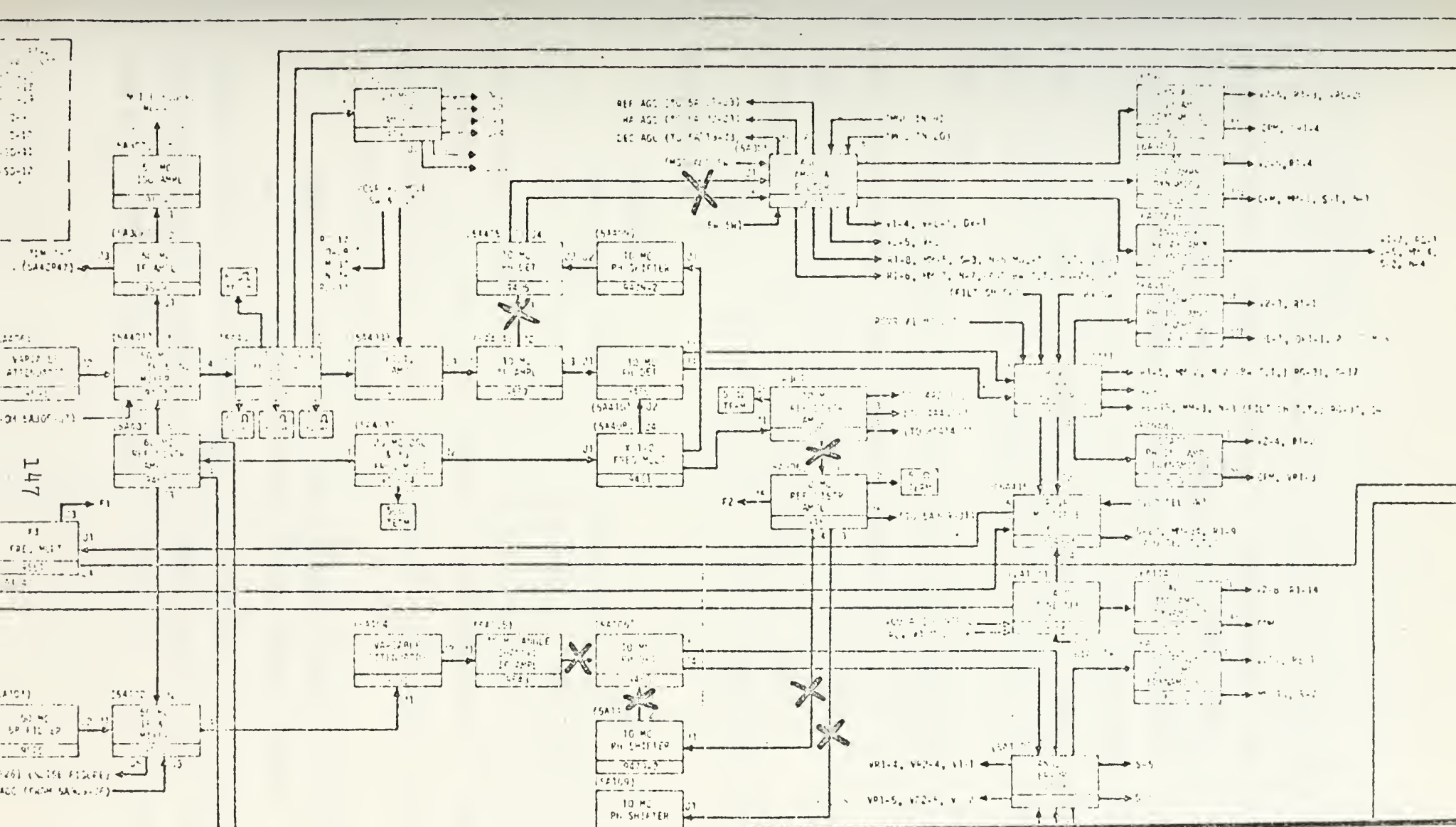

Figure 64 PART OF DSN S-BAND RF RECEIVER/EXCITER SUBSYSTEM BLOCKDIAGRAM WHERE CORRELATION POLARIMETER WAS CONNECTED TO.

(Cable Connections)

3. Adjustments

The GTS receiver was set to operate in the linear amplifier region of its response. The polarizer was turned to 0°-position and the input amplifier in the reference channel of the correlation polarimeter was adjusted to give the standard signal level of 0.4 volt rms at the BPF outputs. With the polarizer at 90°-position the error channel amplifier gain was set to provide a signal at the BPF outputs of 0.4 volt rms.

The multipliers in both loops were calibrated properly; the Z_o-position of the variable attenuator in the angle channel was used to completely attenuate the error signal, the polarizer was at 45° to the calculated 2.0 volts.

The AGC output voltage was 1.0 volt for the standard signal level.

4. AGC Test

With the polarizer at 0°-position the AGC voltage of 1.0 volt was applied to the AGC amplifier. The gain control was working properly and the response times for the three available loop bandwidths seemed to be comparable to those for the phase-locked-loop operation for which they are about 1.5, 0.15, and 0.05 seconds. [11]

5. Response Time of the Polarization Tracking System

The test transmitter delivered a strong signal. The signal levels in the correlation polarimeter were adjusted to the 0.28 volts rms behind the band-pass filters; the polarizer was set to 45°. Servo voltage was 2.0 volts. On the tracking

command the polarizer turns towards the reference position (0°), overshoots and then settles down to the reference position. For different servo loop bandwidths the response times (first crossing of the reference position) have been measured:

TABLE 2

RESPONSE TIMES OF POLARIZATION TRACKING SYSTEM

Bandwidth No.	Response Time (sec)
1	110
2	93
3	inoperative
4	25
5	9.5
6	3

6. Error Signal Curve

For a strong input signal the polarizer was turned with constant speed. The servo input voltage provided by the correlation polarimeter was recorded versus polarizer angle (Fig. 65).

Due to the hard-limiter in the reference channel the servo voltage curve does not show the sinusoidal shape of Section III.B., since the limiter keeps the reference multiplier input at a constant level, even for a decreasing reference signal. Now as the polarizer approaches 90° the error channel signal is near its maximum the reference signal

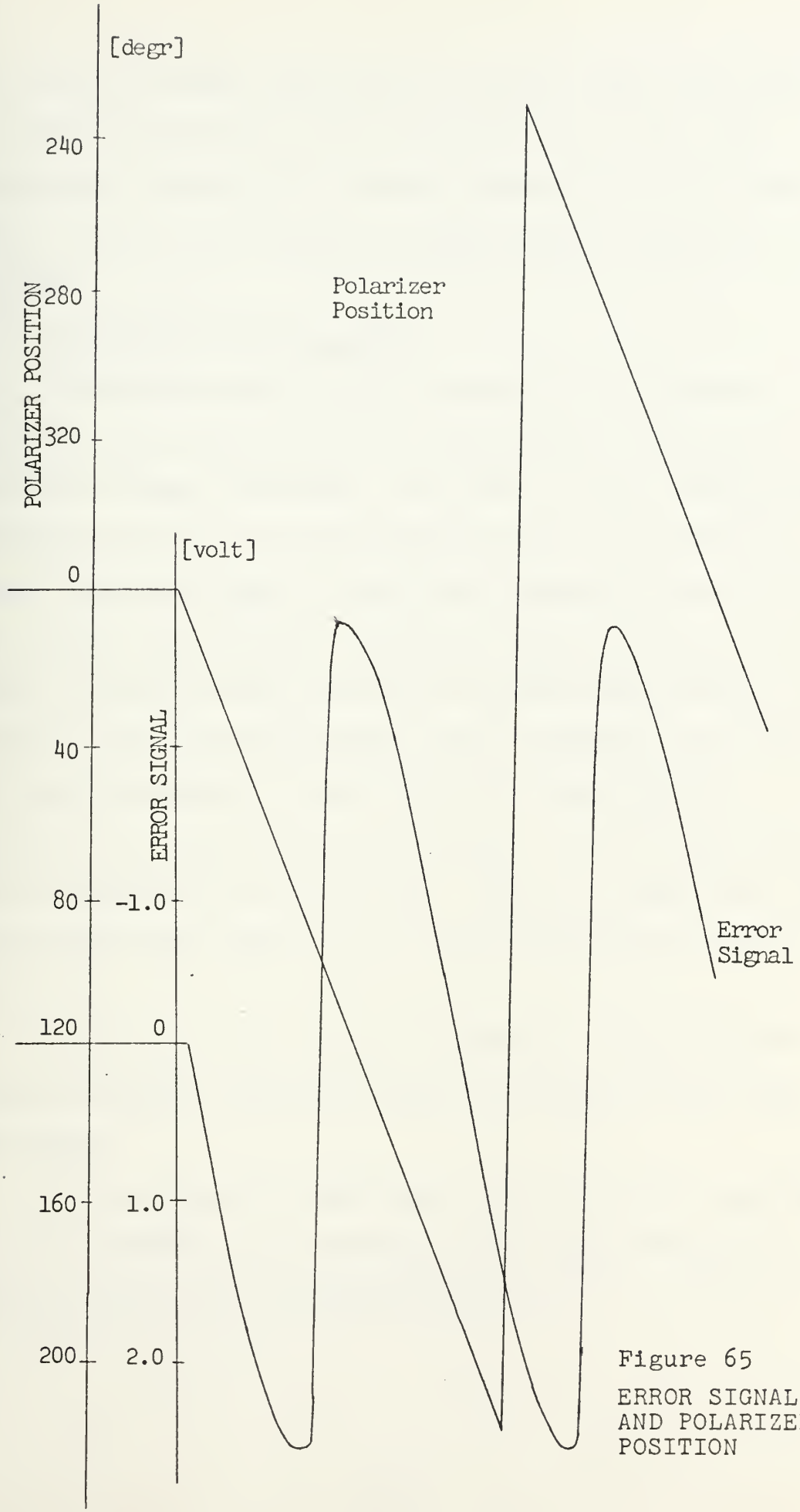

Figure 65

ERROR SIGNAL CURVE AND POLARIZER POSITION

drops below a certain value and the square wave behind the hard-limiter breaks down, but it builds up as fast with opposite sign beyond 90°. Another possibility is that the SNR gets low in the reference channel and the signal is suppressed.

7. Tracking of Probe Signal

The servo output of the correlation polarimeter electronics was connected to the correlation polarimeter. For various signal strengths — the gains in the correlation polarimeter were set to the standard level — the polarizer tracked the probe signal. The system temperature was 25° K. Table 3 shows the results. These are only preliminary data. Further the probe signal at various system temperatures (up to 1000° K) are necessary before final comments can be made about the performance of the correlation polarimeter.
To get the very high system temperatures, the 64 meter antenna must be directed close to the sun. Prior to these noise tests the receiver gains must be set so that saturation does not occur.

Tracking of the telemetry carrier of a spacecraft by the correlation polarimeter has to be part of the final test series.

The correlation polarimeter could be fully operational by 1974 during the German/American Project "HELIOS," a satellite to the far side of the sun.

TABLE 3

TRACKING RESULTS

Signal-Strength[1]	BPF bandwidth	Servo loop bandwidth	Response Time	Standard Deviation of Polarizer Angle
dBm	Hz		sec	degrees
-160	5	#6	3	1.13
-160	125	#6	3	1.73
-165	5	#6	3	1.2 , 1.46
-147	5	#5	9.5	1.0

[1]The signal strength was determined from the AGC curve of receiver 2 which was operating in phase-locked-loop configuration. Prior to these measurements both receiver systems were calibrated.

VII. CONCLUSION

It was shown by means of the working model that the theory of the correlation polarimeter is valid.

An actual system for the Goldstone Tracking Station 64-meter antenna was designed and constructed. This then was integrated into the GTS receiver system and showed its capability of tracking the plane of polarization of a linearly polarized test signal injected into the feed system by probes.

A high noise test has not yet been performed. Prior to the use of the correlation polarimeter at high noise temperatures the amplifier gains in the GTS receiver must be set so that saturation does not occur. Also test data should be taken with high noise temperature so a final check can be made versus the theory.

The crosstalk between the two 250 Hz band-pass filters can be eliminated or at least significantly reduced by separating them in the chassis.

Modifications of the correlation polarimeter chassis or development of a standard version should consider the following suggestions:

As far as possible, error and reference channel components should be physically separated to eliminate crosstalk. The multipliers should be replaced by actual phase detectors which are passive devices so that DC drift problems would be minimal. The output of the correlation polarimeter chassis

for the servo voltage should be floated from ground (i.e. high and low outputs) to be directly compatible with the GTS receiver system and to help prevent DC ground loop problems. An ellipticity channel as provided by the coherent polarimeter should be included in the correlation polarimeter.

APPENDIX A

COMPONENTS OF THE WORKING MODEL

No.	Description	Manufacturer	Model No.
For transmitting part:			
1	Signal generator	Hewlett-Packard Synthesizer	5105 A
		and Driver	5110 B
2	RF amplifier	Advantek	ADP - 3T
3	Attenuator	Telonic	TAB - 40A
4	Dipole		
For receiving part:			
1	Crossed dipole arrangement with DC-servomotor	Inland Motor Corp.	
	Shaft-angle-encoder	Decitrak	
2	Mixer	Relcom	M 6 E
3	Signal generator	Hewlett-Packard	608 C
	(as local oscillator)		
4	Trombone line	General Radio Corp	874-LTL
	(as phase shifter)		
5	Amplifier	Hewlett-Packard	465 A
		- " -	461 A
		- " -	450
		Krohn Hite	DCA - 50
6	Filter	Allison	2 C
		Krohn Hite	310 C
		self built LC	

No.	Description	Manufacturer	Model No.
7	Noise generator	General Radio Corp	1390 B
8	Power supplies	Power Design Inc	3650 - S
		- " -	3240
		Power Mate Corp	BP 34 D
9	DC-servo amplifier	Inland Controls	150 A
10	Multiplier	Teledyne Philbrick Nexus	4452
11	Integrator		
	using operat. ampl.	Burr Brown	3112/12C
		Fairchild	A 741
12	Inverter		
	using op. amp.	Burr Brown	3112/12C
13	Inverter		
	using	Fairchild	A 741
For the tests:			
1	Voltmeter, true rms	Hewlett-Packard	3400 A
2	Counter, Freq.	Computer Measurement Corp.	AN/USM 207
3	Strip chart recorder	Moseley Autograf	7100 B
4	Oscilloscope		
5	Set up to measure polarization angle (see Fig. 34)		
6	Vector Voltmeter	Hewlett-Packard	8405 A
7	Phasemeter, digital	Wiltron Comp.	355

APPENDIX B

CIRCUIT DIAGRAMS OF WORKING MODEL COMPONENTS

Shown are the integrator and inverter circuits. The power supply connections are not drawn.

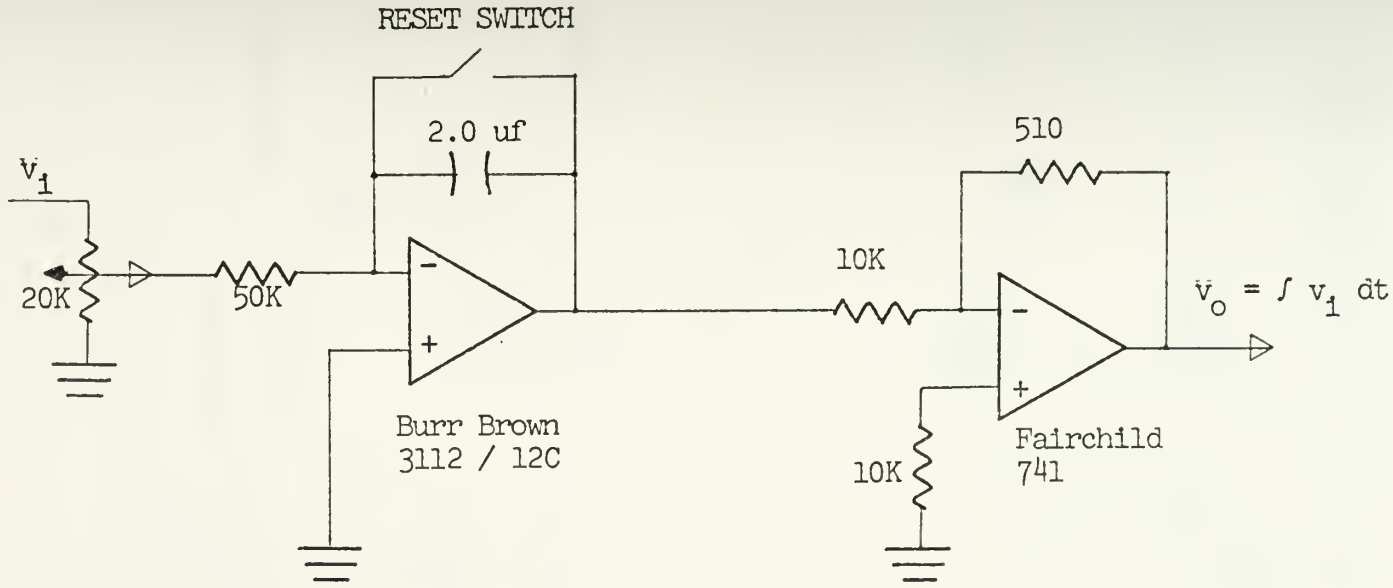

Figure 66 INTEGRATOR WITH INVERTER STAGE
(used in working model)

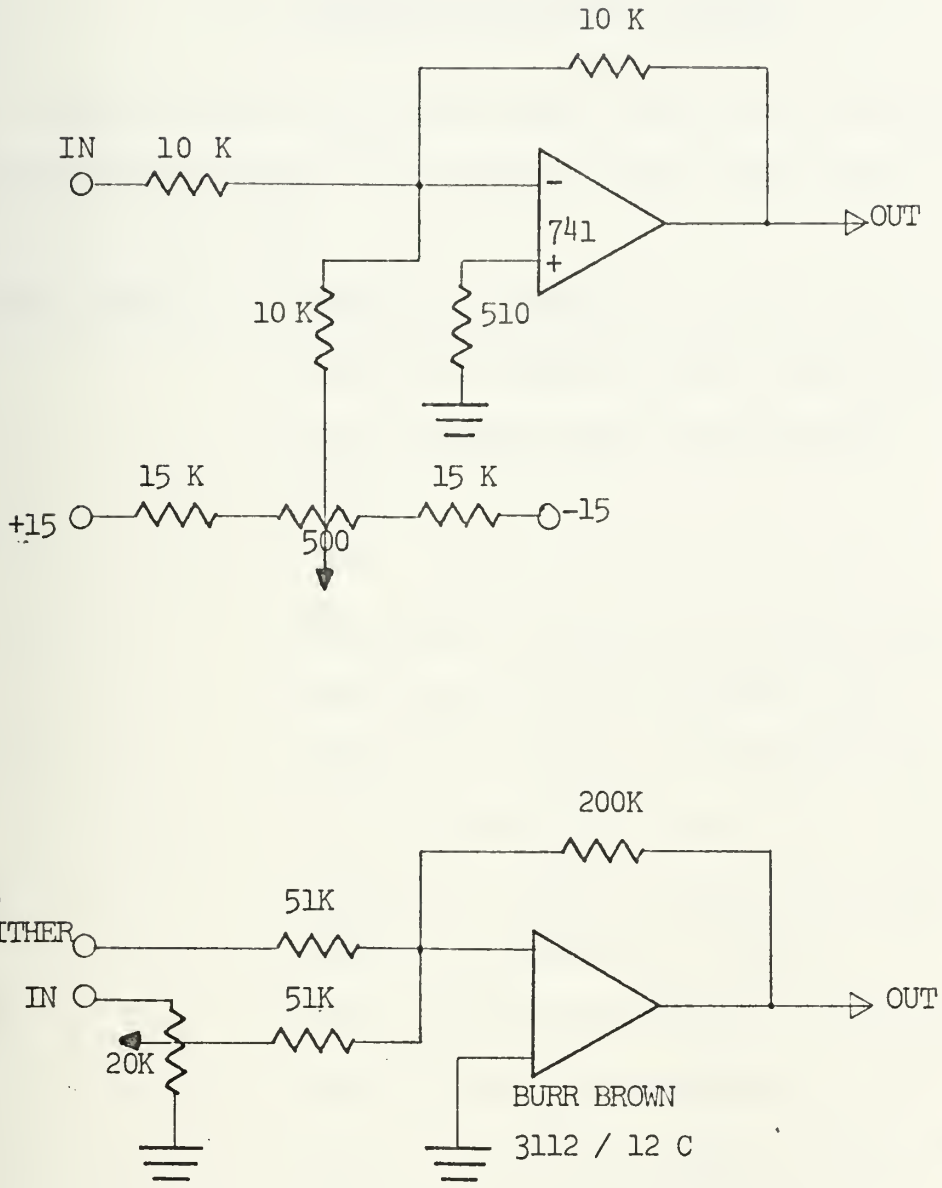

Figure 67 a) INVERTER, to invert multiplier output and to cancel multiplier output offset
b) INVERTER, second input to add a Dither signal
(both used in working model)

APPENDIX C

LISTING OF CIRCUIT BOARDS

Looking from the front panel into the correlation polarimeter chassis the circuit boards from left to right (see Fig. 52) are:

Board Number	Circuit on Board
1	Reference channel input amplifiers
2	Error channel input amplifiers
3	AFC
4	AGC
5	Band-pass filters with 250 Hz bandwidth (Bw) about the center frequency (f_c) of 5 KHz
6	Reference channel band-pass filter, BW: 5 Hz, 12.5 Hz, and 25 Hz about f_c = 250 Hz
7	Reference channel band-pass filters, BW: 50 Hz and 125 Hz about f_c = 250 Hz
8	Error channel band-pass filters, BW: 5 Hz, 12.5 Hz, and 25 Hz about f_c = 250 Hz
9	Error channel band-pass filters, BW: 50 Hz and 125 Hz about f_c = 250 Hz
10	Multiplier of inner loop
11	Multiplier of outer loop
12	Amplifiers (4^{th} IF, outer loop output, servo input)
13	4750 Hz local oscillator

APPENDIX D

IDENTIFICATION OF TRIM POTS ON BOARDS

The trim pots on the circuit boards are numbered. The following table is a summary of their functions.

Trim pot No.	Value	Function
1 - 8, 10-14, 16, 18 - 21, 47 - 48, 50 - 51, 53 - 54, 56 - 57, 59, 61, 64	10 K	Zeroing of the DC offset of the operational amplifiers with corresponding numbers
9	10 K	DC offset adjustment of low-pass filter on in AFC circuit
15	10 K	Gain adjustment for AFC input
22	10 K	Gain adjustment for AGC input
23	20 K	Frequency adjustment of reference channel band-pass filter (Ref. BPF), BW = 5 Hz
24	500	Input level adjustment to ref. BPF, BW = 5 Hz
25	20 K	Frequency adjustment of ref. BPF, BW = 12.5 Hz
26	500	Input level adjustment to ref. BPF, BW = 12.5 Hz

Trim pot No.	Value	Function
27	10 K	Frequency adj. of ref. BPF, BW = 25 Hz
28	500	Input level adj. to ref. BPF, BW = 50 Hz
29	20 K	Frequency adj. of ref. BPF, BW = 50 Hz
30	500	Input level adj. to ref. BPF, BW = 50 Hz
31	20 K	Frequency adj. of ref. BPF, BW = 125 Hz
32	500	Input level adj. to ref. BPF, BW = 125 Hz
33	20 K	Frequency adj. of ref. spare
34	500	Input level adj. to ref. spare
35 - 46		Frequency and input level adj. for error channel BPF's, same order as for reference channel
49	50 K	Input level adj. of error signal input to multiplier of inner loop
52	50 K	Input level adj. of reference signal input to multiplier of inner loop
55	50 K	Input level adj. of error signal input to multiplier of outer loop
58	50 K	Input level adj. of reference signal input to multiplier of outer loop
62	1 K	Input level adj. to reference 4th IF amplifier
63	1 K	Input level adj. to error channel 4th IF amplifier
72	100	Adj. of center frequency of BPF in the 4750 Hz LO output
73	50 K	Gain adj. of the BPF in the 4750 Hz LO output
74	10 K	Adj. of AFC threshold voltage

APPENDIX E

CIRCUIT DIAGRAMS

The diagrams of the circuits realized on the boards of the correlation polarimeter chassis and for the working model are shown in Figs 68-76.

For simplicity the power supply connections for the circuit components are not drawn.

In order to make identification of the operational amplifiers used in these circuits possible, all amplifiers are numbered on the boards and these numbers are shown circled on the diagrams.

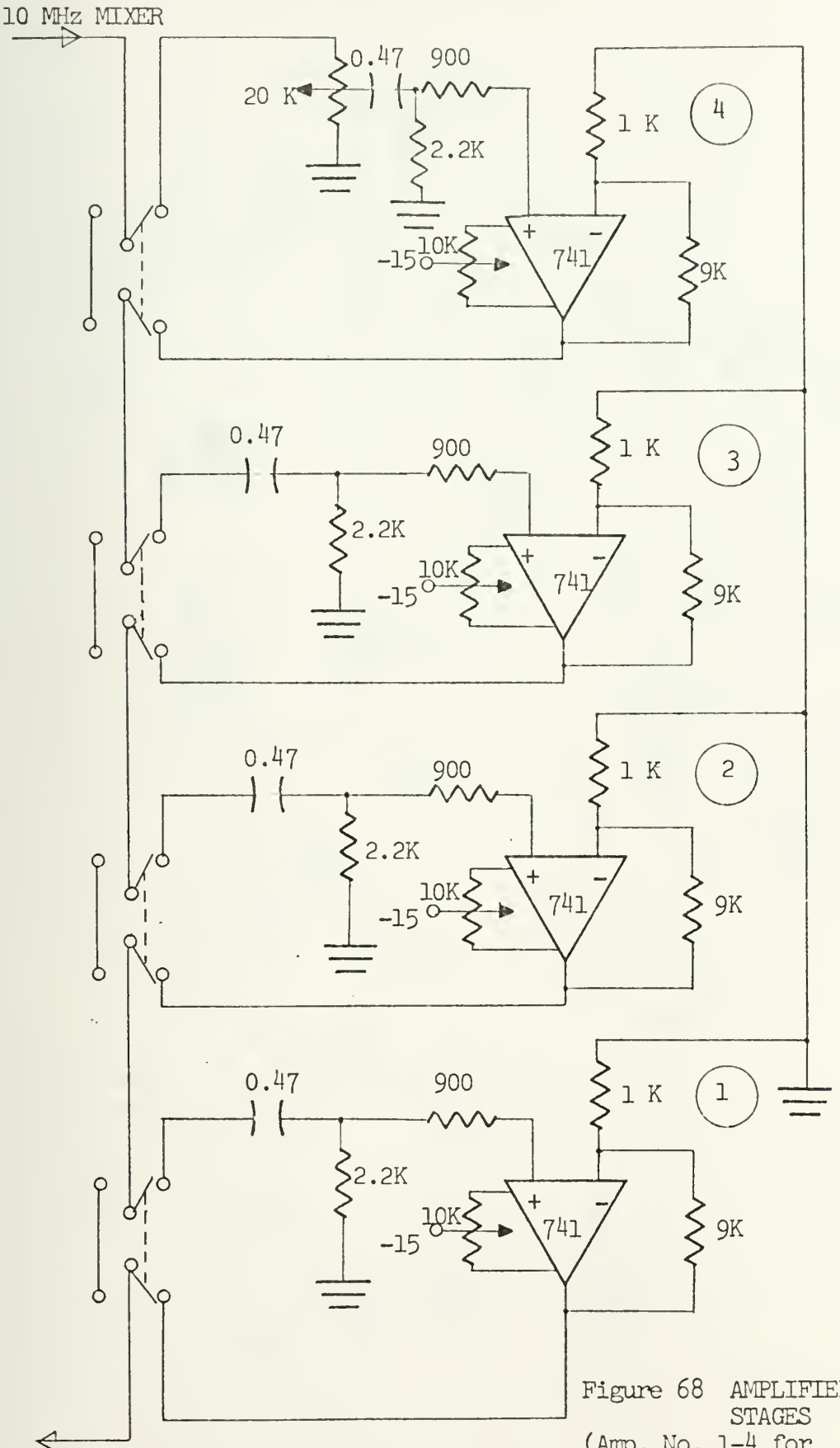

Figure 68 AMPLIFIER STAGES
(Amp. No. 1-4 for REFERENCE; 5-8 for ERROR CHANNEL)

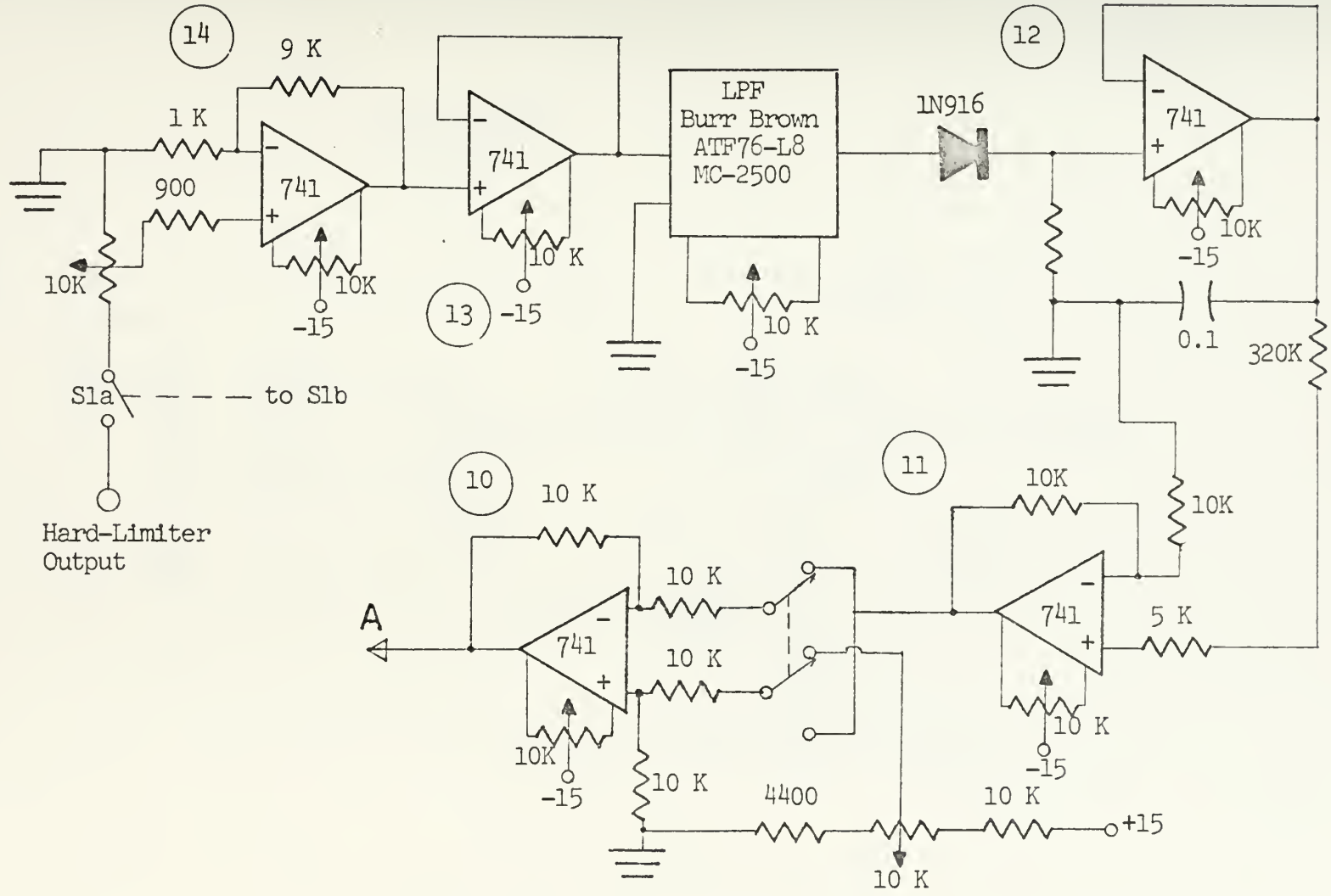

Figure 69 AFC CIRCUIT

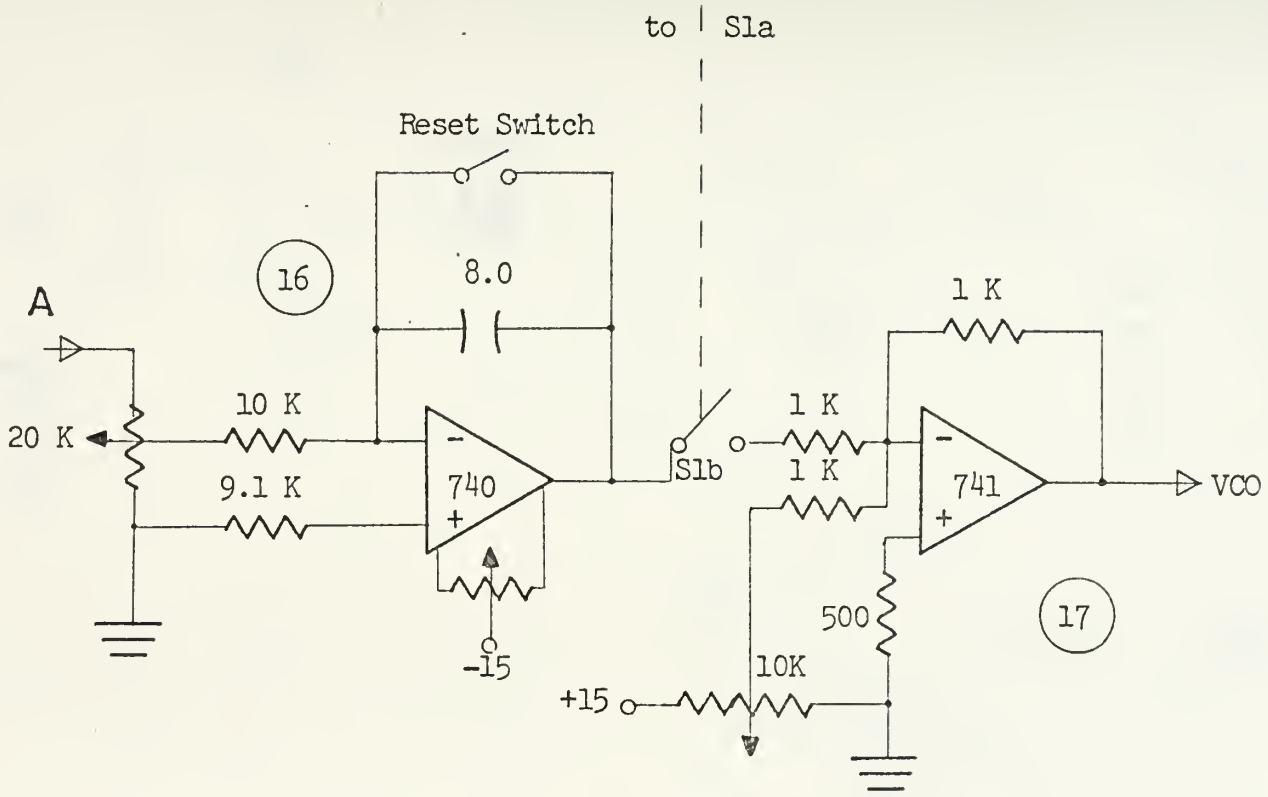

Figure 69 AFC CIRUIT (cont'd)

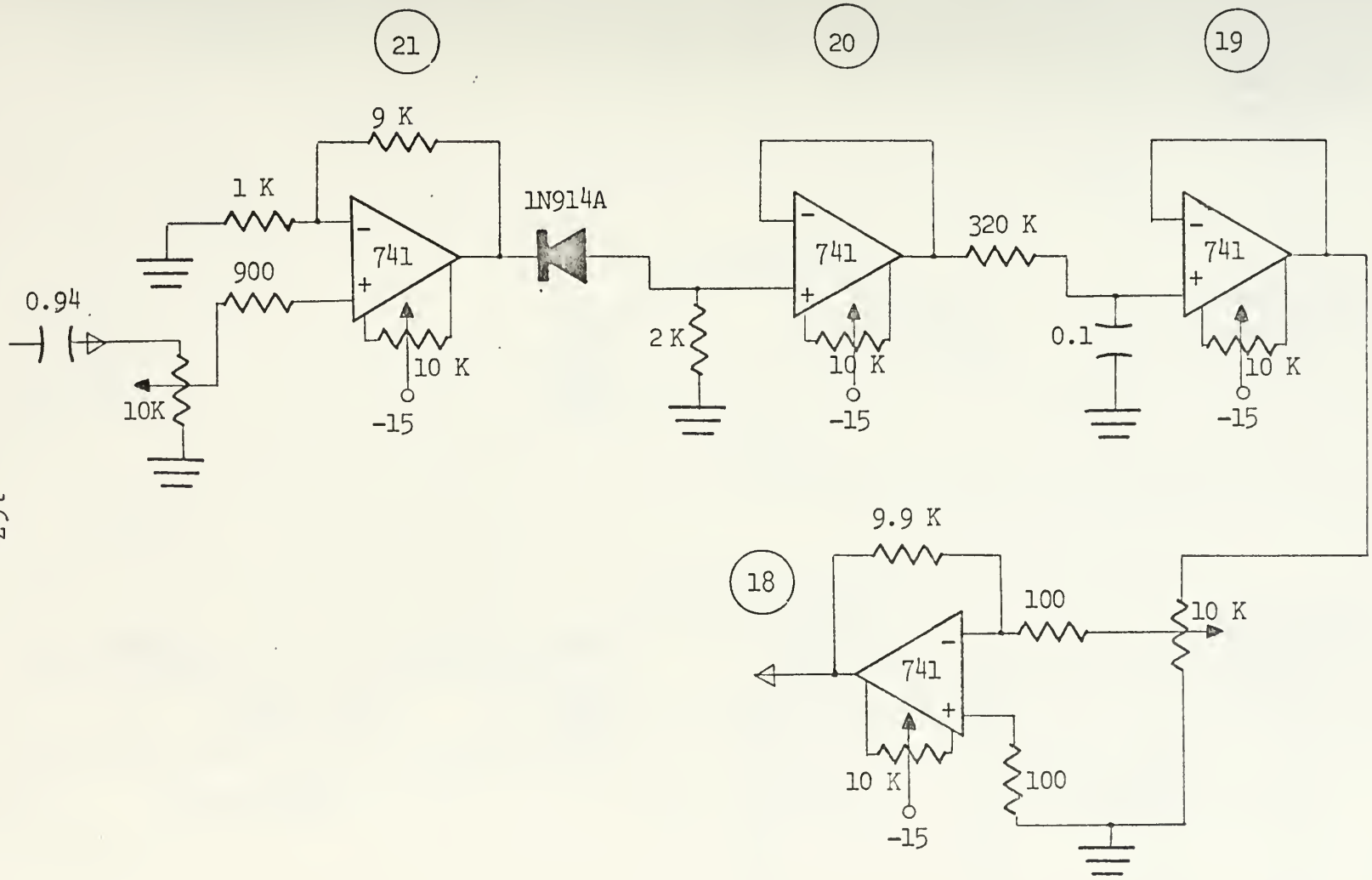

Figure 70 AGC CIRCUIT DIAGRAM

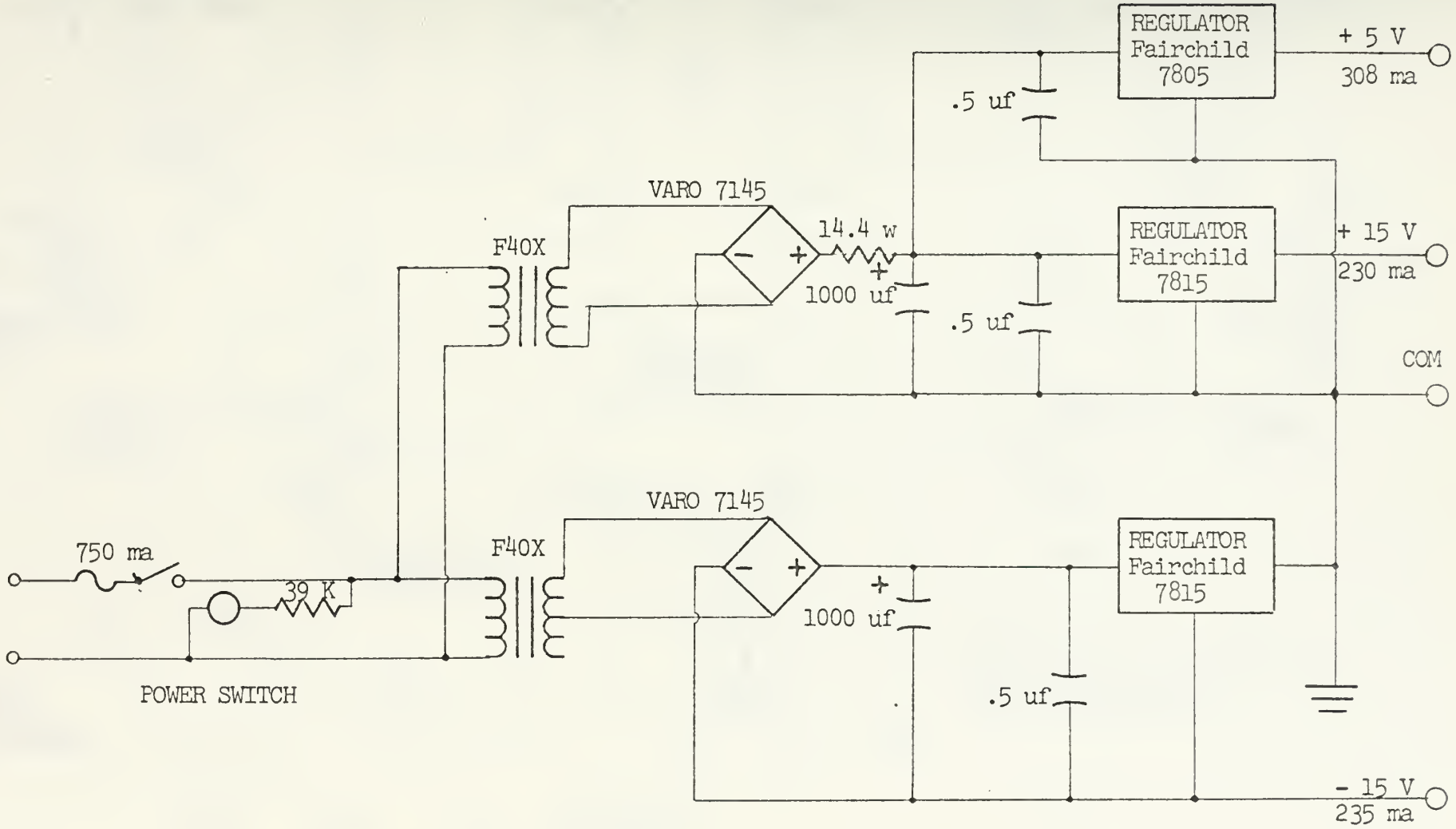

Figure 71 SYSTEM POWER SUPPLY (the current values are those delivered to the connected system, not maximum values)

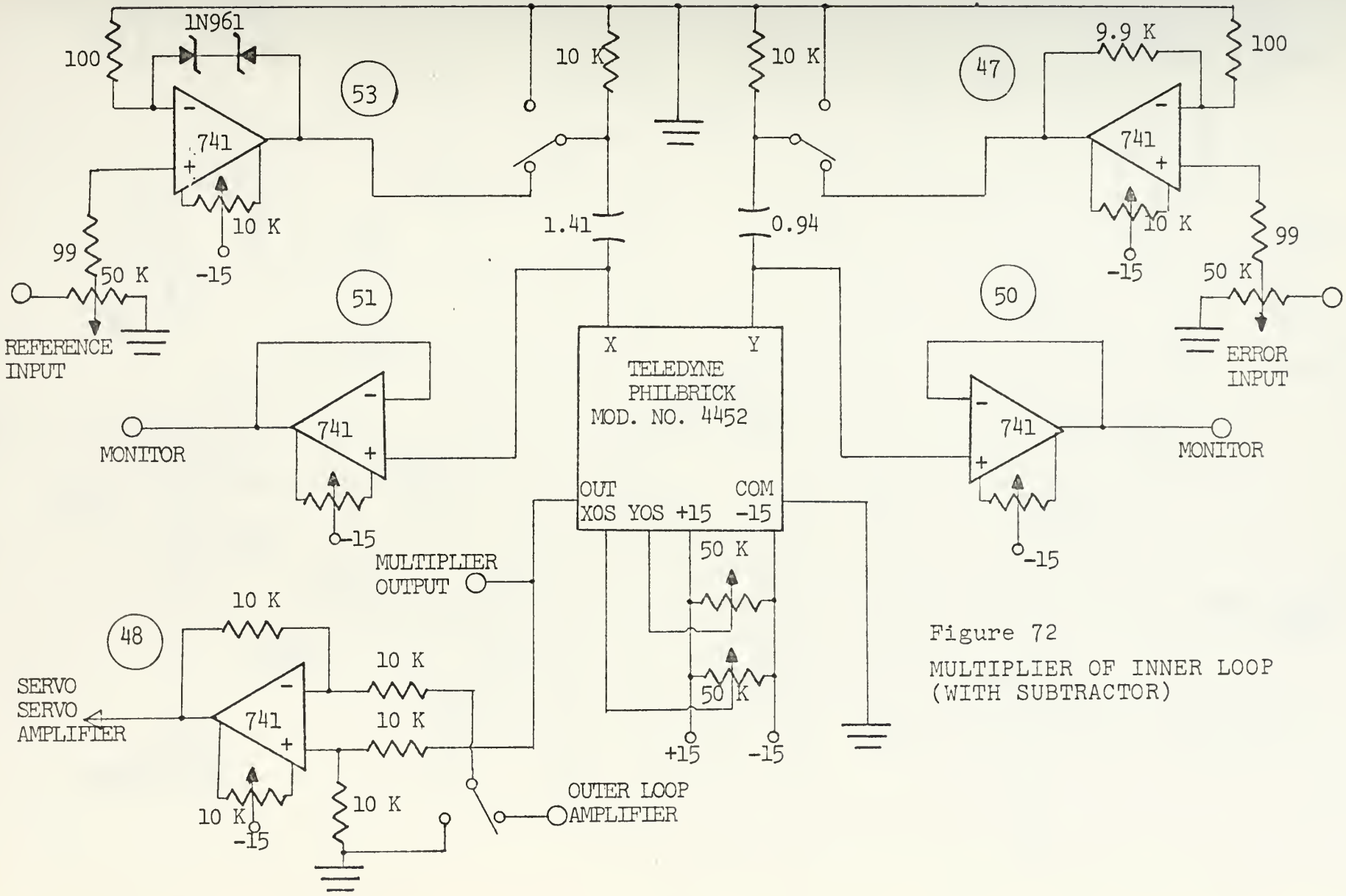

Figure 72

MULTIPLIER OF INNER LOOP
(WITH SUBTRACTOR)

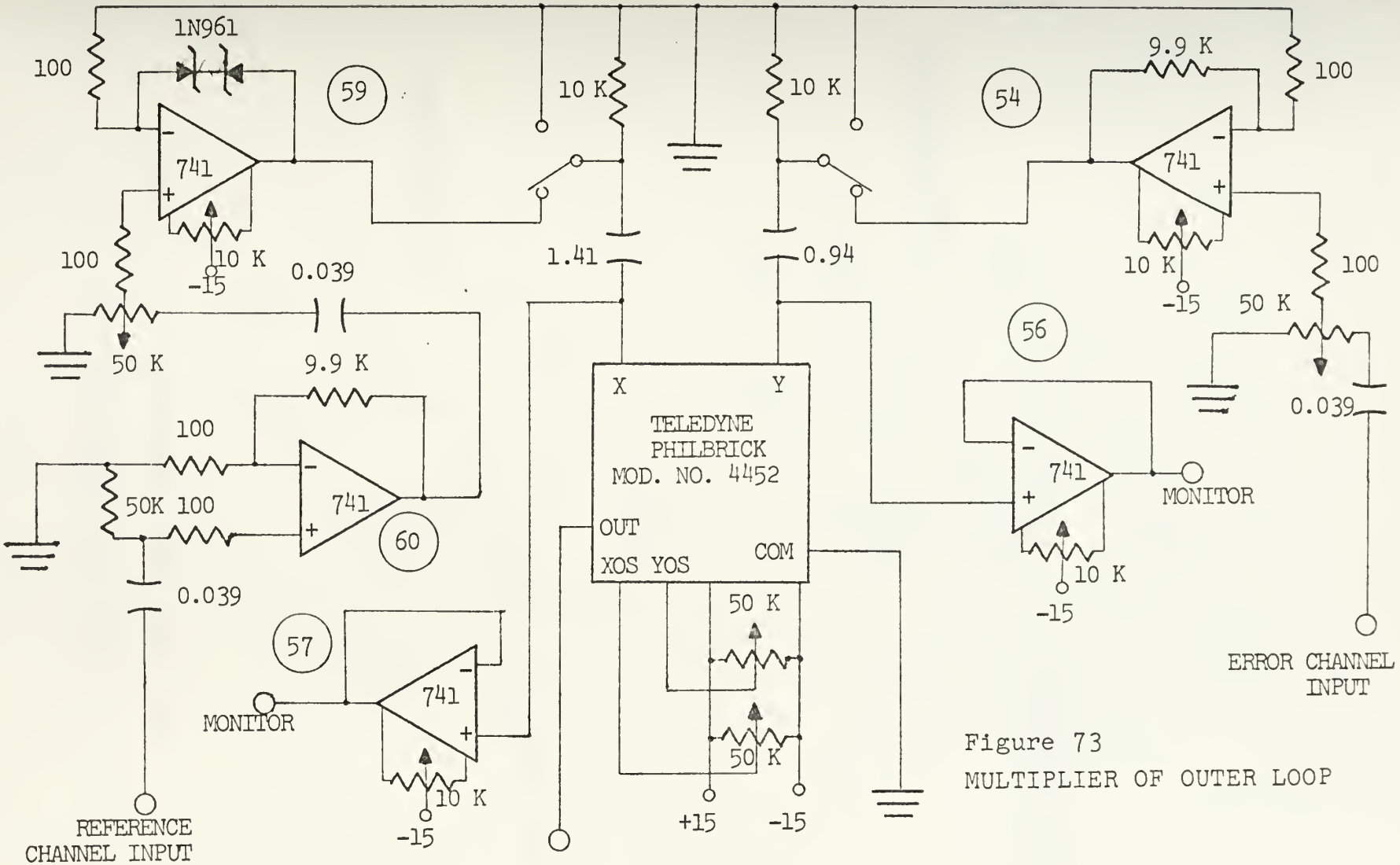

Figure 73
MULTIPLIER OF OUTER LOOP

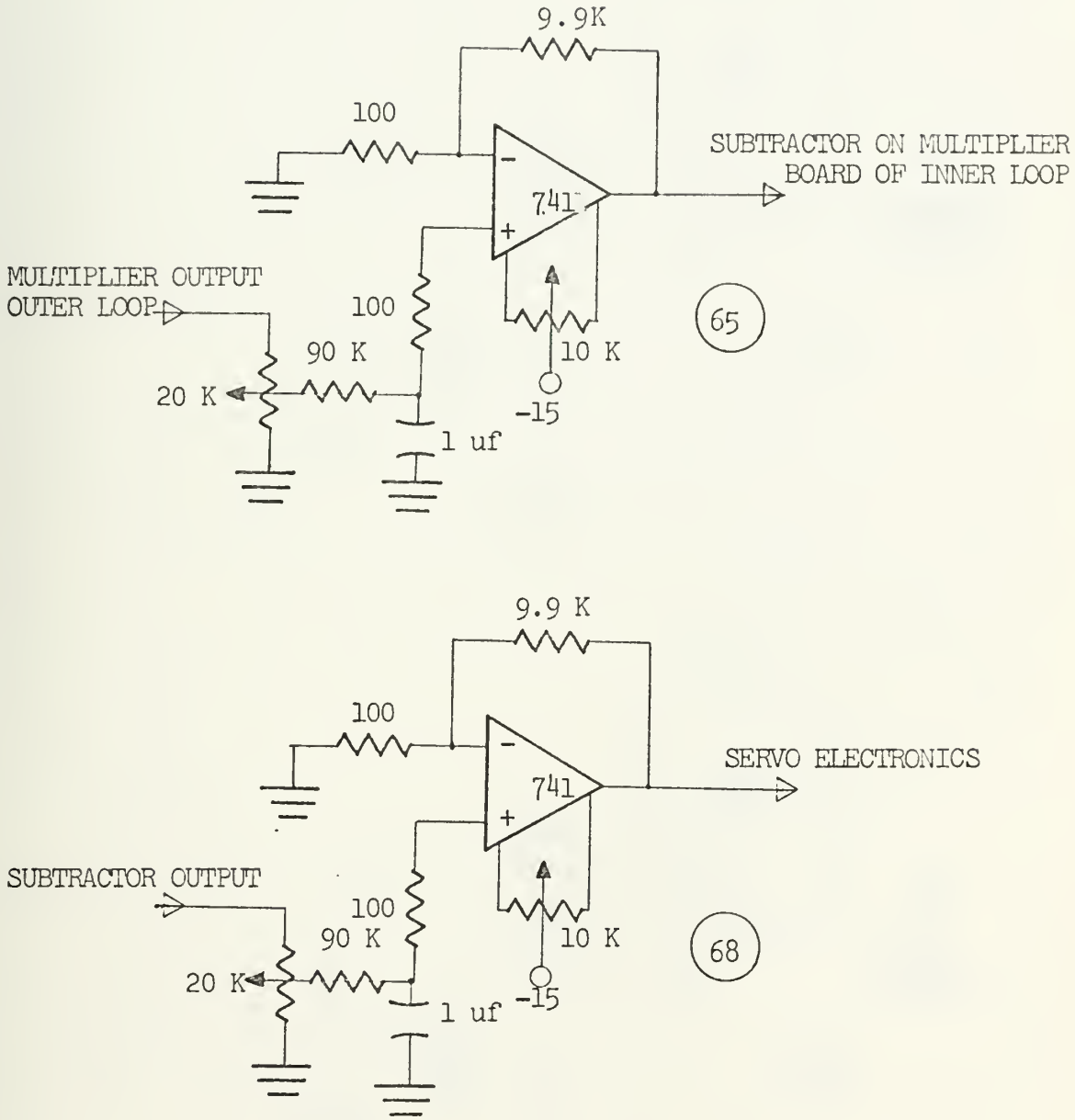

Figure 74 a) AMPLIFIER, OUTER LOOP GAIN

b) AMPLIFIER, SERVO GAIN

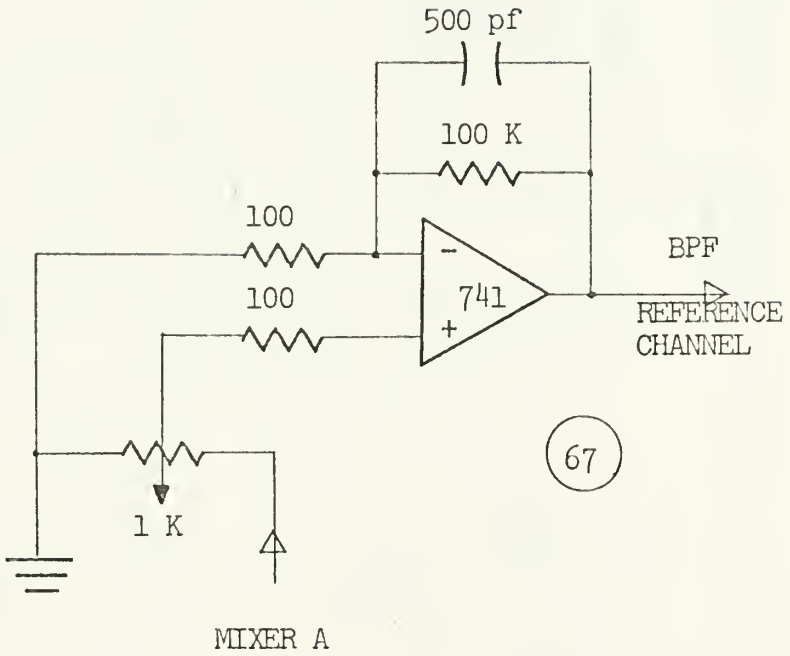

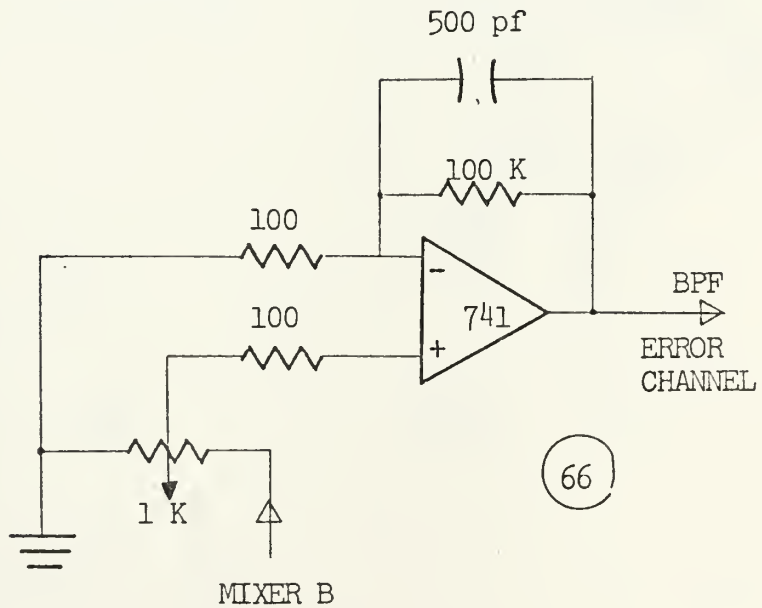

Figure 75 AMPLIFIER IN FRONT OF BPF (BW: 250 Hz)

a) REFERENCE CHANNEL

b) ERROR CHANNEL

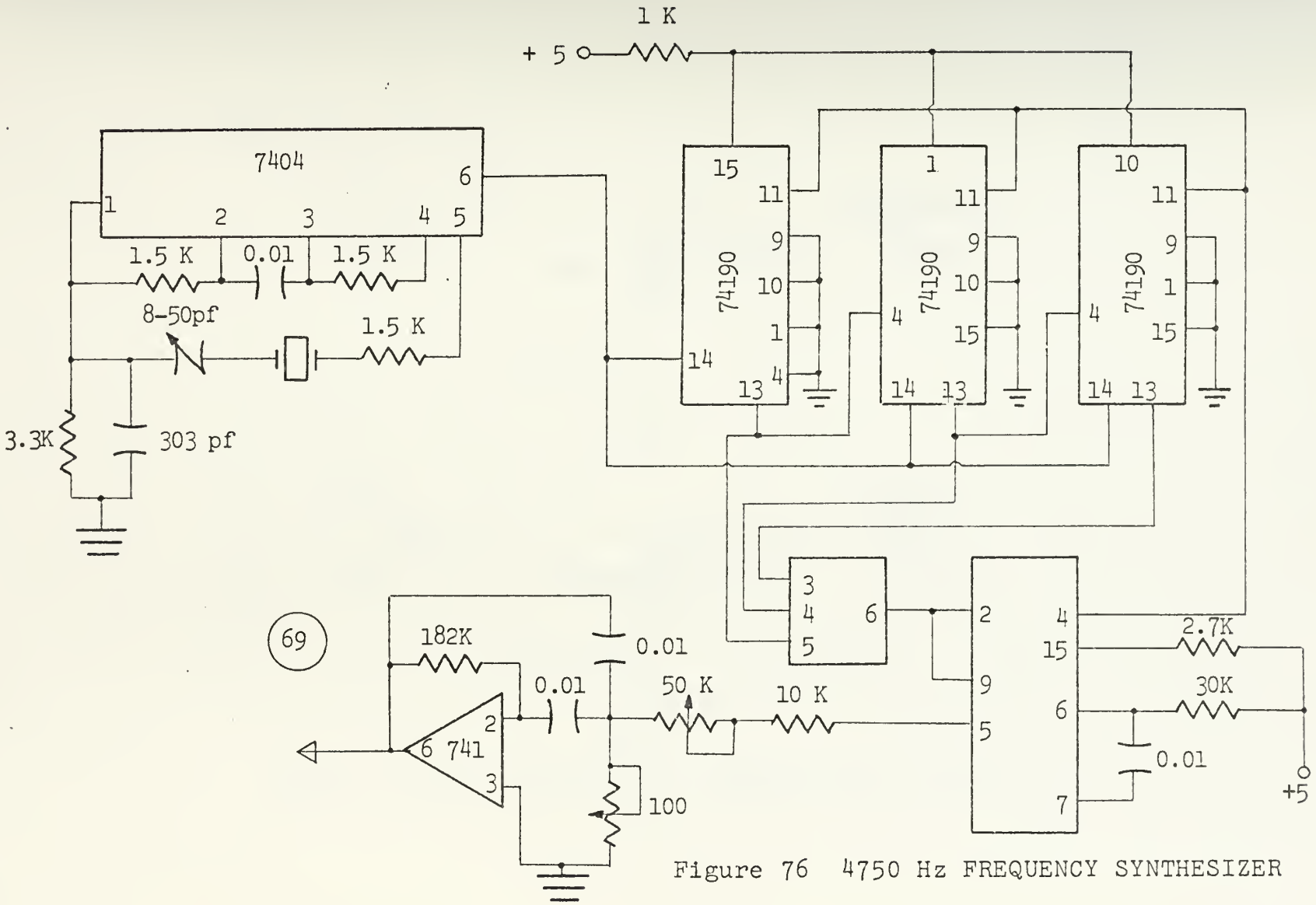

Figure 76 4750 Hz FREQUENCY SYNTHESIZER

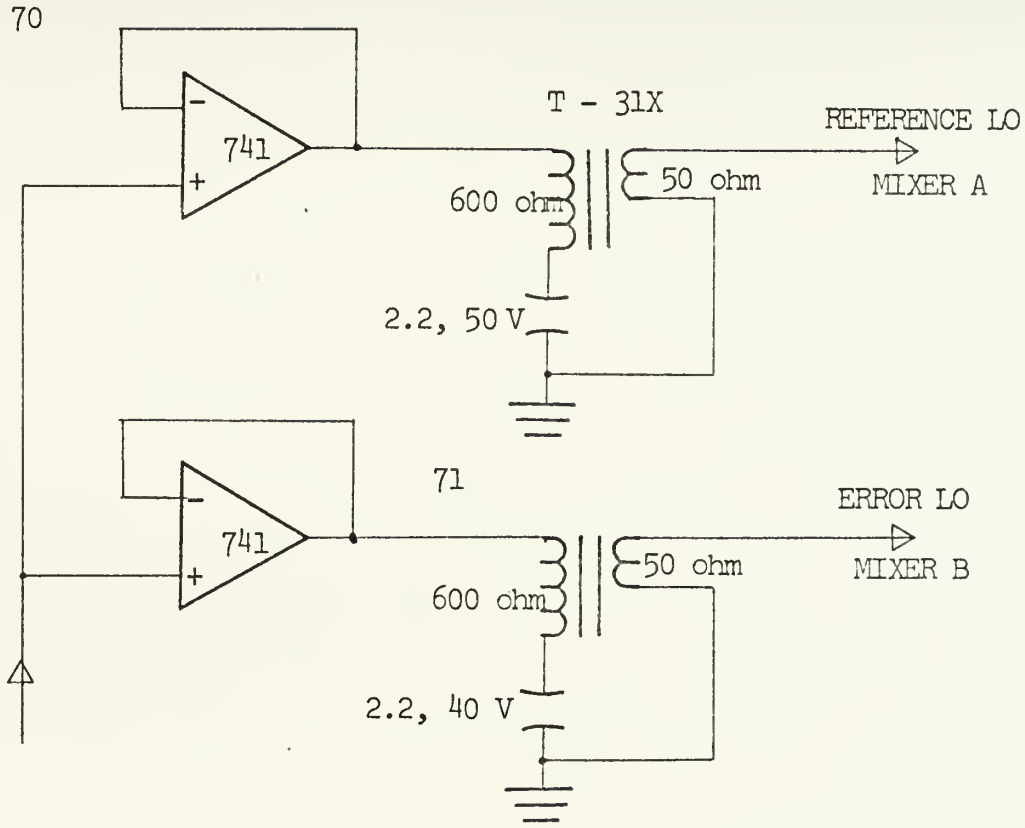

Figure 76 4750 Hz FREQUENCY SYNTHESIZER (Cont'd)

APPENDIX F

WIRING DIAGRAMS

The wiring diagrams according which all the inter-connection between the circuit-boards and the other system components had been done are given as Figs. 77-90.

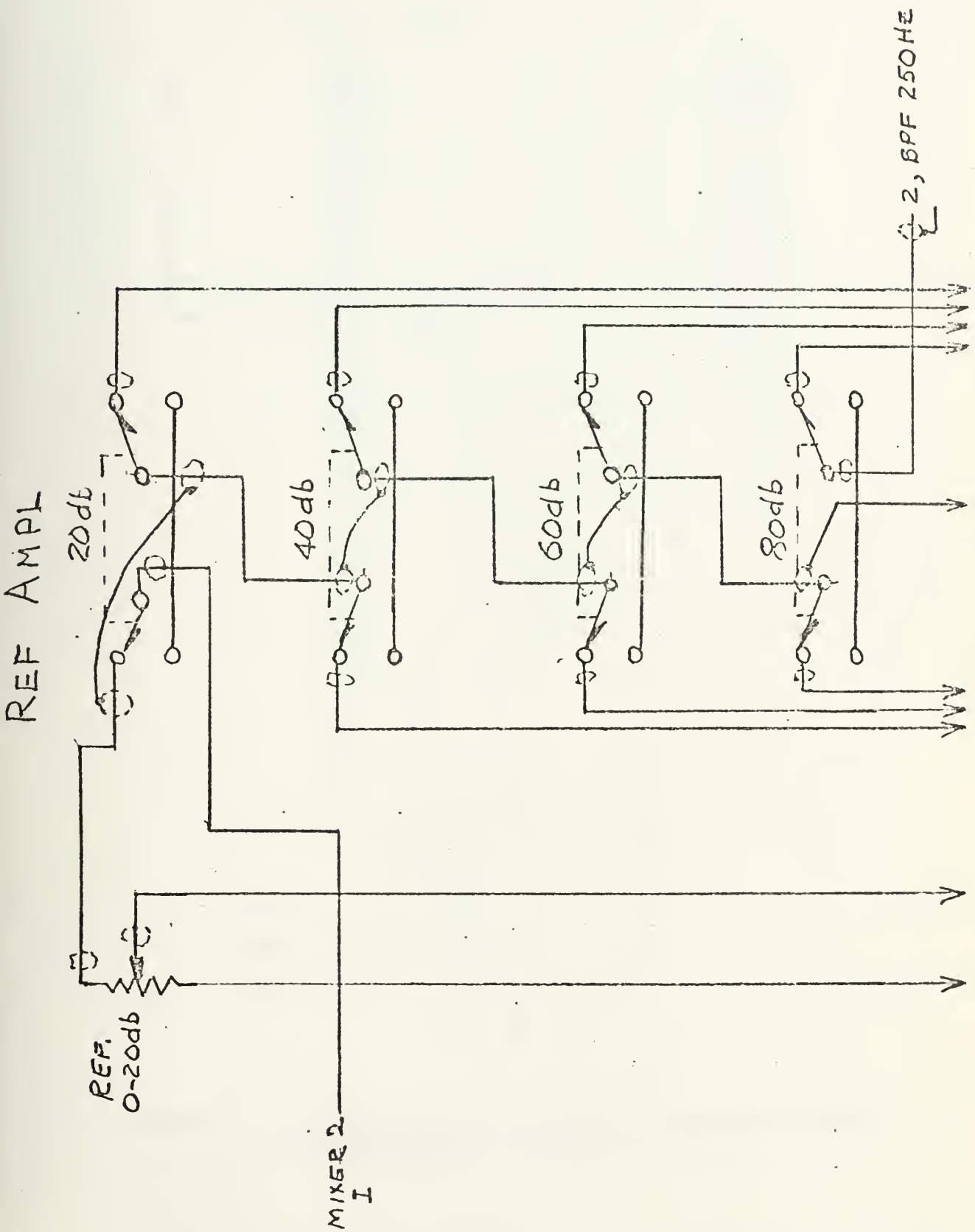

Figure 77. REFERENCE CHANNEL INPUT AMPLIFIER WIRING

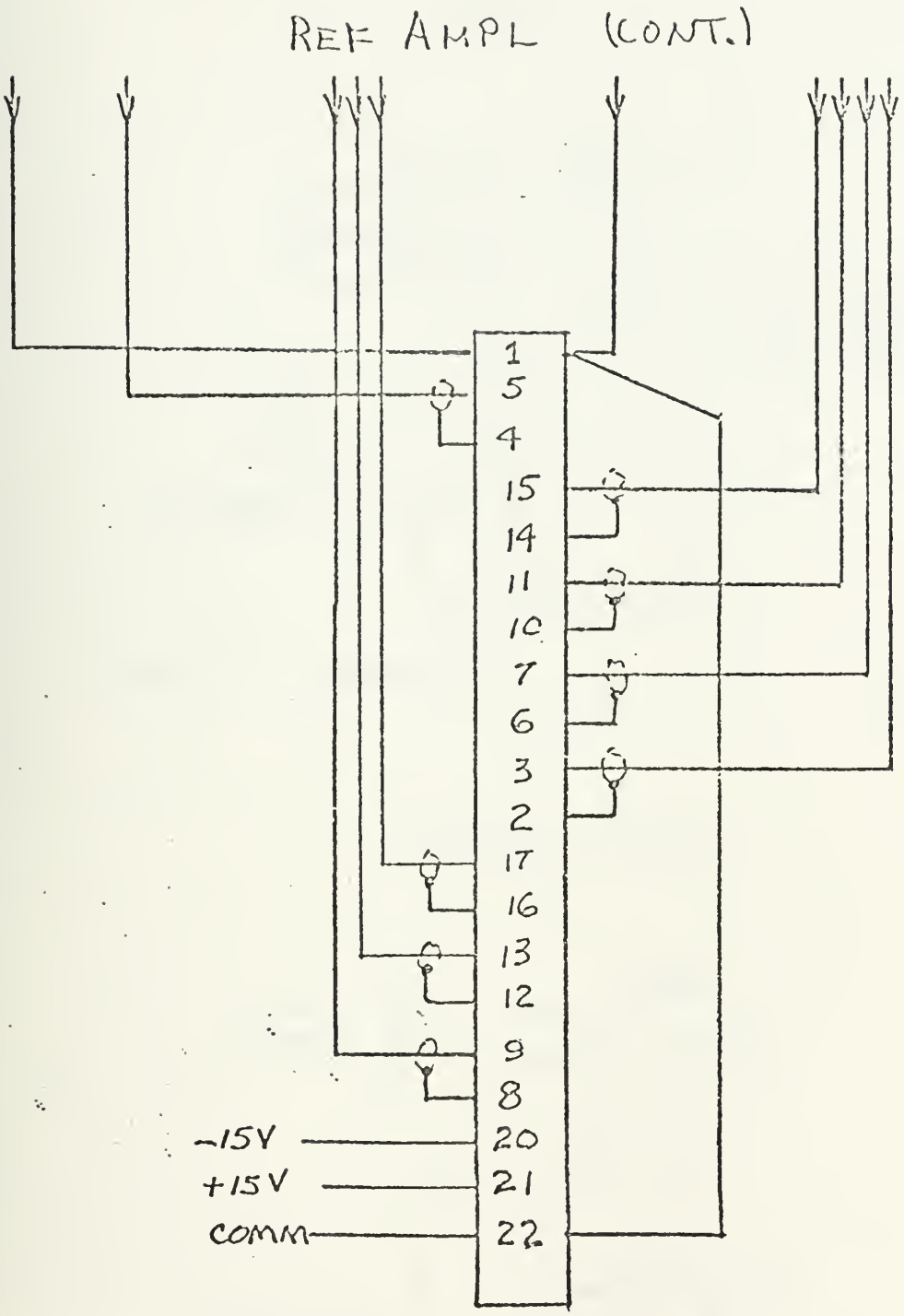

Figure 77. REFERENCE CHANNEL INPUT AMPLIFIER WIRING (continued)

AGC

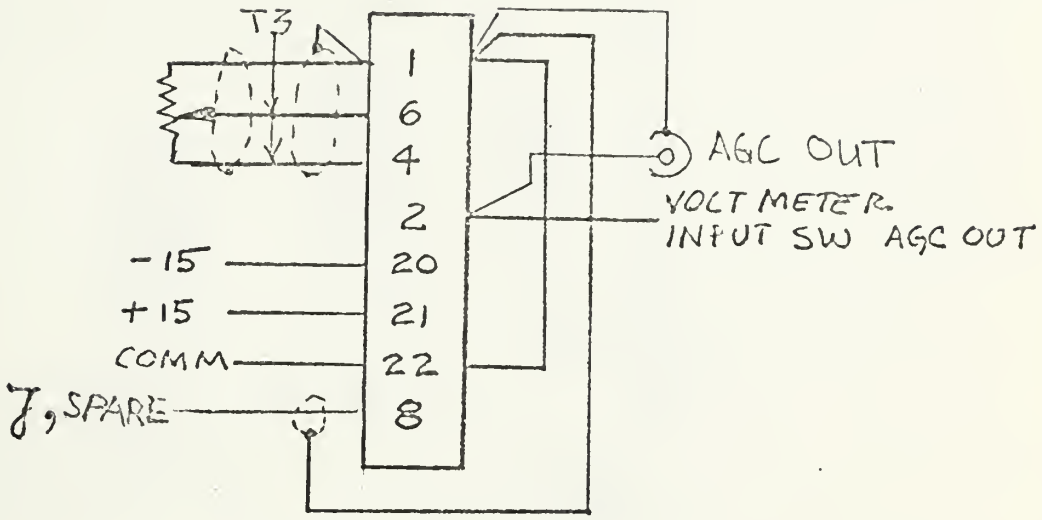

Figure 78. AGC WIRING

ERROR. AMPL.

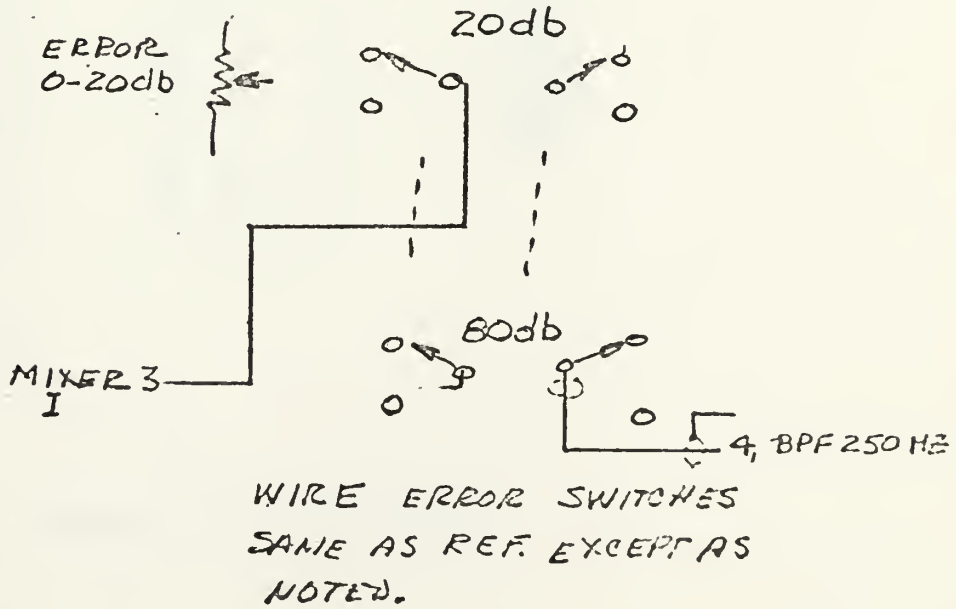

Figure 79. ERROR CHANNEL INPUT AMPLIFIER WIRING

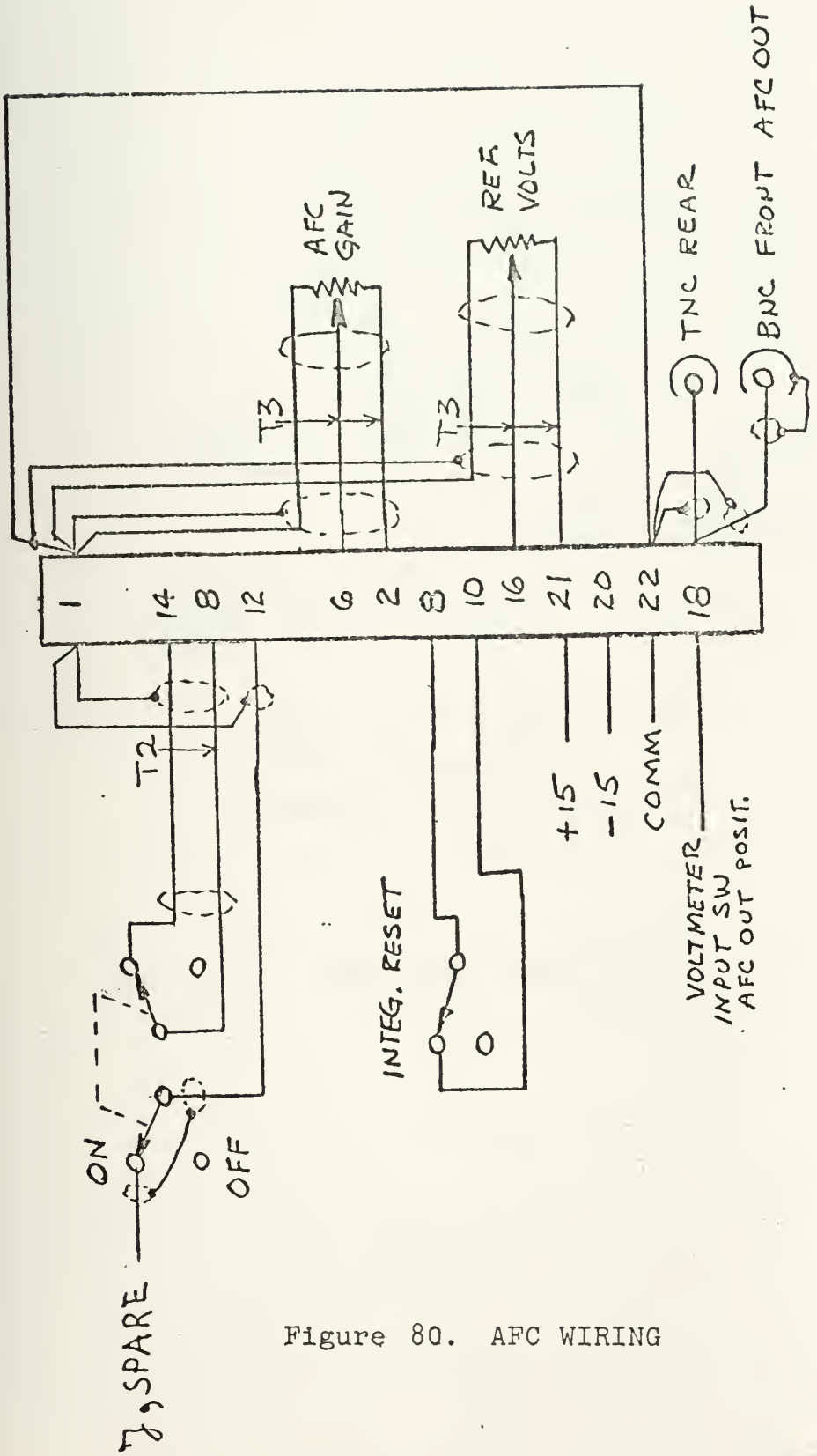

Figure 80. AFC WIRING

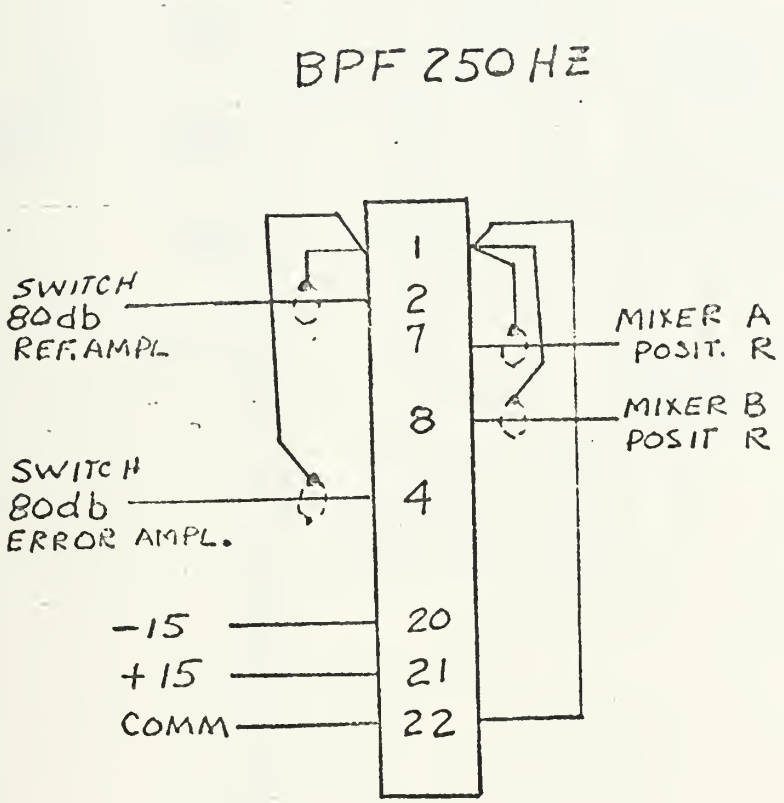

Figure 81. BAND-PASS FILTER, 250 Hz, WIRING

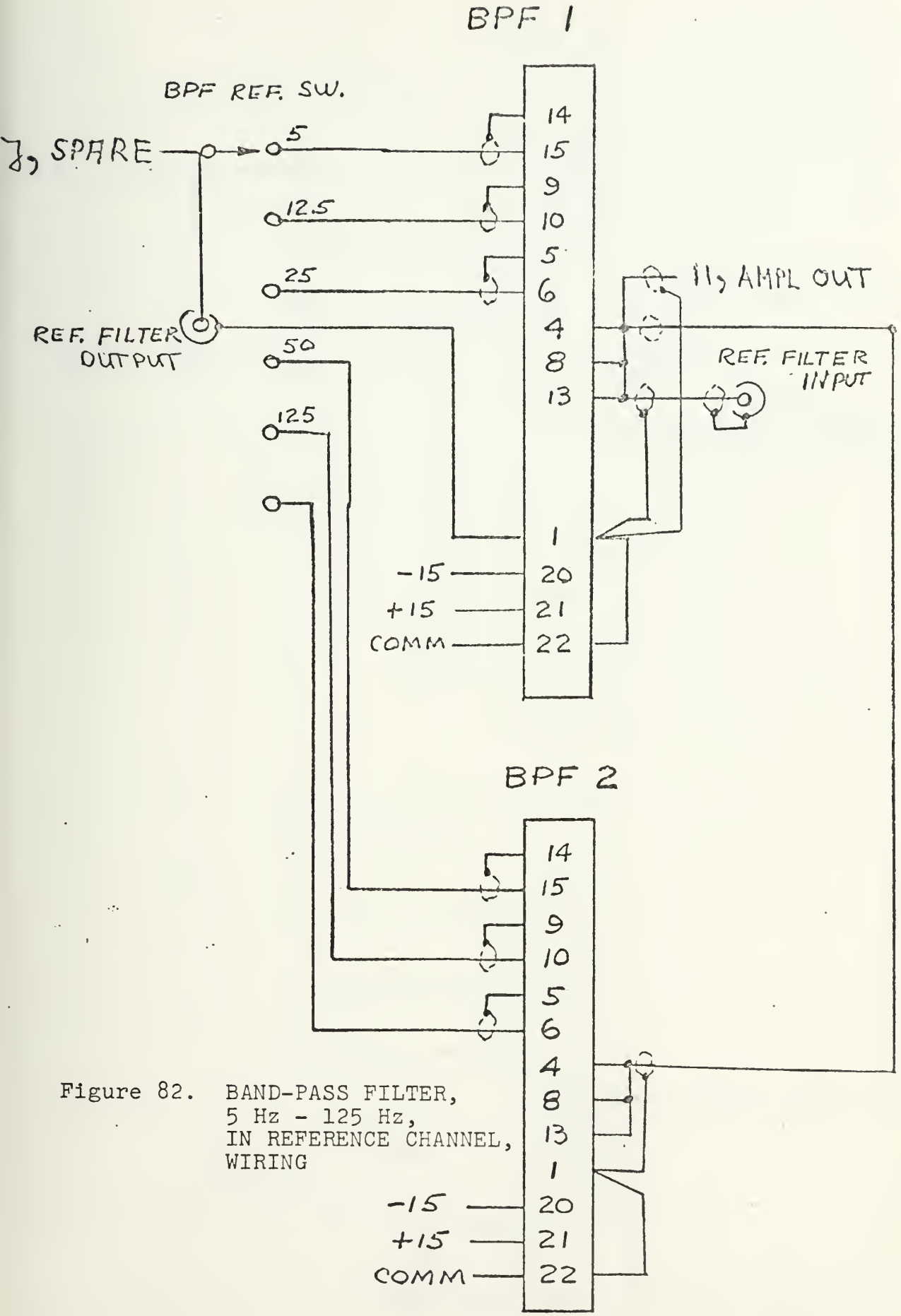

Figure 82. BAND-PASS FILTER, 5 Hz - 125 Hz, IN REFERENCE CHANNEL, WIRING

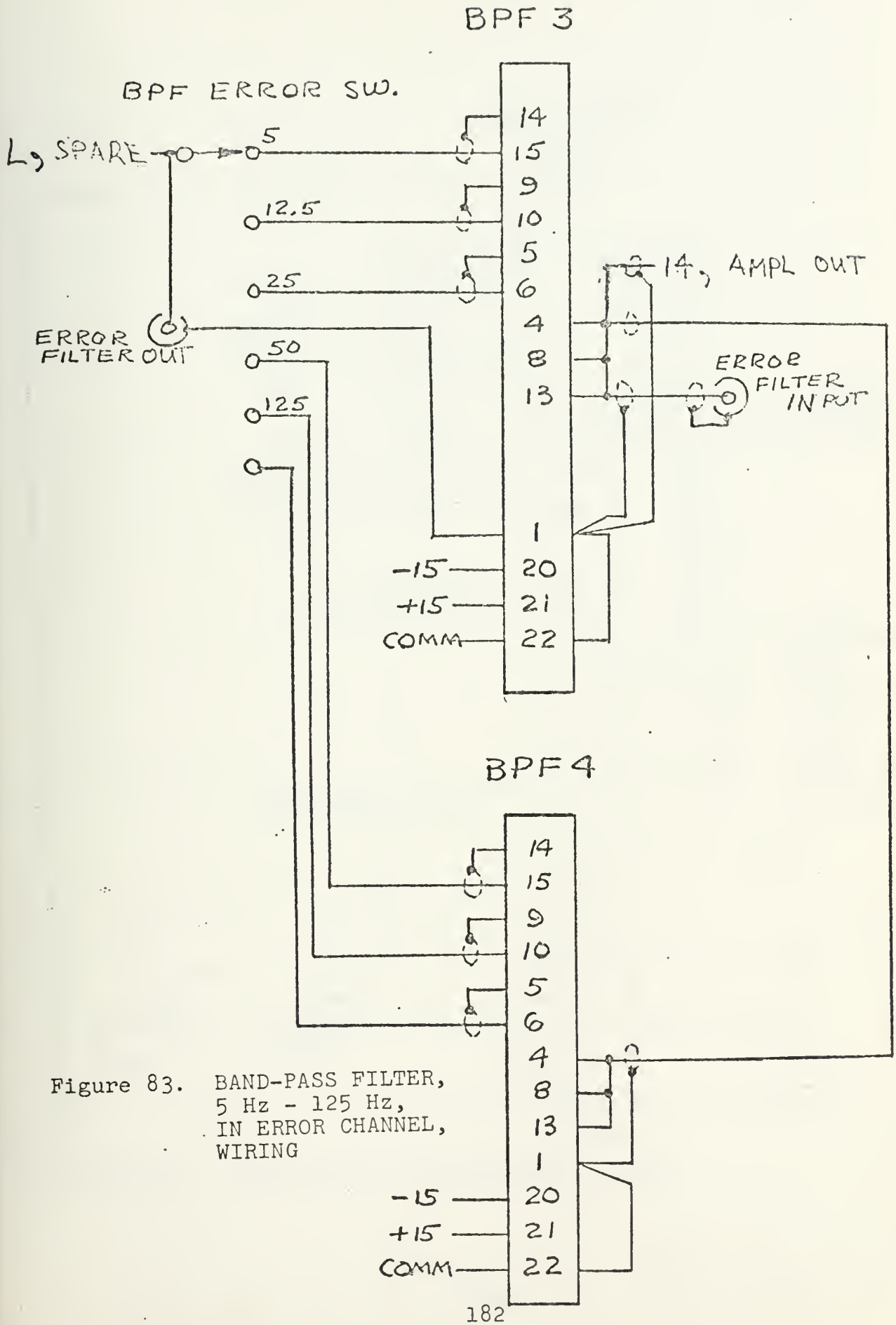

Figure 83. BAND-PASS FILTER, 5 Hz - 125 Hz, IN ERROR CHANNEL, WIRING

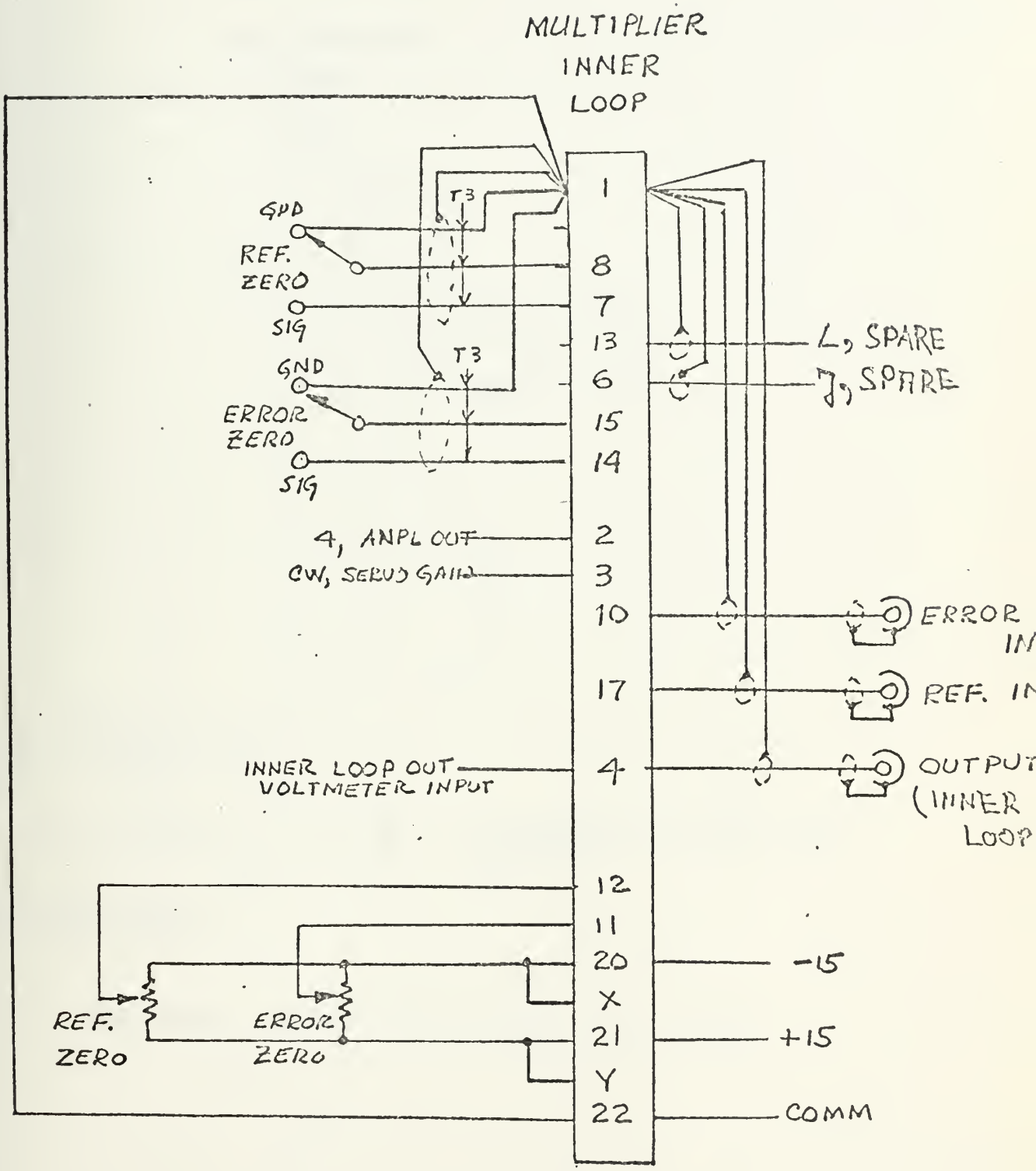

Figure 84. MULTIPLIER OF INNER LOOP, WIRING

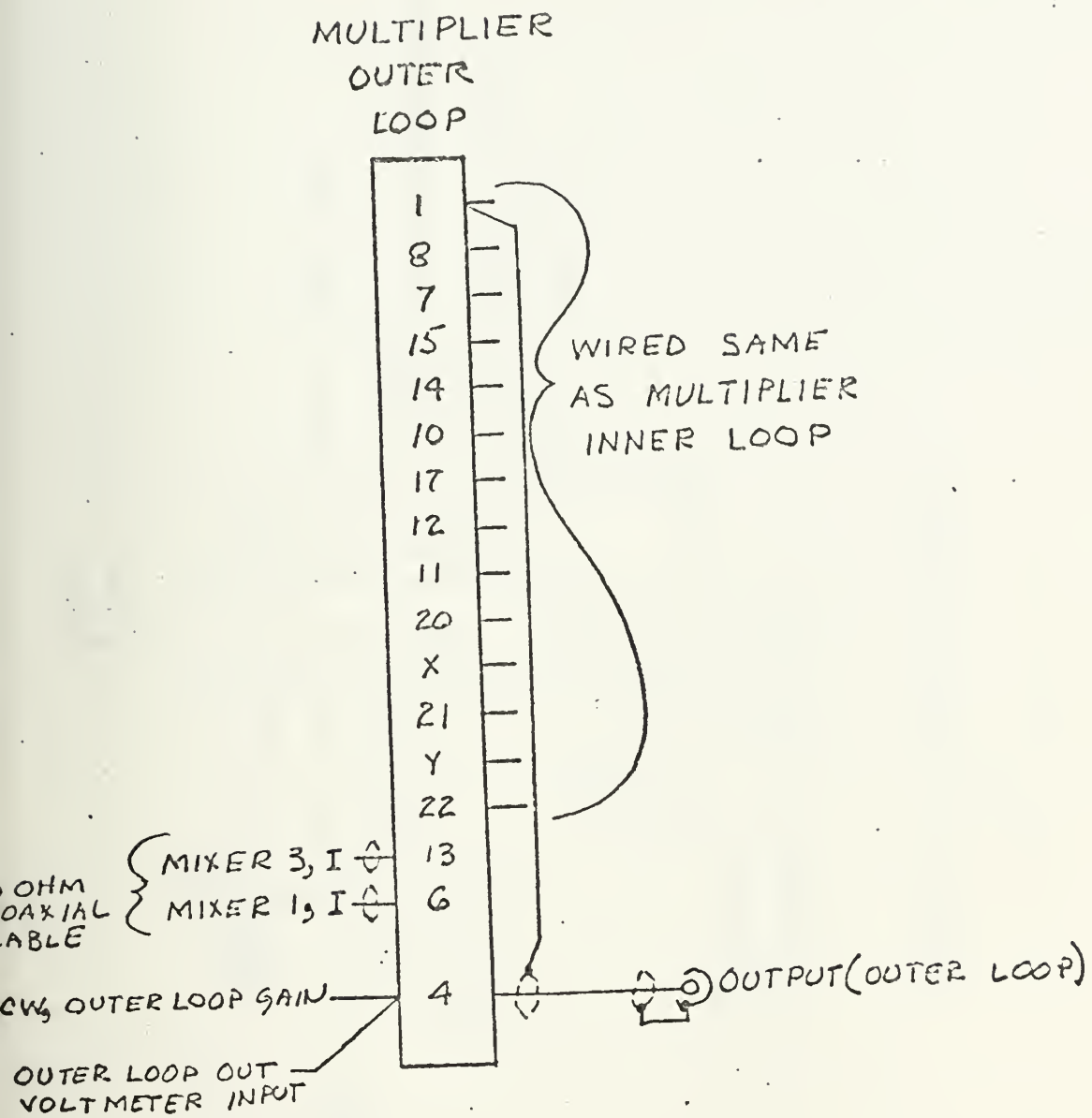

Figure 85. MULTIPLIER OF OUTER LOOP, WIRING

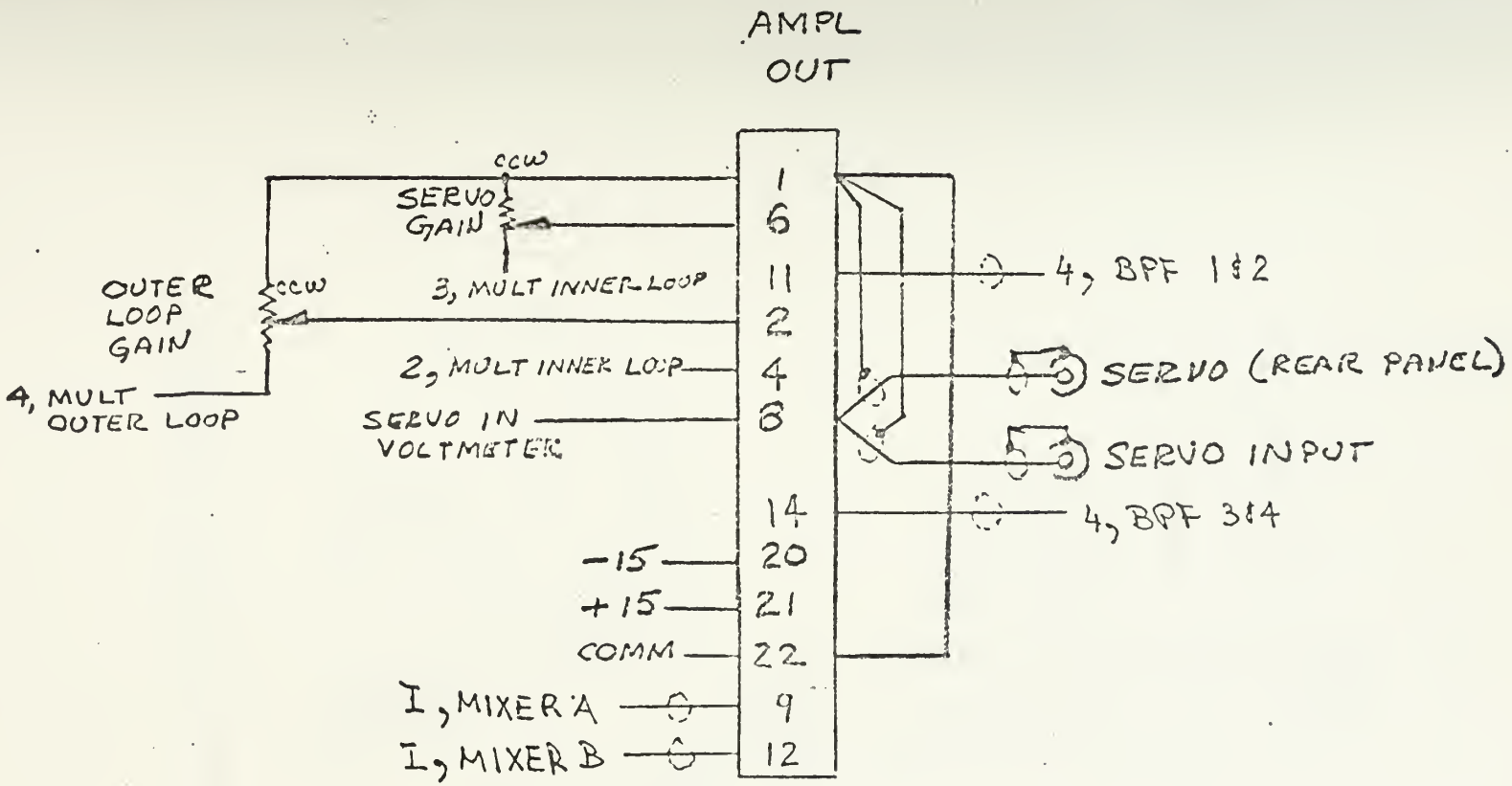

Figure 86. AMPLIFIER WIRING

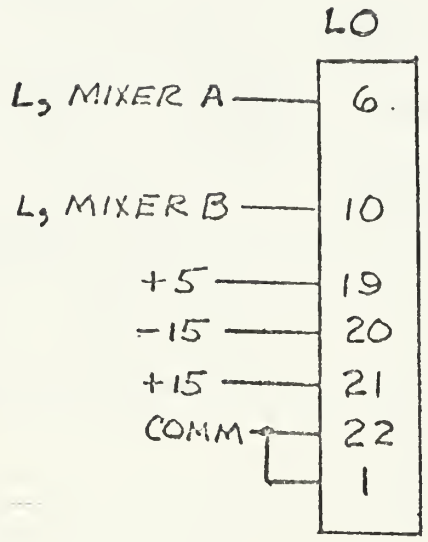

Figure 87.

LOCAL OSCILLATOR WIRING

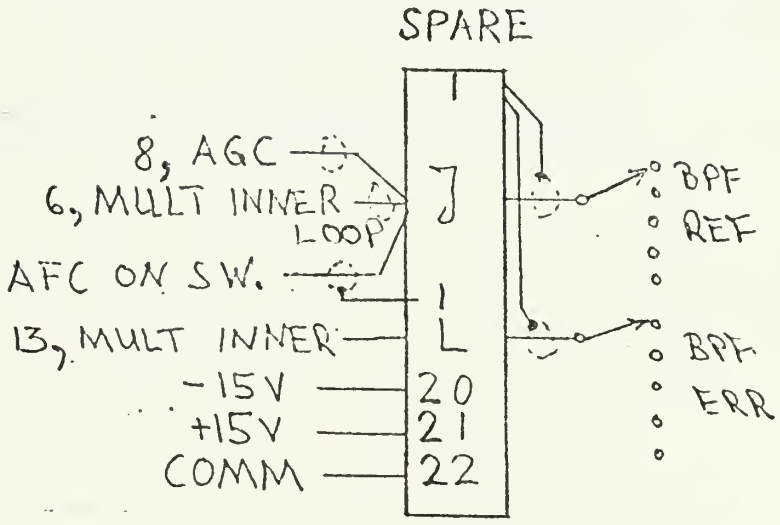

Figure 88. WIRING OF SPARE CONNECTOR

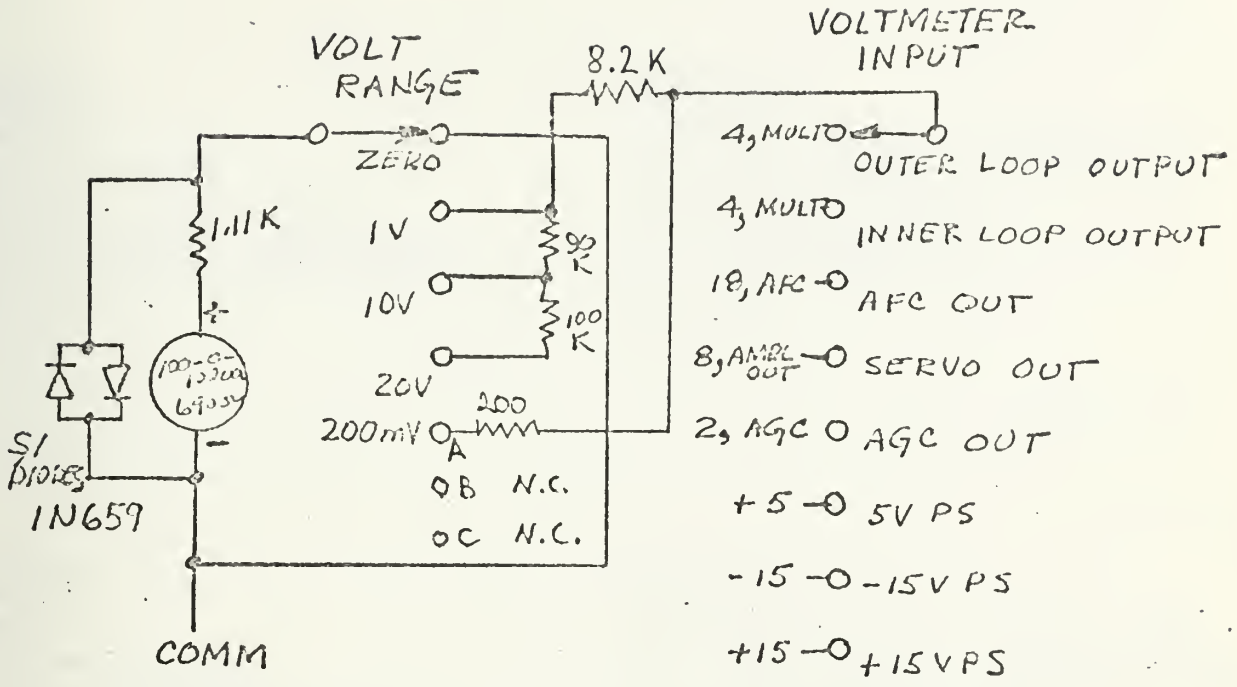

Figure 89. VOLTMETER CONNECTION

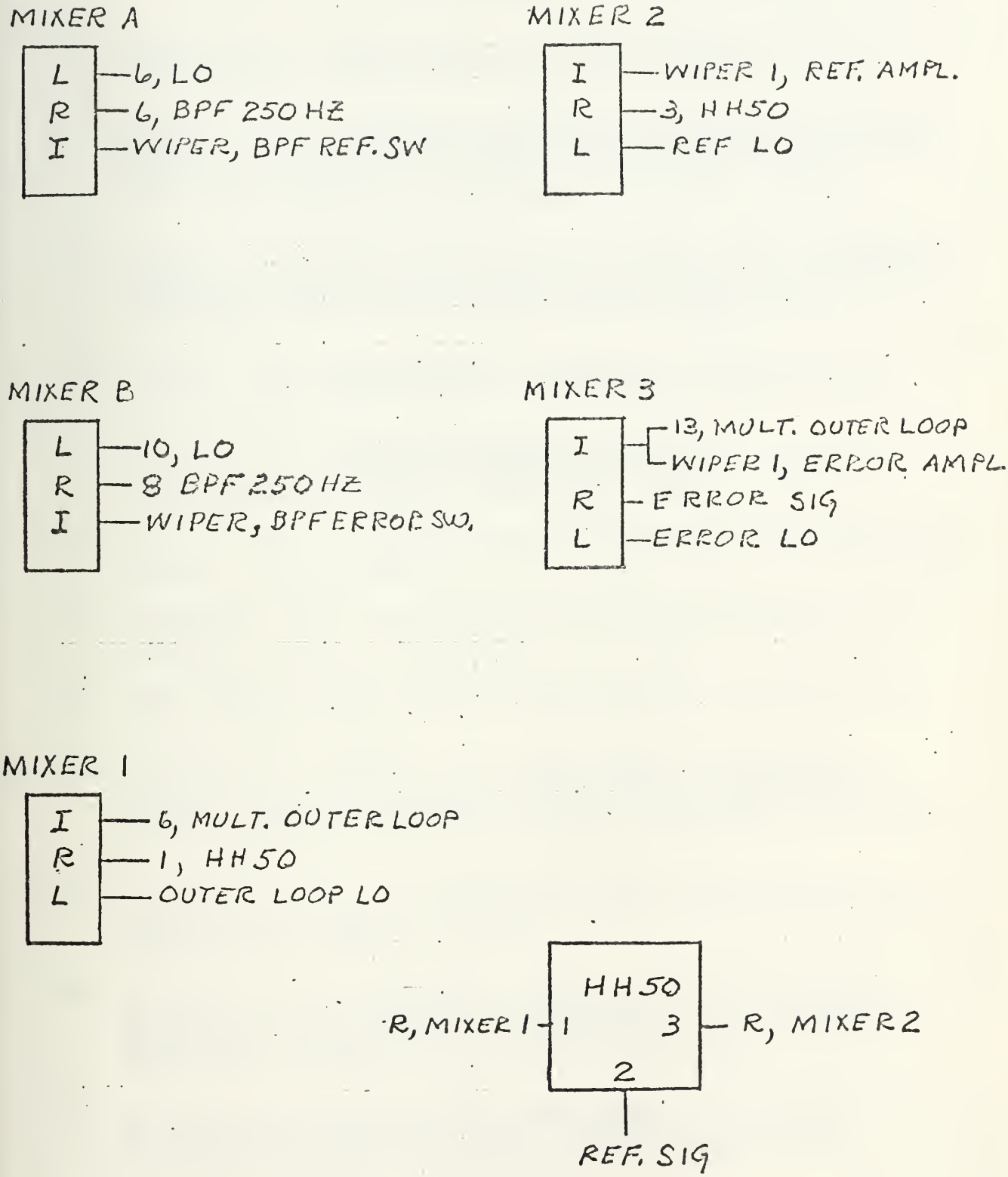

Figure 90. MIXER CONNECTIONS

BIBLIOGRAPHY

1. Skolnik, M.I., Introduction to Radar System, McGraw-Hill, 1962.

2. Taylor, R.E., Automatic Electronic Polarization Tracking System, NASA TR X-523-67-302, National Aeronautics and Space Administration, Goddard Space Flight Center, Greenbelt, Maryland, June 1967.

3. Ohlson, J.E., Levy, G.S., and Stelzried, C.T., A Tracking Polarimeter for Measuring Solar and Ionospheric Faraday Rotation of Signals from Deep Space Probes, to be published.

4. Ohlson, J.E., Correlation Polarimetry for Noise-Like Signals, to be published.

5. Taylor, R. E., RosmanII Antenna Automatic Polarization Tracking Modification, v. II, Technical Proposal, Philco WDL-TP 2031, Oct. 1965.

6. Thomas, J.B., An Introduction to Statistical Communication Theory, Wiley, 1969.

7. Goldstein, R.M., Superior Conjunction of Pioneer 6, Science, v. 166, p. 598-601, Oct. 1969.

8. Amer. Radio Relay League, Antenna Book, West Hartford, Connecticut, 1955.

9. Strum, R.D., Demetry, J.S., The Step and Frequency Response of Second-Order Linear Systems with no Zeros, Handout, Naval Postgraduate School, Monterey, California, February 1965.

10. DiStefano III, J.J., Stubberud, A.R., and Williams, I.J., Feedback and Control Systems, Schaum's Outline Series, McGraw Hill, 1967.

11. Jet Propulsion Laboratory , Block III C DSIF Ground Equipment S-Band RF Receiver/Exciter Subsystem Detail Specification for, Code ID No. 23835, Spec No. DOR-1276-DTL A, Pasadena, California, June 1967.

12. Jet Propulsion Laboratory, DSN S-Band RF Receiver/ Exciter Subsystem Block III C Diagram, Code No ID No 23835, Pasadena, California, March 1967.

13. Davenport, W.B., Signal-to-noise Ratios in Band-Pass Limiters, Journal of Applied Physics, v. 24, No. 6, p. 720-727, June 1953.

14. Viterbi, A.J., Principles of Coherent Communication, McGraw-Hill, 1966.

15. Blachman, N.M., The Output Signal-to-Noise Ratio of a Bandpass Limiter, IEEE Transaction on Aerospace and Electronics Systems, p. 635, July 1968.

INITIAL DISTRIBUTION LIST

		No. Copies
1.	Defense Documentation Center Cameron Station Alexandria, Virginia 22314	2
2.	Library, Code 0212 Naval Postgraduate School Monterey, California 93940	2
3.	Dokzent Bundeswehr - See 53 Bonn Friedrich Ebert Allee 34 West- Germany	1
4.	Marineamt - In EBM 294 Wilhelmshaven Gökerstrasse West- Germany	1
5.	Associate Professor John Ohlson, Code 52OL Department of Electrical Engineering Naval Postgraduate School Monterey, California 93940	3
6.	G. S. Levy 238 - 737 Jet Propulsion Laboratory Pasadena, California	1
7.	LCDR Wolff-R. Zimmermann, FGN 307 Nienburg/Weser Roonstrasse 23 West- Germany	1

SECURITY CLASSIFICATION OF THIS PAGE (When Data Entered)

REPORT DOCUMENTATION PAGE		READ INSTRUCTIONS BEFORE COMPLETING FORM
1. REPORT NUMBER	2. GOVT ACCESSION NO.	3. RECIPIENT'S CATALOG NUMBER
4. TITLE (and Subtitle) A Correlation Polarimeter for Deep Space Tracking		5. TYPE OF REPORT & PERIOD COVERED Engineer's Thesis; September 1973 6. PERFORMING ORG. REPORT NUMBER
7. AUTHOR(s) Wolff-Rüdiger Zimmermann		8. CONTRACT OR GRANT NUMBER(s)
9. PERFORMING ORGANIZATION NAME AND ADDRESS Naval Postgraduate School Monterey, California 93940		10. PROGRAM ELEMENT, PROJECT, TASK AREA & WORK UNIT NUMBERS
11. CONTROLLING OFFICE NAME AND ADDRESS Naval Postgraduate School Monterey, California 93940		12. REPORT DATE September 1973 13. NUMBER OF PAGES 193
14. MONITORING AGENCY NAME & ADDRESS(if different from Controlling Office) Naval Postgraduate School Monterey, California 93940		15. SECURITY CLASS. (of this report) Unclassified 15a. DECLASSIFICATION/DOWNGRADING SCHEDULE

16. DISTRIBUTION STATEMENT (of this Report)

Approved for public release; distribution unlimited.

17. DISTRIBUTION STATEMENT (of the abstract entered in Block 20, if different from Report)

18. SUPPLEMENTARY NOTES

19. KEY WORDS (Continue on reverse side if necessary and identify by block number)

Correlation Polarimeter
Deep Space Tracking
Polarization Tracking

20. ABSTRACT (Continue on reverse side if necessary and identify by block number)

The tracking polarimeter implemented on the 64-meter National Aeronautics and Space Administration/Jet Propulsion Laboratory (NASA/JPL) parabolic antenna at Goldstone, California uses a pair of waveguide quarter-wave plates to allow synthesis of a rotating cross-polarized linear feed system, and a phase-locked-loop (PLL) to coherently determine an error signal from the

DD FORM 1 JAN 73 1473 EDITION OF 1 NOV 65 IS OBSOLETE
S/N 0102-014-6601 |

SECURITY CLASSIFICATION OF THIS PAGE (When Data Entered)

(20.)

signal component in the error channel. This error signal drives the feed system until the error axis is orthogonal to the signal axis.

Because the PLL has the normal "loss of lock" problem at low signal-to-noise ratios a correlation polarimeter has been developed. The PLL is replaced by a multiplier as a correlator. The correlation between the signal components in the reference and error channels accomplishes a detection of the error signal because both have same phase, since they are just different projections of the same signal vector.

The analysis, the investigation of the theory by means of a working model, the development of the actual correlation polarimeter and the test series performed are described.